Time-of-Flight Inelastic Neutron Scattering

Ray Osborn
Materials Science Division
Argonne National Laboratory

Acknowledgements

Brian Rainford
Department of Physics and Astronomy
University of Southampton, UK

Toby Perring
ISIS Pulsed Neutron Facility
Rutherford Appleton Laboratory, UK

The moving finger …

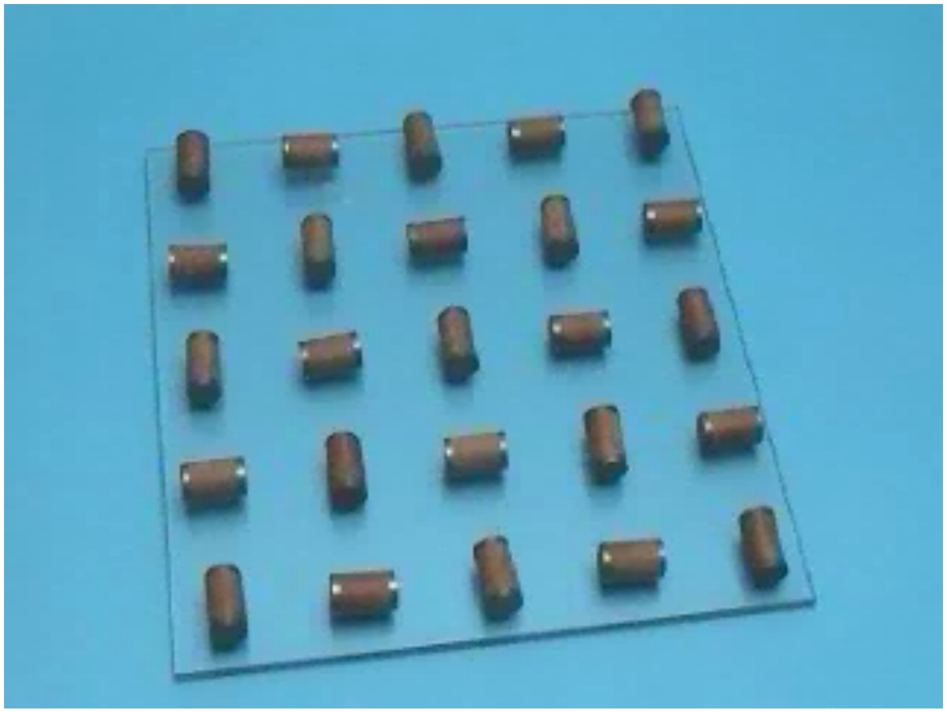

Courtesy of ISIS Pulsed Neutron and Muon Source, Rutherford Appleton Laboratory

Acknowledgements: W. Press, A. Hueller, M. Prager, C. Carlile

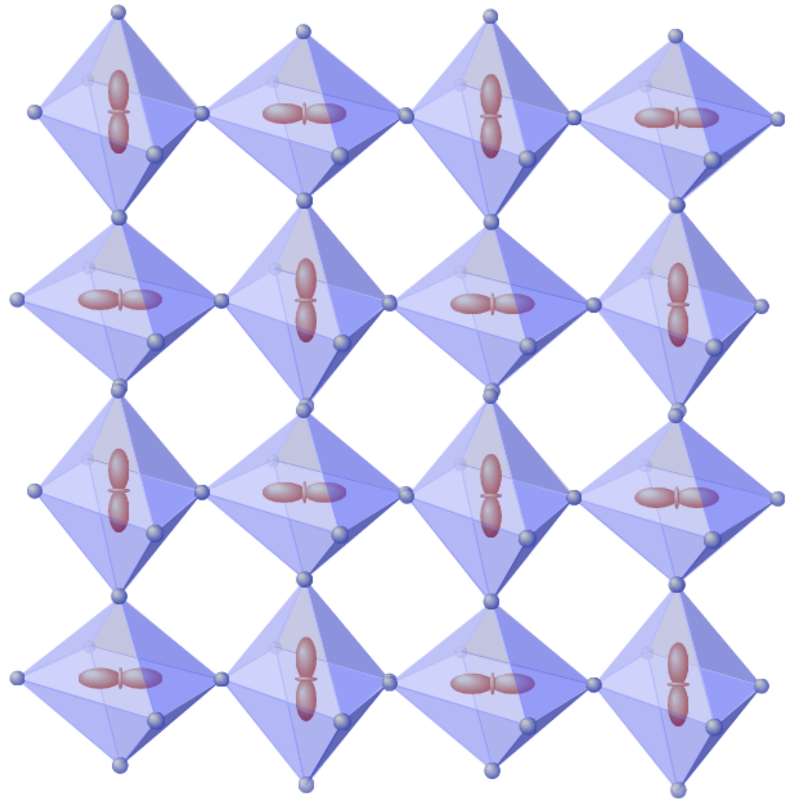

$LaMnO_3$

Direct Geometry vs Indirect Geometry

Direct geometry

- Fixed incident energy
- All final energies

→ $-\infty < \hbar\omega < E_i$

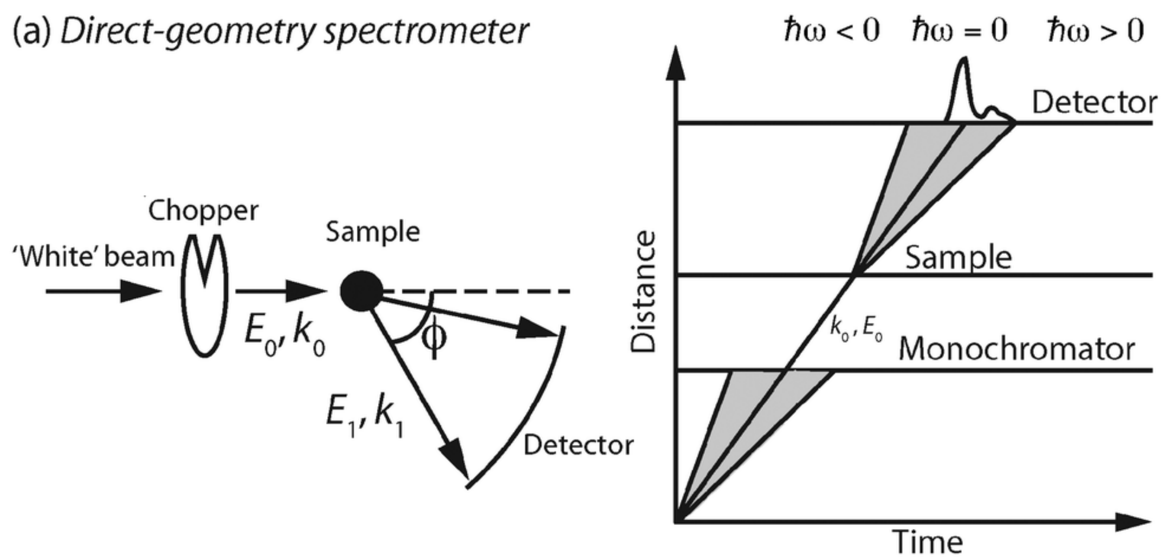

Indirect geometry

- All incident energies E_i
- Fixed final energy E_f

→ $-E_f < \hbar\omega < \infty$

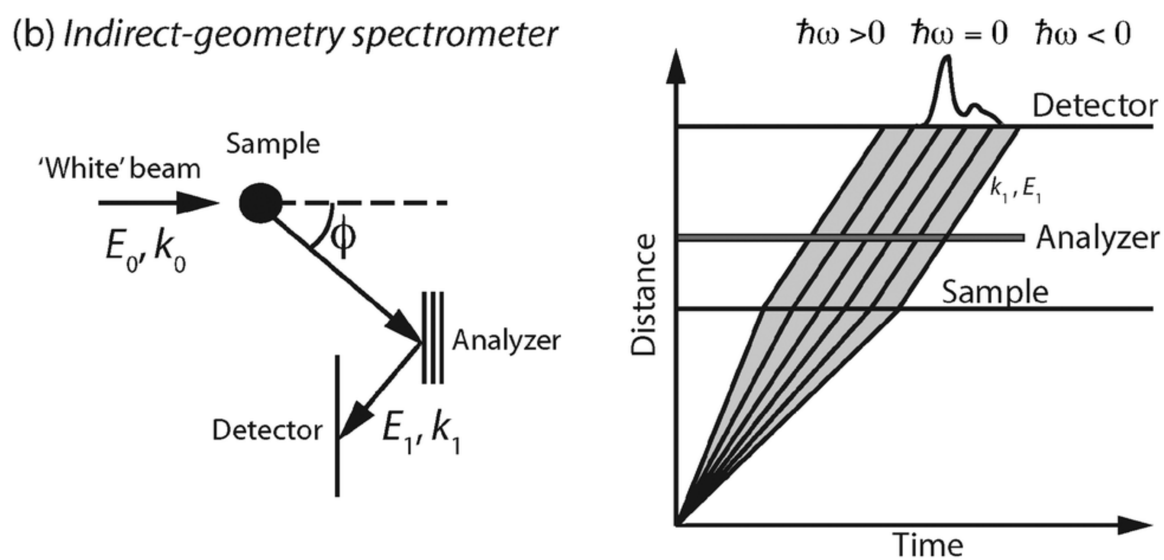

Direct Geometry Chopper Spectrometer

- e.g., IN4 (ILL), MARI, MERLIN, MAPS (ISIS), ARCS, SEQUOIA (SNS)

ARCS - A wide Angular Range Chopper Spectrometer

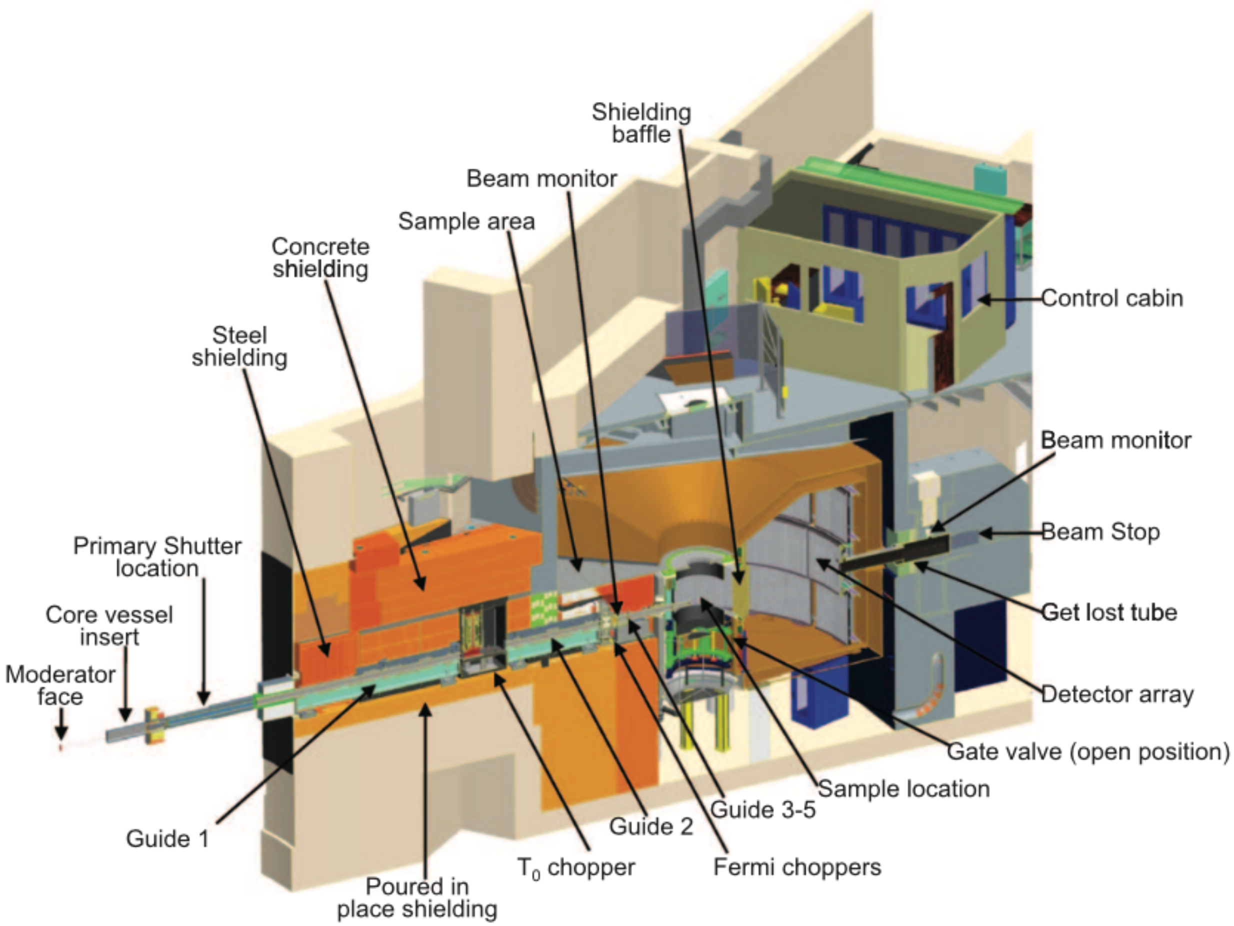

- Primary Flight Path: 11.6m
- Secondary Flight Path: 3m
- Angular range :
  - -30°-150° (Horizontal)
  - -30°-30° (Vertical)
- Incident energy : 10meV-1.5eV
- Energy resolution : 2-5%Ei
- Detectors : Position sensitive
- Supermirror guide
- Oscillating collimator
- Provision for polarization analysis

D. L. Abernathy *et al.*, Review of Scientific Instruments. **83,** 015114 (2012).

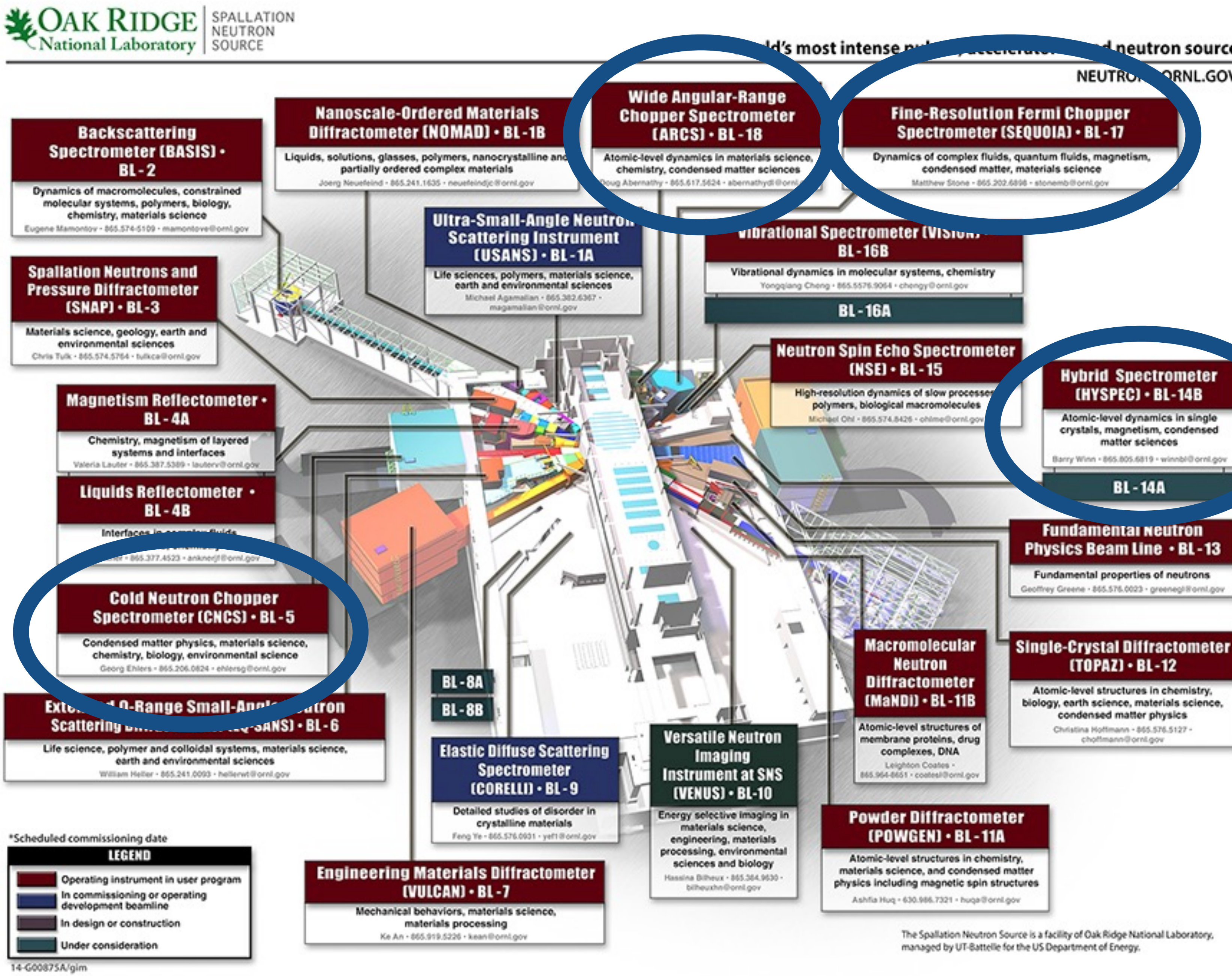
OAK RIDGE National Laboratory
SPALLATION NEUTRON SOURCE
neutron source
NEUTRON ORNL.GOV
Backscattering Spectrometer (BASIS) • BL-2
Dynamics of macromolecules, constrained molecular systems, polymers, biology, chemistry, materials science
Nanoscale-Ordered Materials Diffractometer (NOMAD) • BL-1B
Liquids, solutions, glasses, polymers, nanocrystalline and partially ordered complex materials
Wide Angular-Range Chopper Spectrometer (ARCS) • BL-18
Atomic-level dynamics in materials science, chemistry, condensed matter sciences
Fine-Resolution Fermi Chopper Spectrometer (SEQUOIA) • BL-17
Dynamics of complex fluids, quantum fluids, magnetism, condensed matter, materials science
Ultra-Small-Angle Neutron Scattering Instrument (USANS) • BL-1A
Life sciences, polymers, materials science, earth and environmental sciences
BL-16B
Vibrational dynamics in molecular systems, chemistry
BL-16A
Spallation Neutrons and Pressure Diffractometer (SNAP) • BL-3
Materials science, geology, earth and environmental sciences
Neutron Spin Echo Spectrometer (NSE) • BL-15
High-resolution dynamics of slow processes, polymers, biological macromolecules
Hybrid Spectrometer (HYSPEC) • BL-14B
Atomic-level dynamics in single crystals, magnetism, condensed matter sciences
BL-14A
Magnetism Reflectometer • BL-4A
Chemistry, magnetism of layered systems and interfaces
Liquids Reflectometer • BL-4B
Physics Beam Line • BL-13
Fundamental properties of neutrons
Cold Neutron Chopper Spectrometer (CNCS) • BL-5
Condensed matter physics, materials science, chemistry, biology, environmental science
Macromolecular Neutron Diffractometer (MaNDi) • BL-11B
Atomic-level structures of membrane proteins, drug complexes, DNA
Single-Crystal Diffractometer (TOPAZ) • BL-12
Atomic-level structures in chemistry, biology, earth science, materials science, condensed matter physics
Life science, polymer and colloidal systems, materials science, earth and environmental sciences
BL-8A
BL-8B
Elastic Diffuse Scattering Spectrometer (CORELLI) • BL-9
Detailed studies of disorder in crystalline materials
Versatile Neutron Imaging Instrument at SNS (VENUS) • BL-10
Energy selective imaging in materials science, engineering, materials processing, environmental sciences and biology
Powder Diffractometer (POWGEN) • BL-11A
Atomic-level structures in chemistry, materials science, and condensed matter physics including magnetic spin structures
*Scheduled commissioning date
LEGEND
Operating instrument in user program
In commissioning or operating development beamline
In design or construction
Under consideration
Engineering Materials Diffractometer (VULCAN) • BL-7
Mechanical behaviors, materials science, materials processing
The Spallation Neutron Source is a facility of Oak Ridge National Laboratory, managed by UT-Battelle for the US Department of Energy.
14-G00875A/gim

ARCS T_0 Chopper

- The T_0 chopper to suppress neutrons from the prompt pulse
  - 175kg of Inconel 718 can spin up to 180 Hz

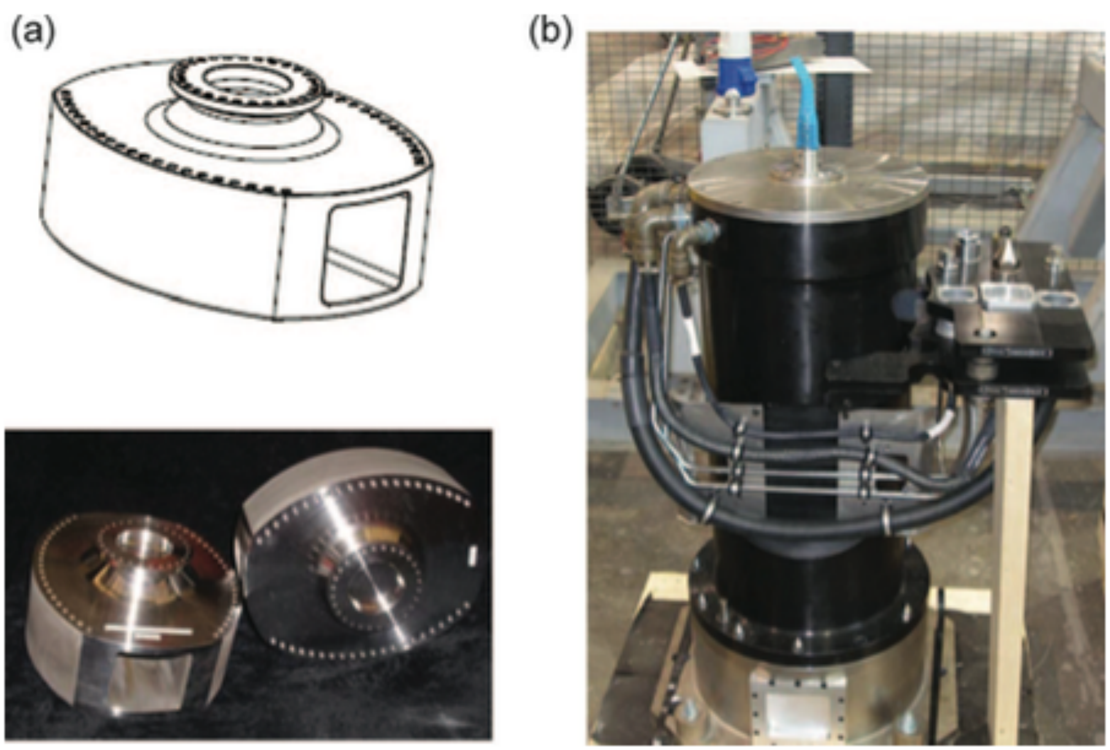

ARCS Fermi Choppers

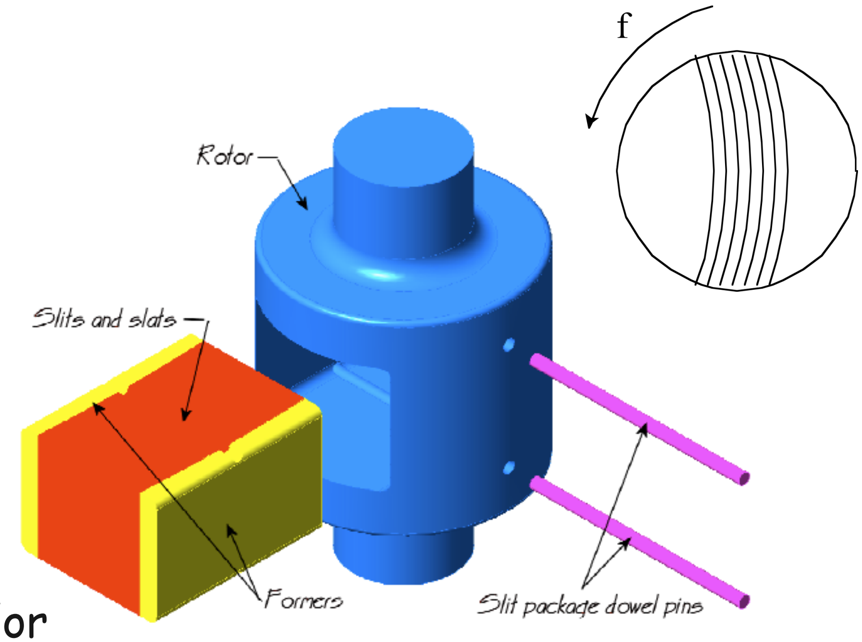

- Fermi choppers monochromate the incident beam
  - Two choppers at a time are mounted on a sliding transition stage
  - Four different slit packages are optimized for different energy bands

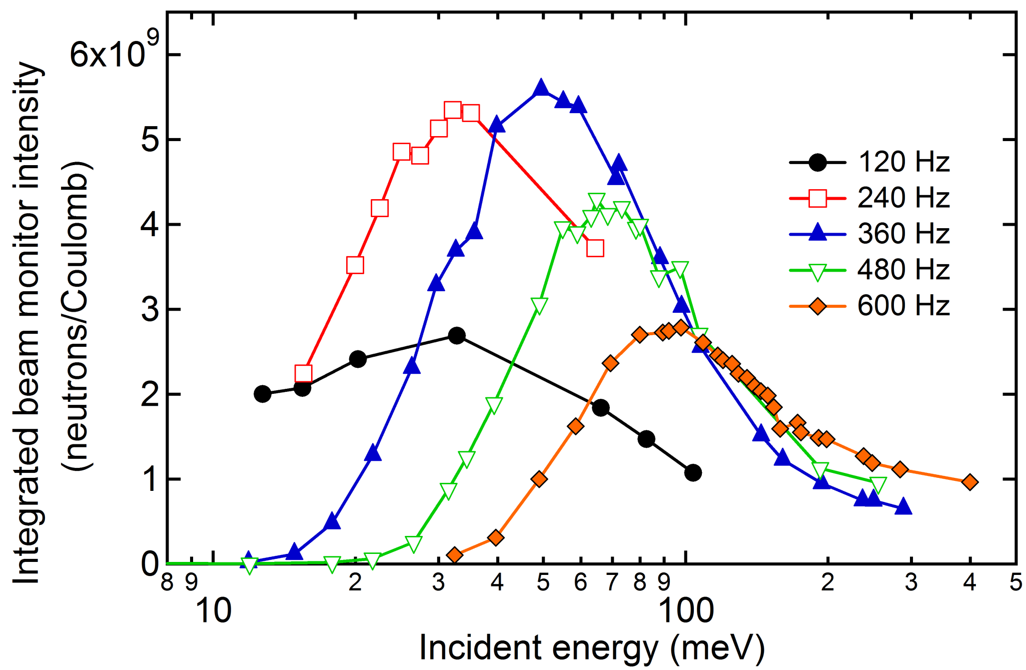

ARCS Detector Tank

- ARCS has 115 detector modules containing 8 ^{3}He linear PSDs of 128 pixels
  - Total = 117,760 pixels
- The secondary flight path is evacuated
  - L2 = 3 to 3.5 m
  - A gate valve isolates the sample area
  - A radial collimator reduces background

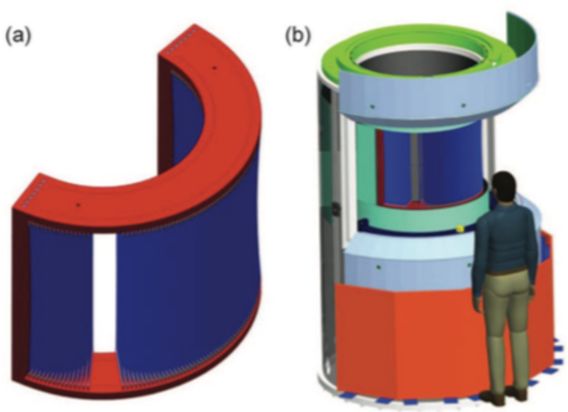

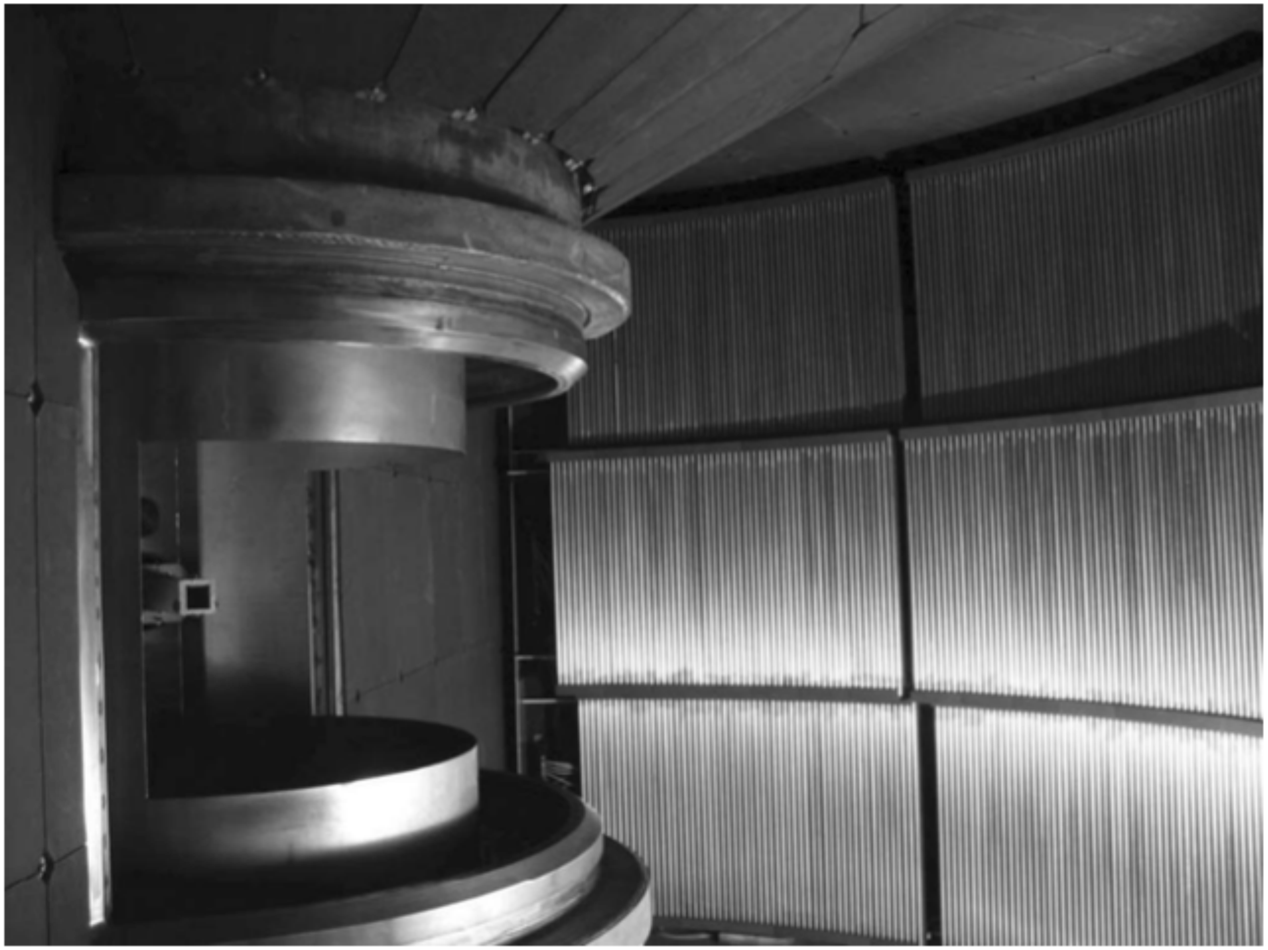

cf MERLIN PSDs

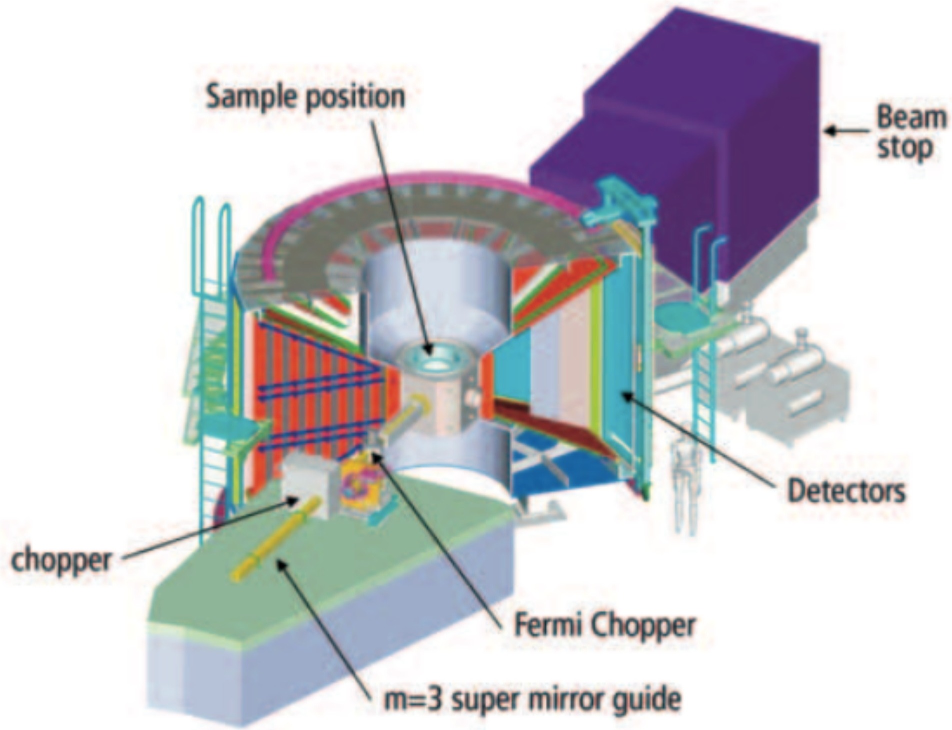

LET

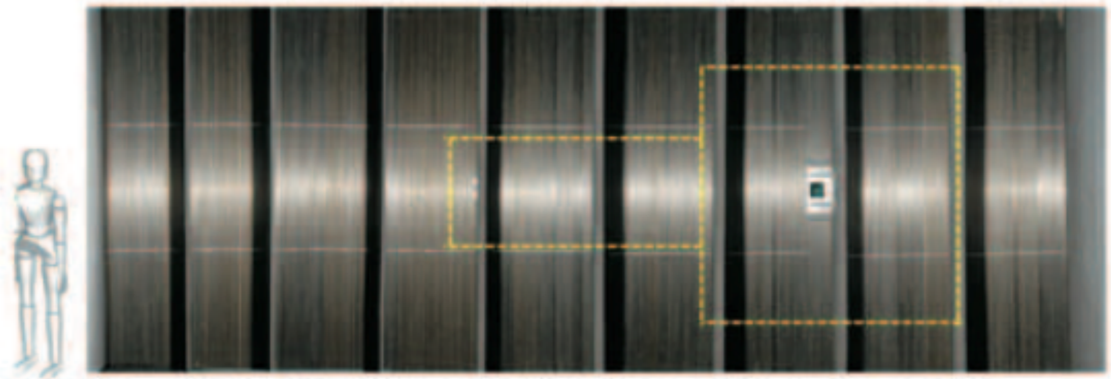

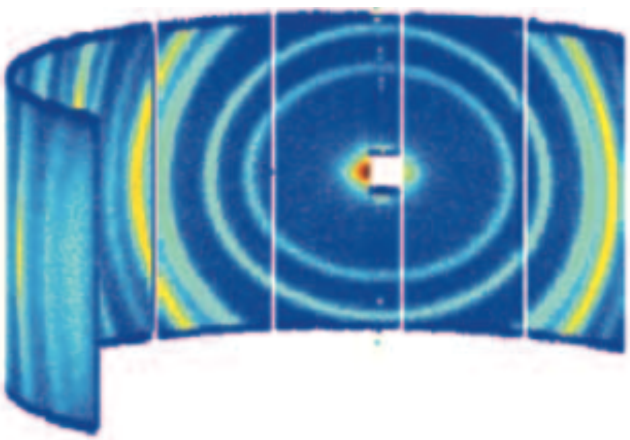

Chopper Resolution

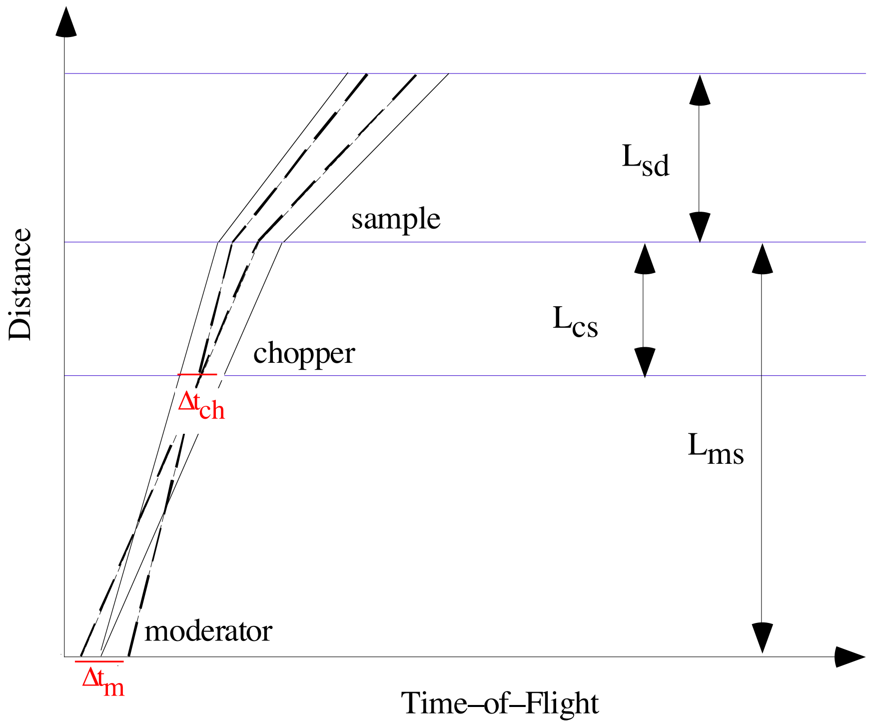

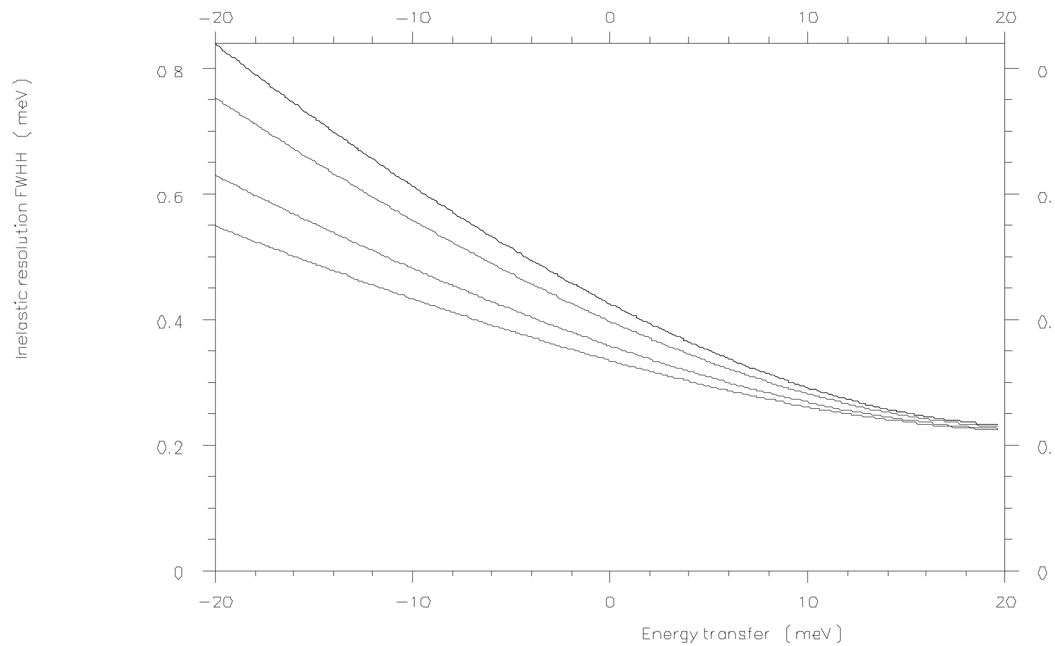

$$\frac{\Delta\varepsilon}{E_i} = \left[\left\{2\frac{\Delta t_{ch}}{t_{ch}}\left(1+\frac{L_{ms}}{L_{sd}}\left[1-\frac{\varepsilon}{E_i}\right]^{\frac{3}{2}}\right)\right\}^2\right]^{\frac{1}{2}} + \left[\left\{2\frac{\Delta t_m}{t_{ch}}\left(1+\frac{L_{cs}}{L_{sd}}\left[1-\frac{\varepsilon}{E_i}\right]^{\frac{3}{2}}\right)\right\}^2\right]^{\frac{1}{2}}$$

Other SNS Direct Geometry Spectrometers

Parameter	CNCS	HYSPEC	SEQUOIA	ARCS
Moderator	c-lH	c-lH	apd-H_2O	apd-H_2O
Source-beam monitor distance (m)	34.85	37.38	18.23	11.831
Source-downstream monitor distance (m)	n/a	n/a	29.003	18.5
Source-sample distance (m)	36.26	40.77	20.01	13.6
Height of beam at sample (cm)	5	3.5	5	5
Width of beam at sample (cm)	1.5	3.5	5	5
Detector tube diameter (cm)	2.54	2.54	2.54	2.54
Detector tube length (m)	2	1.2	1.2	1
Mean sample-detector distance (m)	3.54	4.54	5.53	3.21
Minimum equatorial scattering angle (deg.)	3.8	0[a]	2.0	2.4
Maximum equatorial scattering angle (deg.)	135	135	59.3	136.0
Maximum out of plane scattering angle (deg.)	16	7.5	19.4	27
Solid angle detector coverage[b] (Sr.)	1.606	0.226	0.863	2.196
Incident energy range (meV)[c]	1–80	4–60	8–2000	15–1500
Range of energy resolution ($\%E_i$)[d]	1–5	3–5	1–3	3–5
Radial collimator	Yes	Yes	No	Yes
Entry into user program	2009	2013	2010	2008
Reference	19		20, 34	21

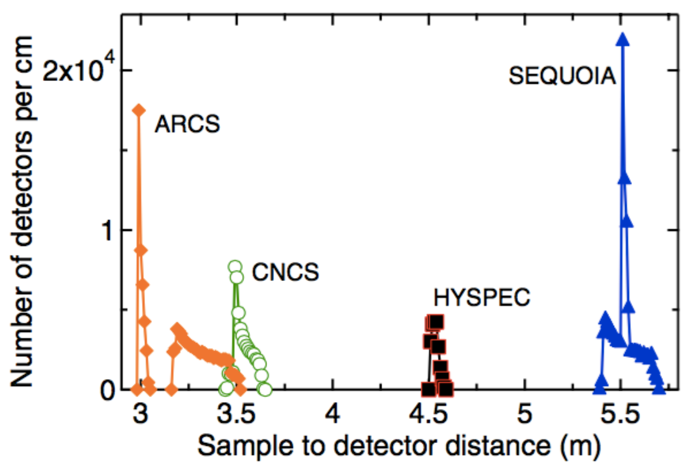

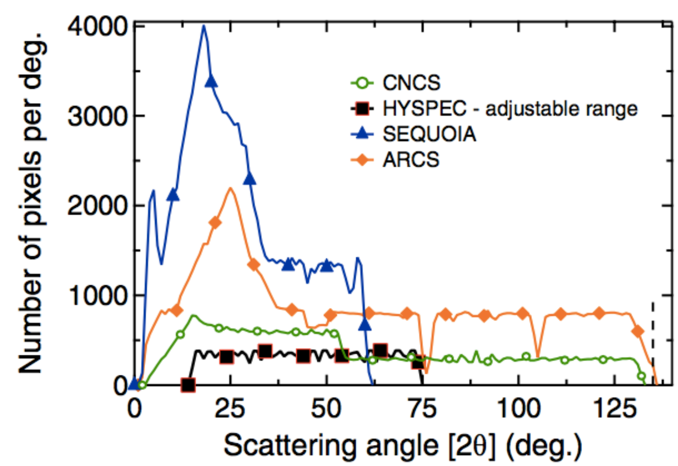

ARCS vs SEQUOIA

- ARCS and SEQUOIA are designed to be complementary
  - ARCS has a wide angular range with moderate resolution
  - SEQUOIA has a more limited angular range with high resolution
- This complementarity efficiently utilizes the limited space between SNS beamlines

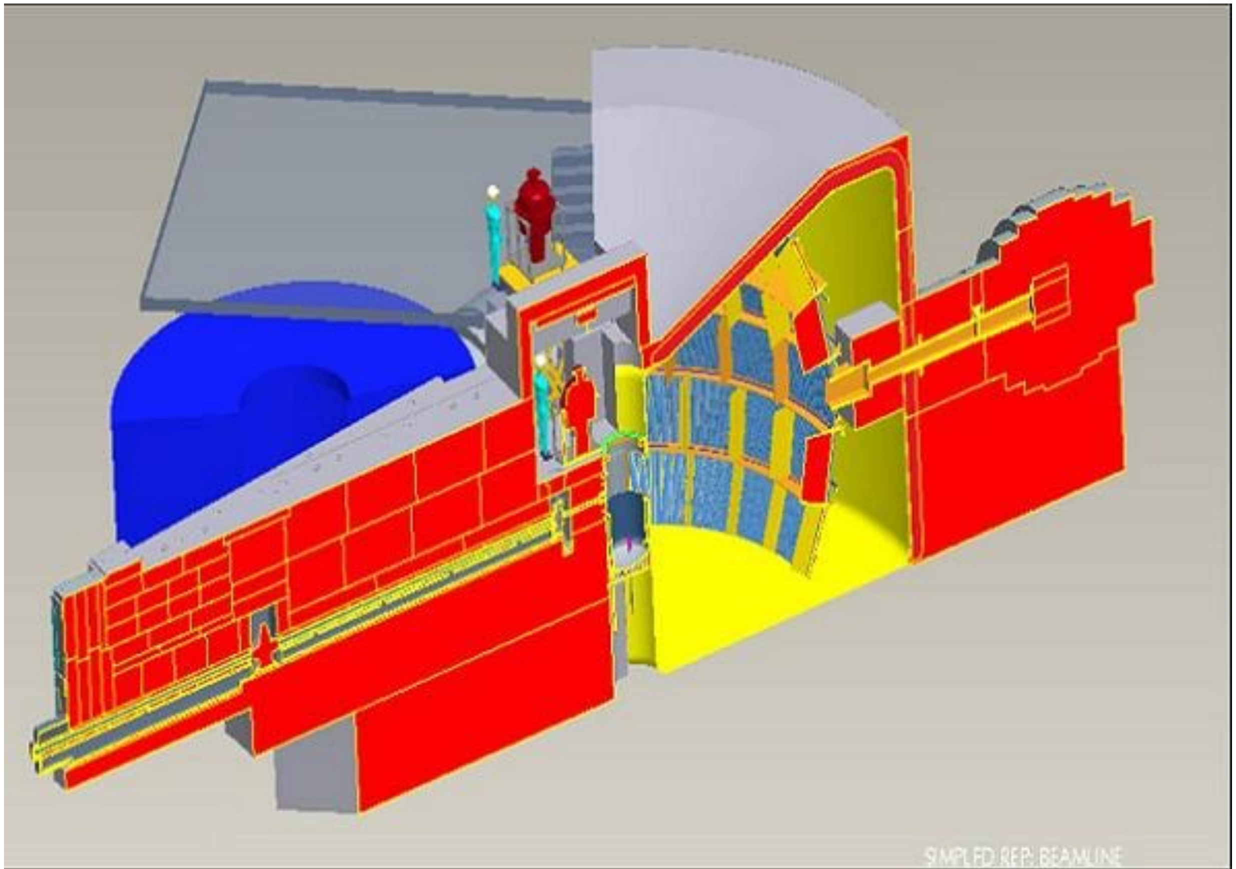

HYSPEC

- The hybrid spectrometer, HYSPEC, combines a Fermi chopper with a crystal monochromator.
- The monochromator focuses the beam from 150x40mm to 20x20mm.
- The detector (160 linear PSDs 1.2 m long), which covers 60°, can rotate about the sample axis.
- The design gives greater sample environment flexibility and allows full polarization analysis (with Heusler monochromator).

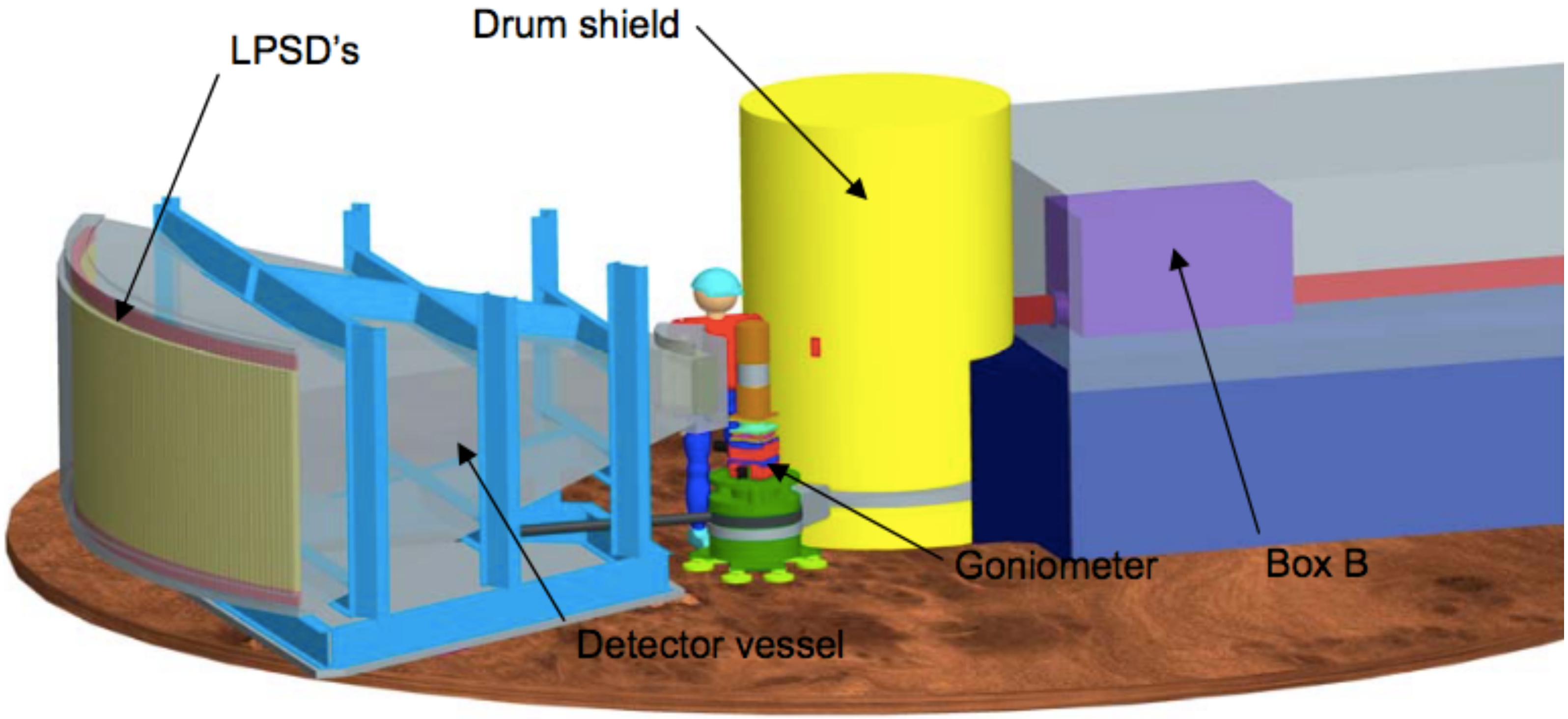

Cold Direct Geometry Spectrometers

- e.g., IN5, IN6 (ILL), LET (ISIS), CNCS (SNS)

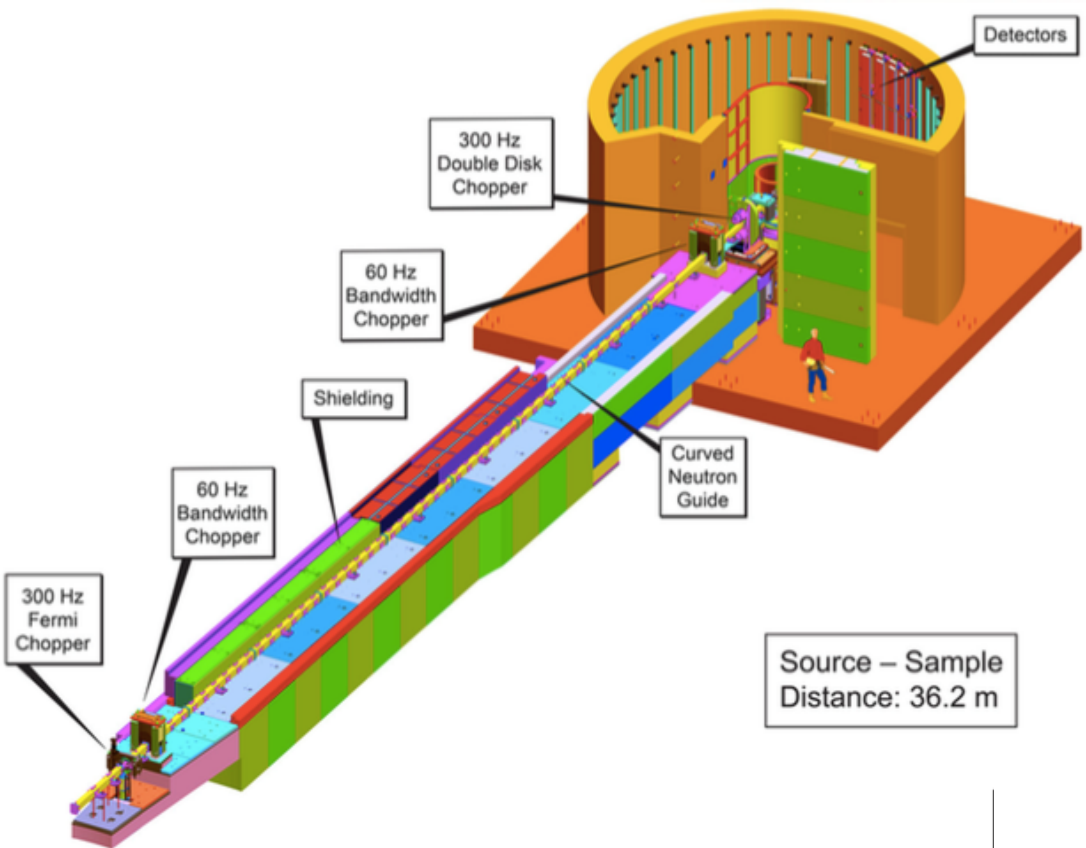

CNCS

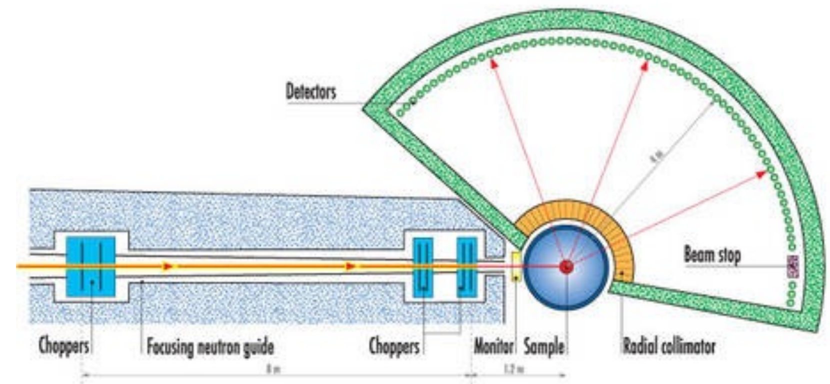

IN5

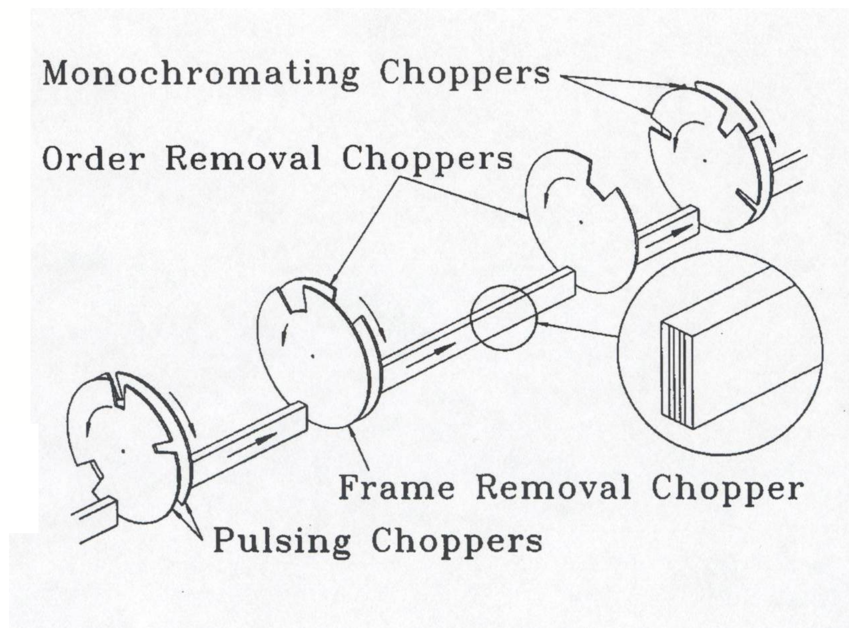

Rep-Rate Multiplication

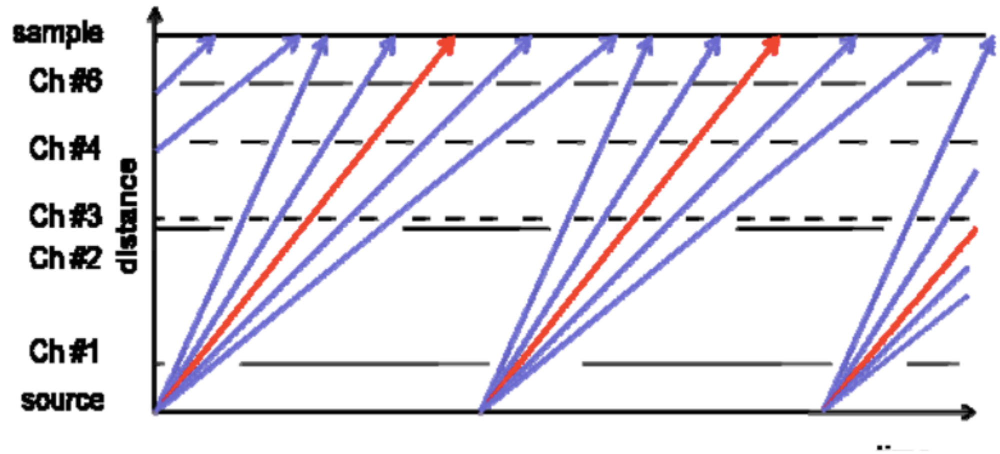

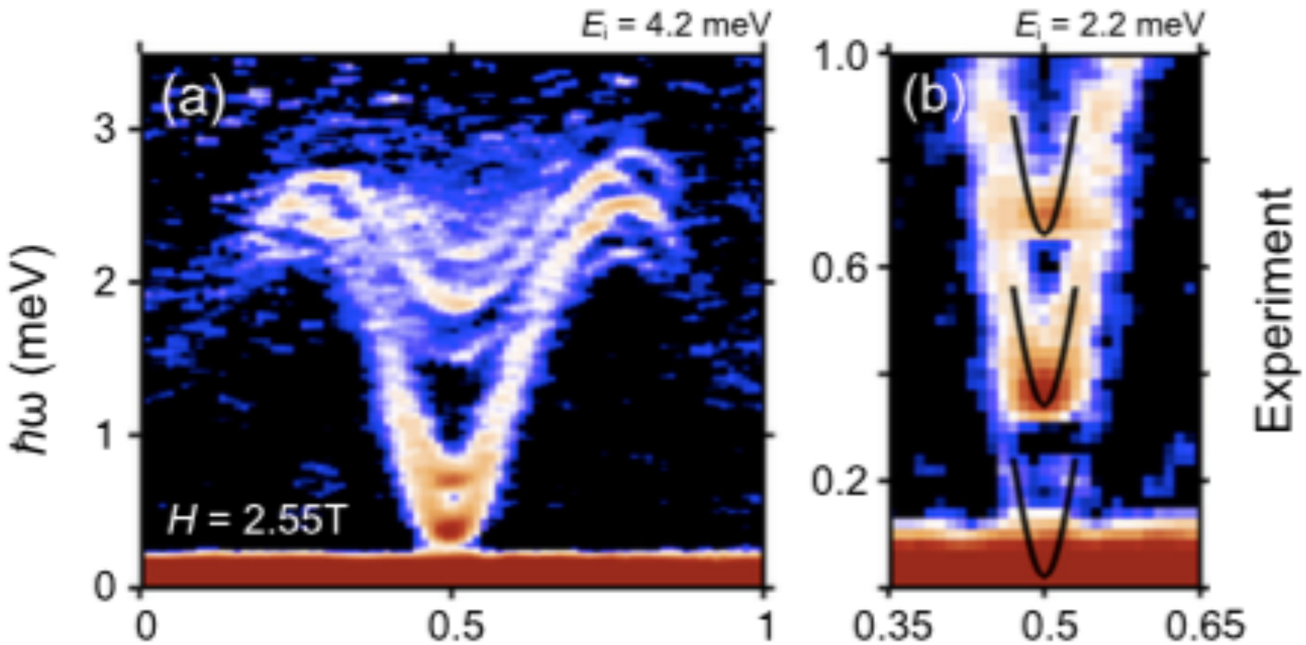

$(C_7H_{10}N)_2$ $CuBr_4$ (DIMPY)

D. Schmidiger, et al. Phys Rev Lett **111**, 107202 (2013).

Neutron Conversion Factors

$$E = \frac{\hbar^2 k^2}{2m} = \frac{h^2}{2m\lambda^2} = \frac{m}{2\tau^2}$$

where τ is the time of flight, or inverse velocity ($\tau = 1/v$).

- E (meV) = 81.80 λ^{-2} (Å^{-2})
- E (meV) = 2.072 k^2 (Å^{-2})
- E (meV) = 5.227 $\times$ 10^6 τ^{-2}($m^2/\mu sec^2$)

- T (K) = 11.604 E (meV)

Inelastic Scattering Processes

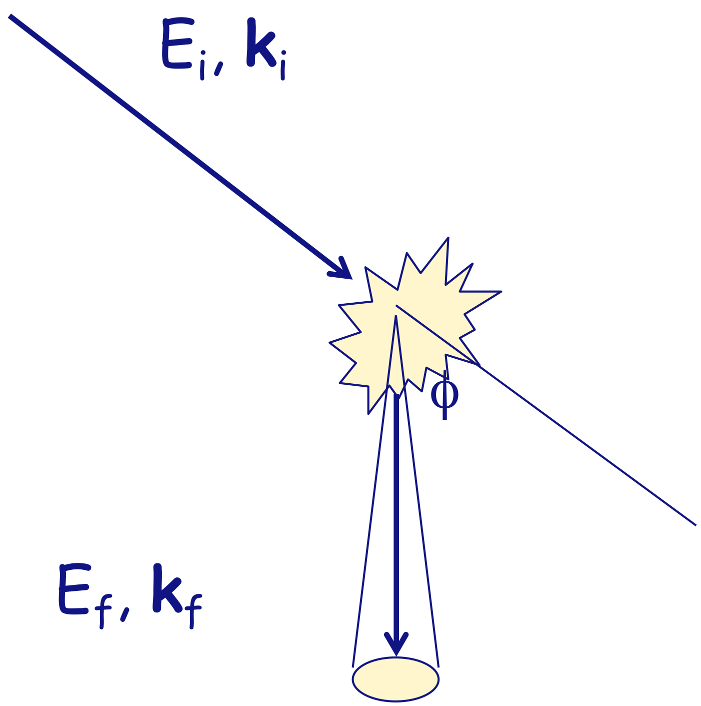

$$\frac{d^2\sigma}{d\Omega\, dE_f} = \frac{k_f}{k_i} S(Q, \varepsilon)$$

Conservation of energy

$$\varepsilon = E_i - E_f$$

Conservation of "momentum"

$$\vec{Q} = \vec{k}_i - \vec{k}_f$$

Reciprocal Space Construction

The scattering triangle

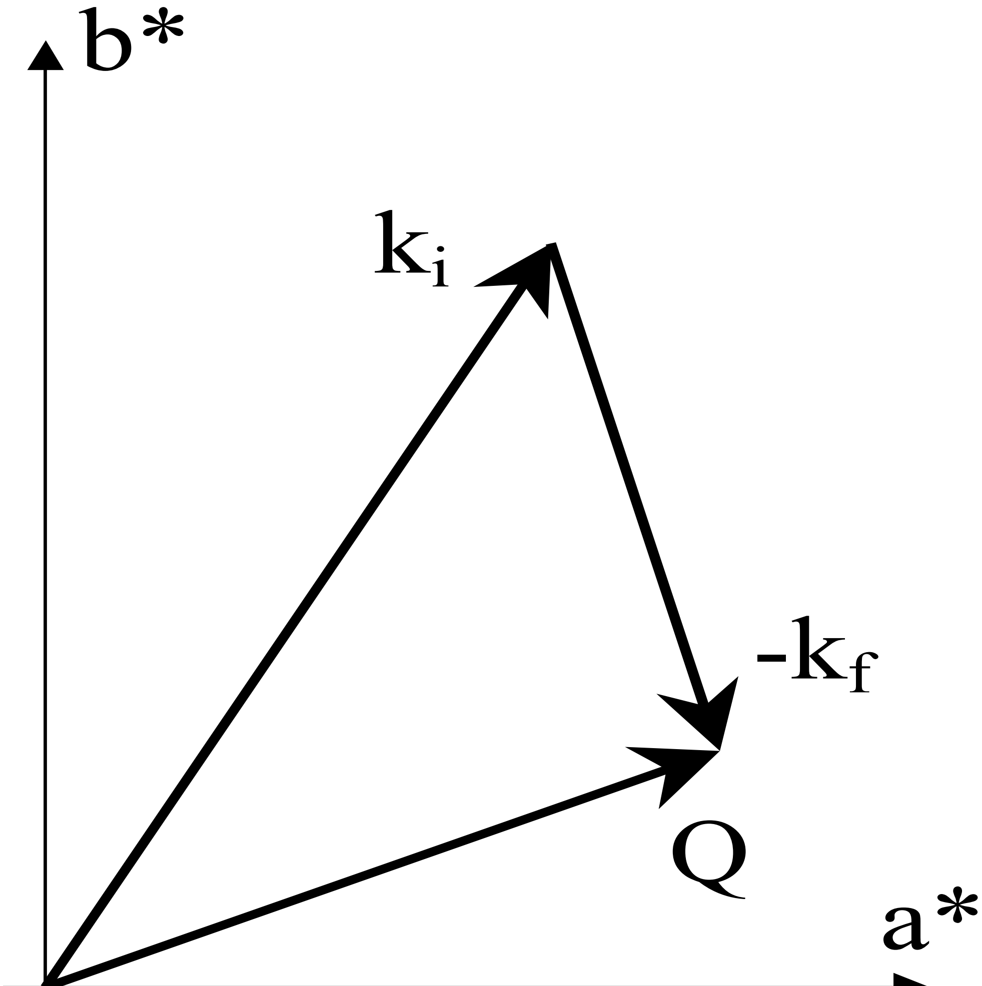

$$\vec{Q} = \vec{k}_i - \vec{k}_f$$

$$\varepsilon = E_i - E_f$$

$$= \frac{\hbar^2}{2m}(k_i^2 - k_f^2)$$

Kinematic Range

From the scattering triangle, we can see that

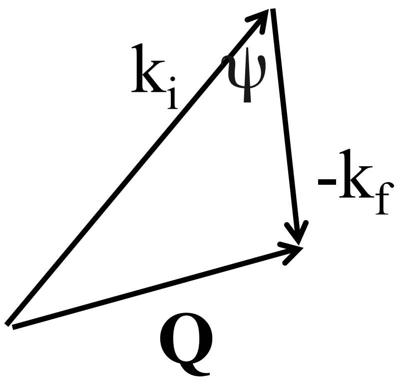

$$Q^2 = k_i^2 + k_f^2 - 2k_i k_f \cos(\psi)$$

from which it follows that

$$\frac{\hbar^2}{2m} Q^2 = E_i + E_f - 2\sqrt{E_i E_f} \cos(\psi)$$

and so putting $E_f = E_i - \varepsilon$

we get $$\frac{\hbar^2}{2m} Q^2 = 2E_i - \varepsilon - 2\sqrt{E_i (E_i - \varepsilon)} \cos(\psi)$$

This equation gives us the locus of (Q, ε) for a given scattering angle ψ.

(N.B. we can write $\hbar^2/2m = 2.072$ for E(meV) and Q in $Å^{-1}$).

Locus of Neutrons in (Q,ε) Space

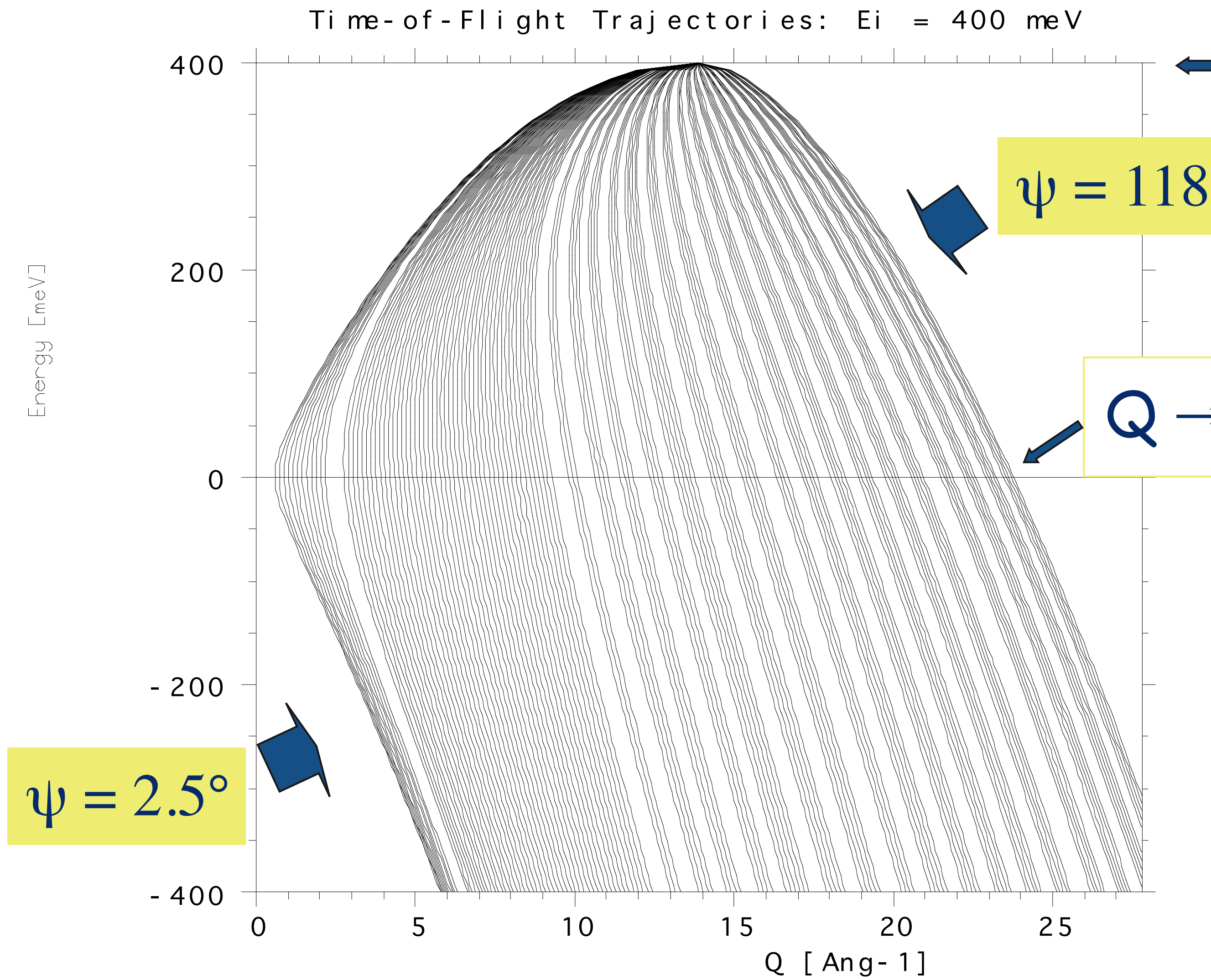

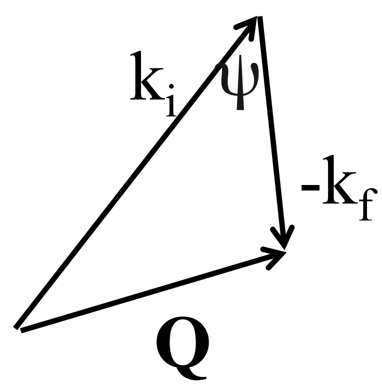

Harmonic Oscillator

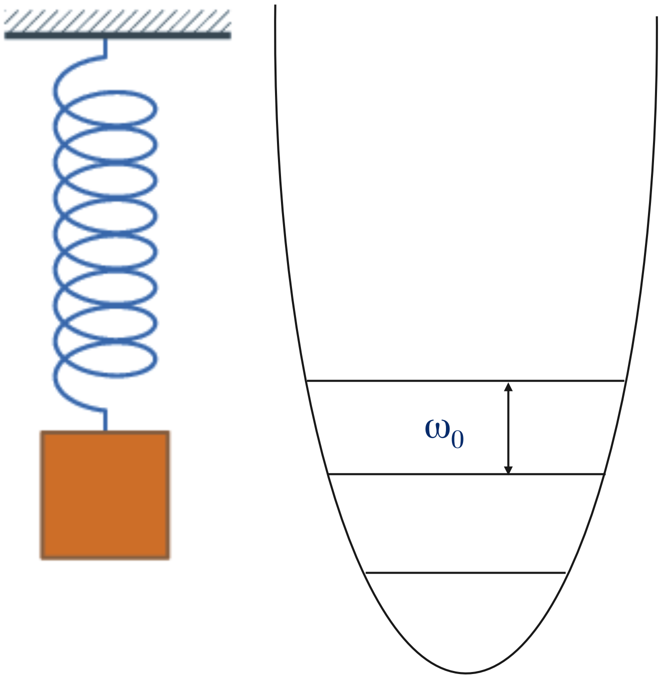

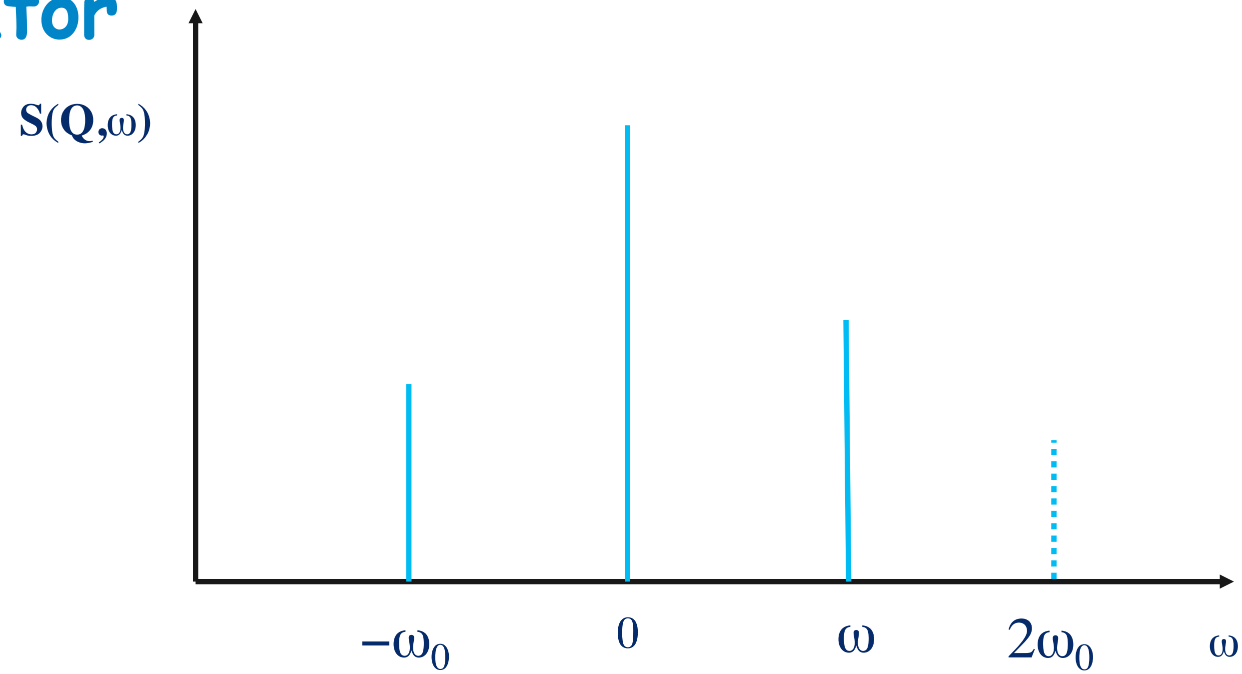

$$S(Q,\omega) = \exp\{-2\,W(Q)\}\left\{\delta(\hbar\omega) + \left(\frac{Q^2}{2m\omega_0}\right)\{n(\omega)+1\}\left[\delta(\omega-\omega_0) - \delta(\omega+\omega_0)\right]\right\}$$

$$\{n(\omega)+1\} = -n(-\omega) = [1-\exp(-\hbar\omega/k_B T)]^{-1}$$

$$V = \tfrac{1}{2}kx^2$$

In general, the neutron can excite n phonons at once

$$S(Q,\omega) = \exp\{-2\,W(Q)\}\sum_n \left(\frac{\hbar Q^2}{4mn\omega_0 \sinh\phi}\right)^n \exp(n\phi)\delta(\omega - n\omega_0)$$

where $\phi = (\hbar\omega_0/2k_B T)$ and $W(Q) = \hbar Q^2 \coth\phi / 4m\omega_0$

Scattering in ZrH_2

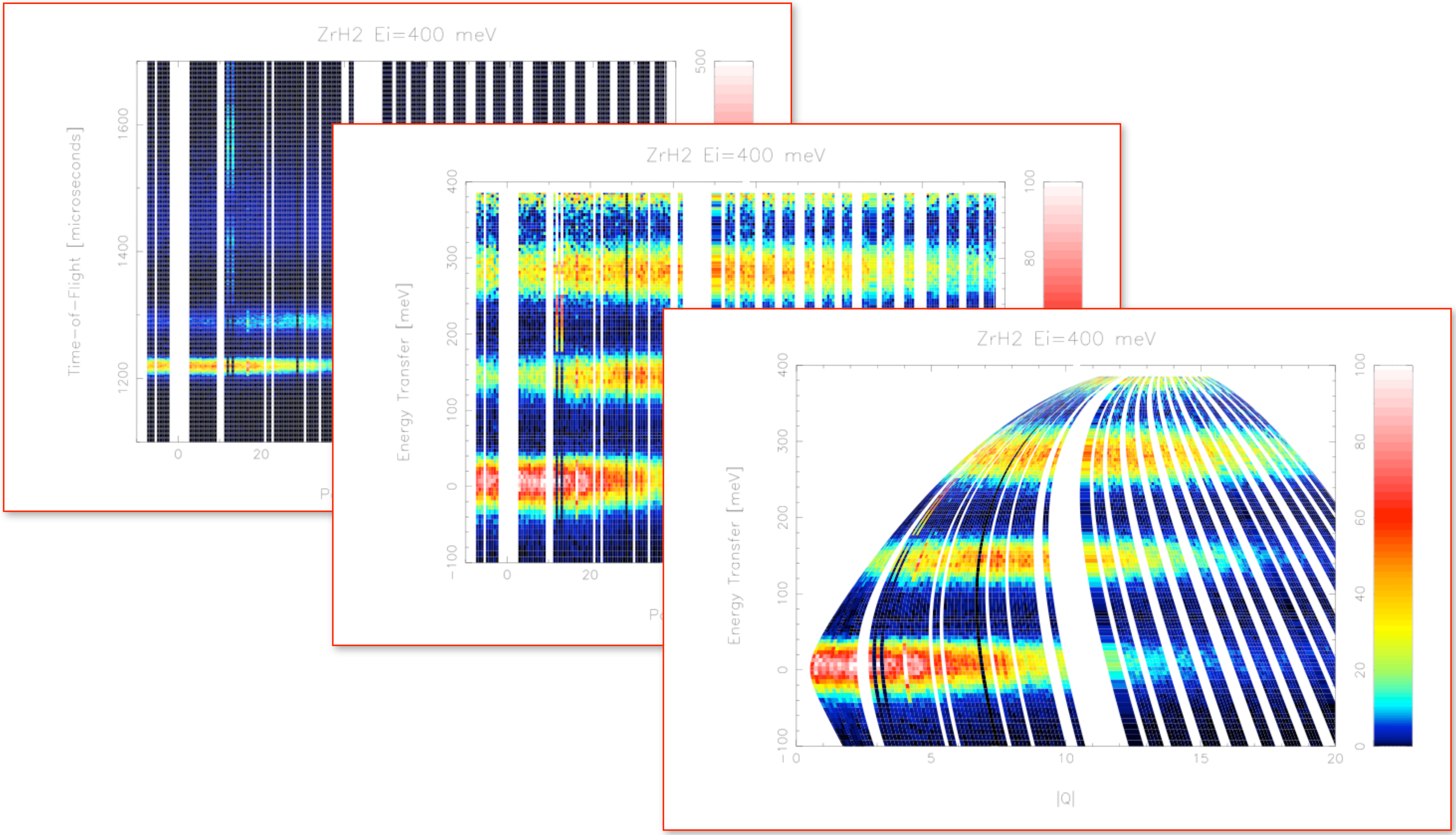

(Q,ε)-Dependence of ZrH_2

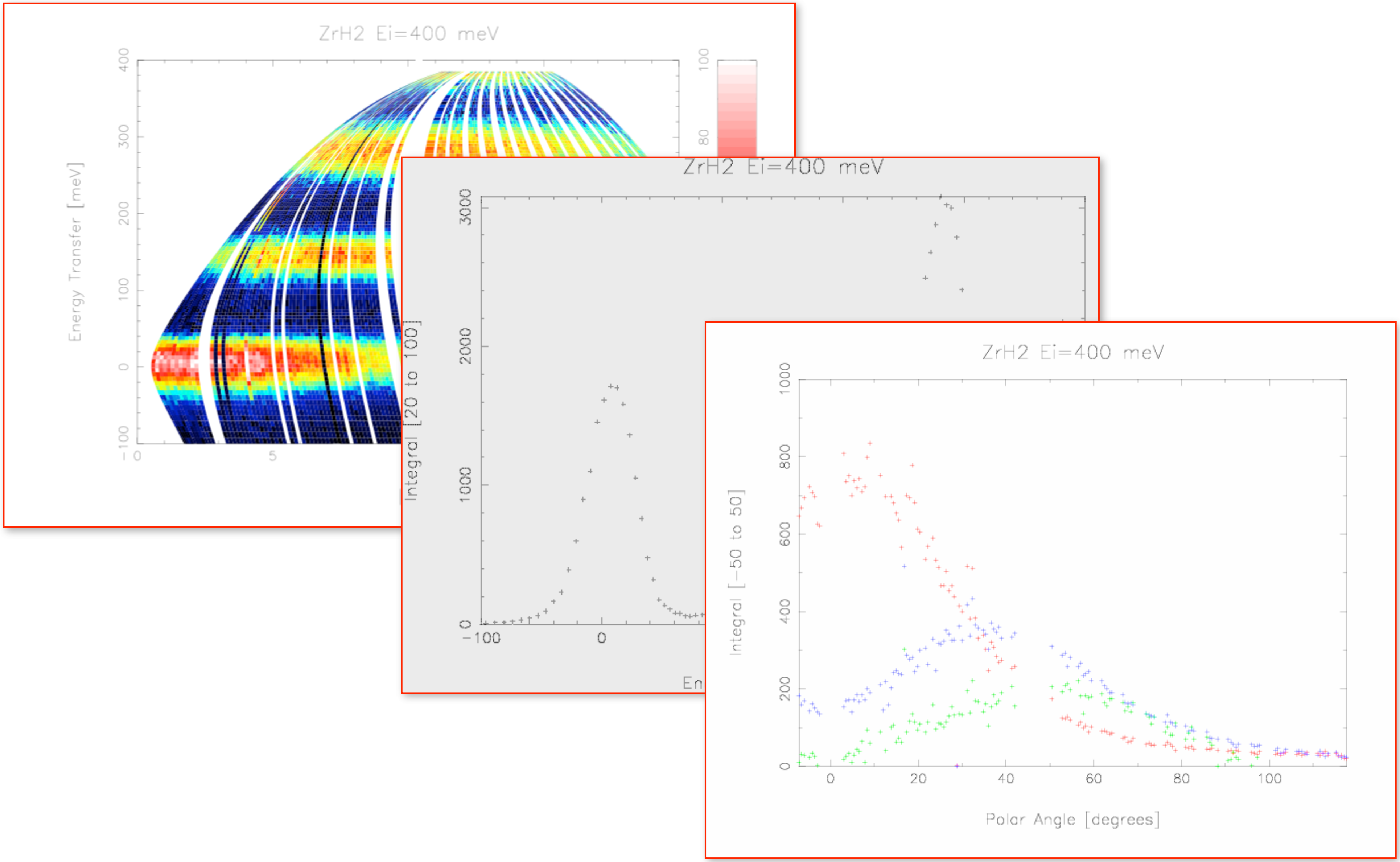

Quantum Oscillations in UN

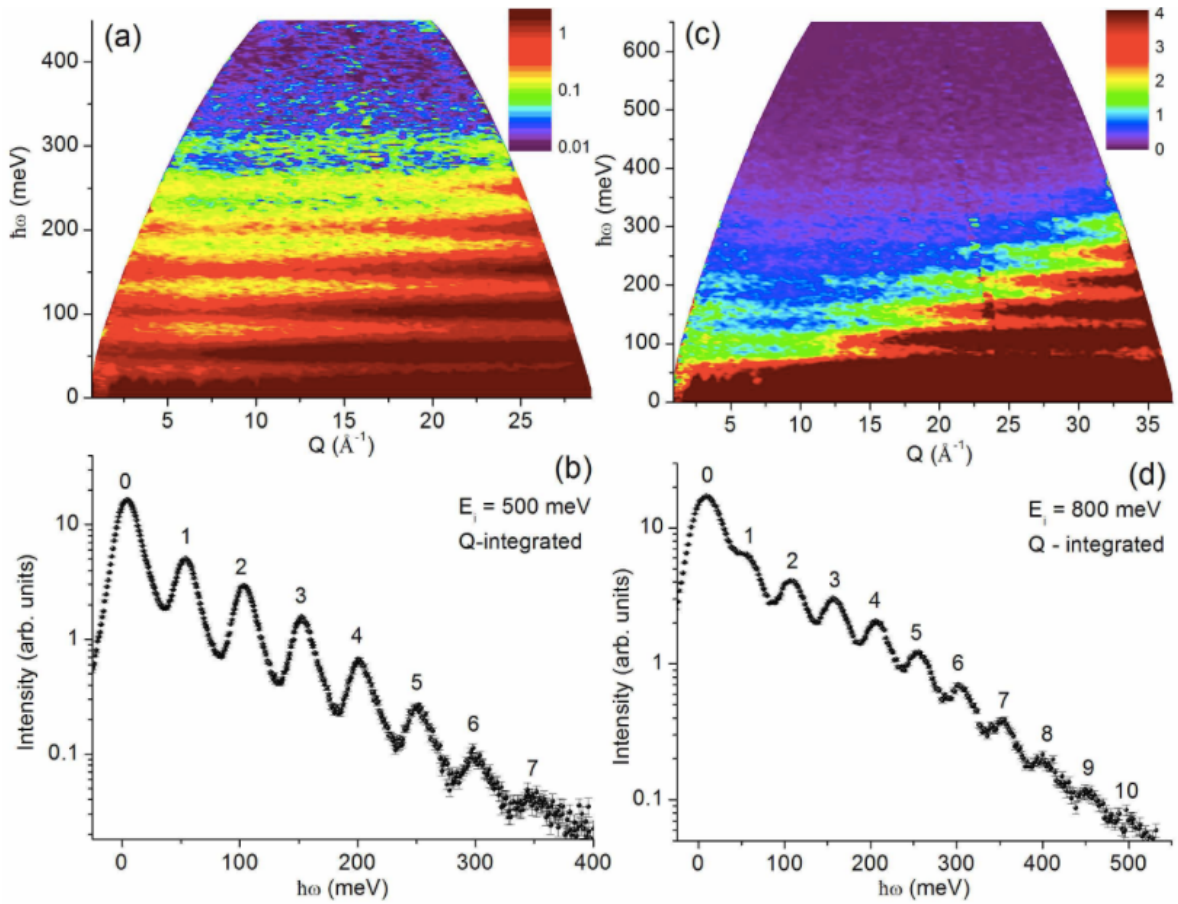

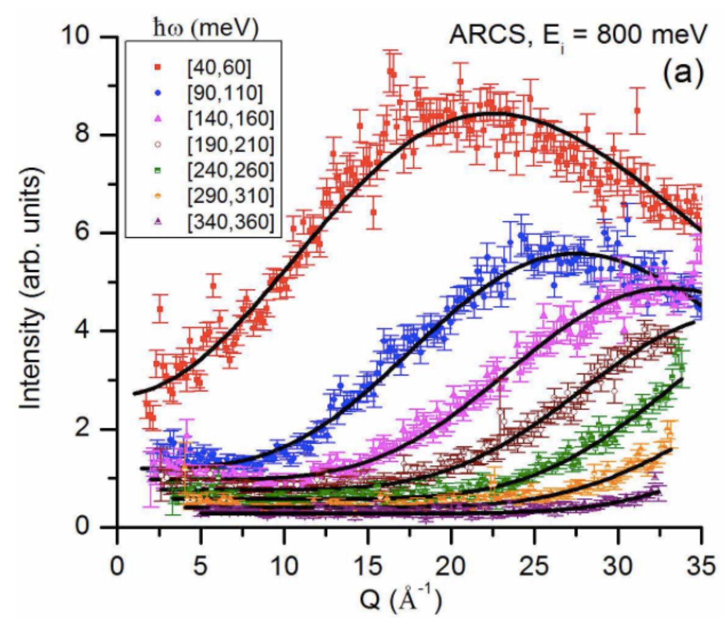

Aczel, A. A. et al. Nat Comm **3**, 1124 (2012).

Coherent Phonons

If the atoms are coupled, the spectrum of lattice vibrations is a function of energy and wave vector

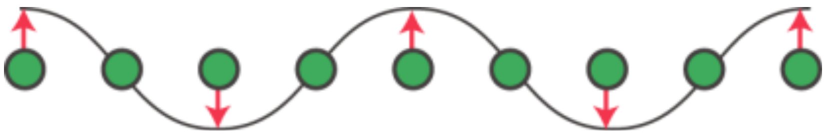

Transverse mode

Longitudinal mode

e.g. simple linear chain of atoms, mass m, coupled together by bonds ("springs") with stiffness S.

Elementary excitations are wave-like with $\lambda = 2\pi/q$;

Displacement of n th atom is: $x_n = A\exp[i(qna - \omega_q t)]$

where $\omega_q = \sqrt{\frac{4S}{m}}\sin(\frac{qa}{2})$

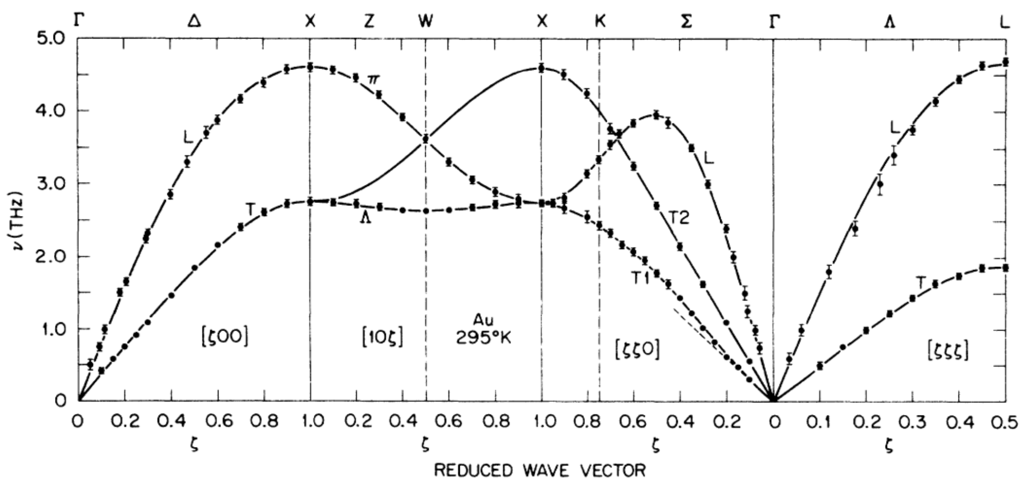

Lynn, *et al.*, *Phys. Rev. B* **8**, 3493 (1973).

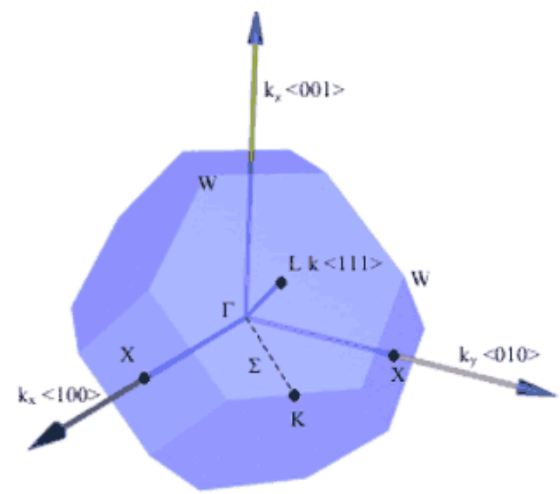

FCC Brillouin zone

Phonon Dispersion in MgB_2

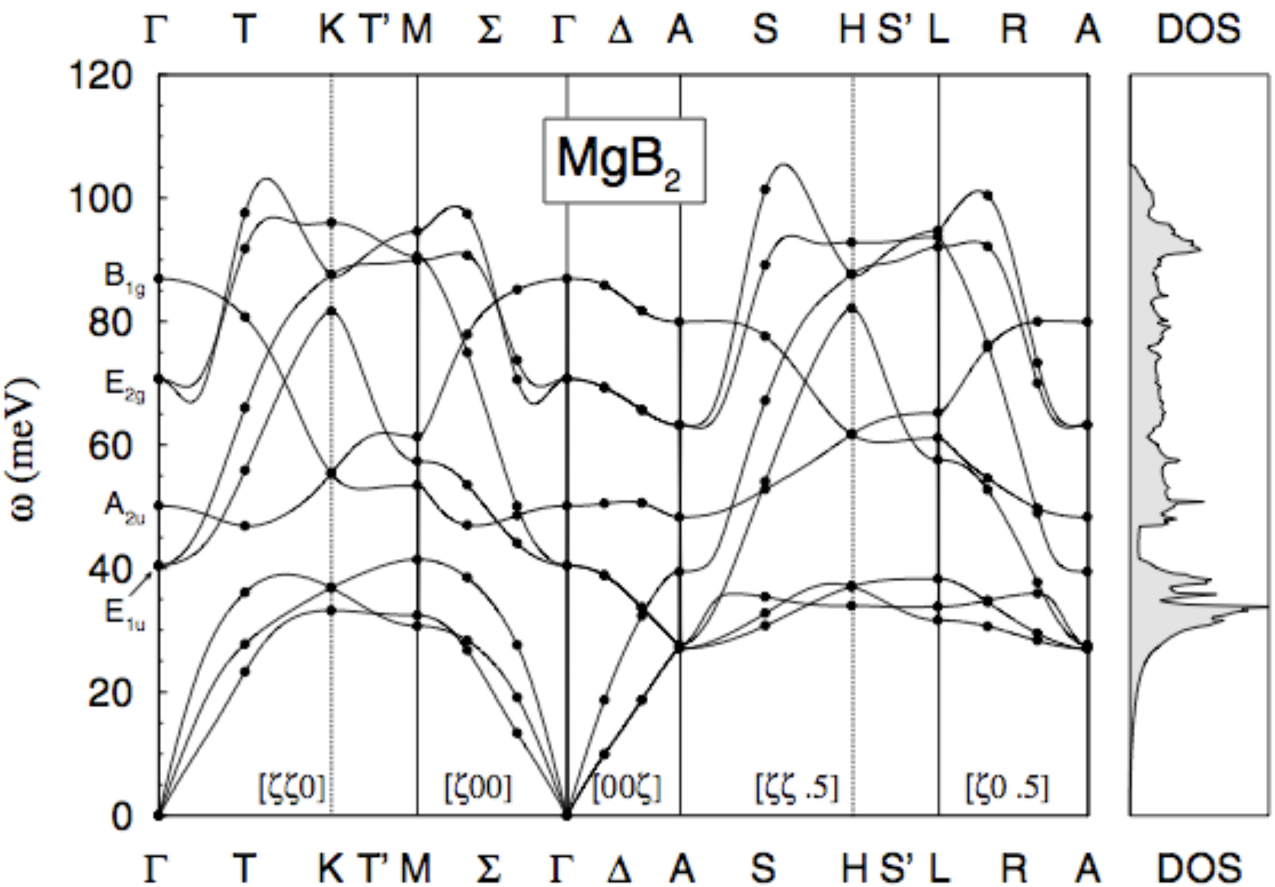

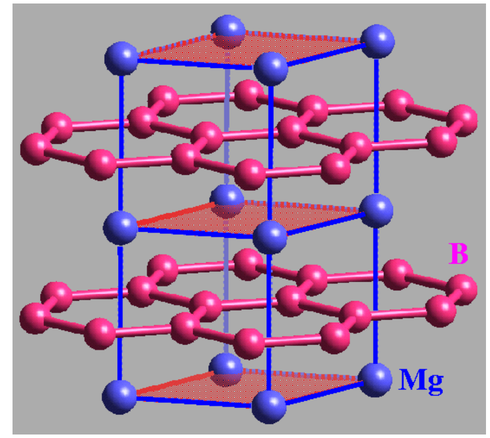

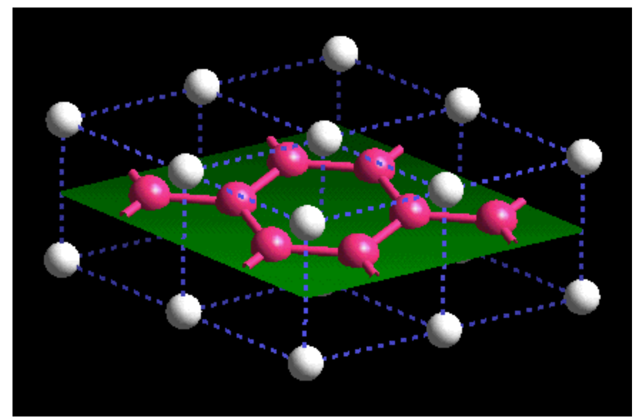

Phonon Density-of-States

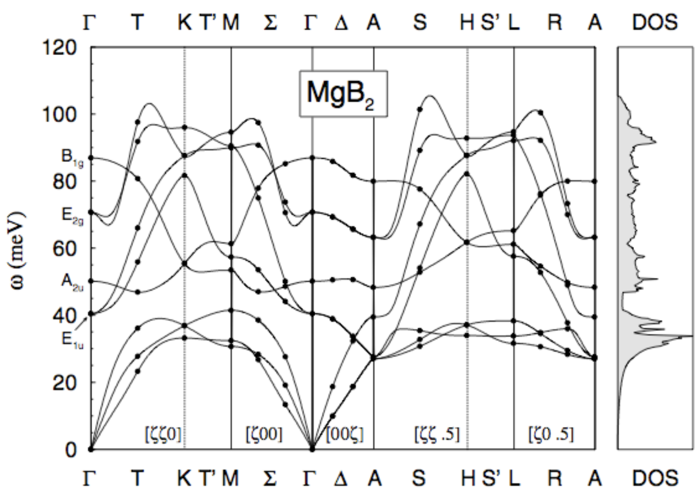

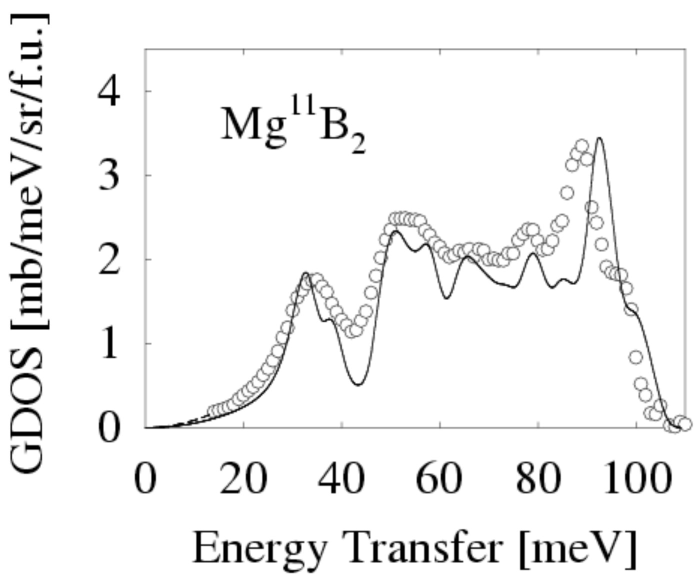

When single crystals are available, phonon dispersion relations (ω vs **q**) can be measured.

However, it is often useful to measure the phonon density-of-states
i.e. the sum over all phonon modes at each energy

In the incoherent approximation,

$$S(Q,\omega) = \exp\left[-2W(Q)\right]\left[\delta(\hbar\omega) + \frac{\hbar Q^2}{2M}\frac{Z(\omega)}{\omega}\left\{n(\omega)+1\right\} + \ldots\right]$$

Strictly speaking, we measure a sum of the partial densities-of-state of each element weighted by σ_i/M_i

Vanadium: A Perfect Incoherent Scatterer

$$S(Q,\omega) = \sum_i \sigma_i \frac{\hbar Q^2}{2M_i} \exp(-2W_i) \frac{Z_i(\omega)}{\omega} \left[n(\omega) + 1 \right]$$

$$W_i = \frac{1}{2} < (\mathbf{Q.u})^2 >= \frac{\hbar Q^2}{2M_i} \int \frac{Z_i(\omega)}{\omega} [2n_B(\omega) + 1] d\omega$$

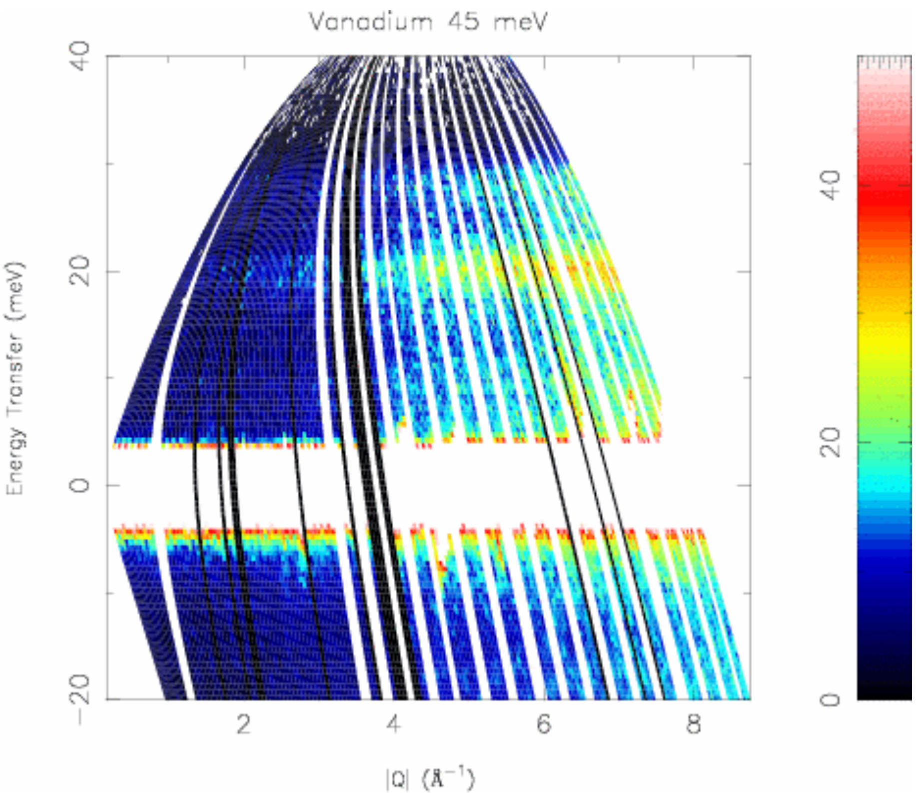

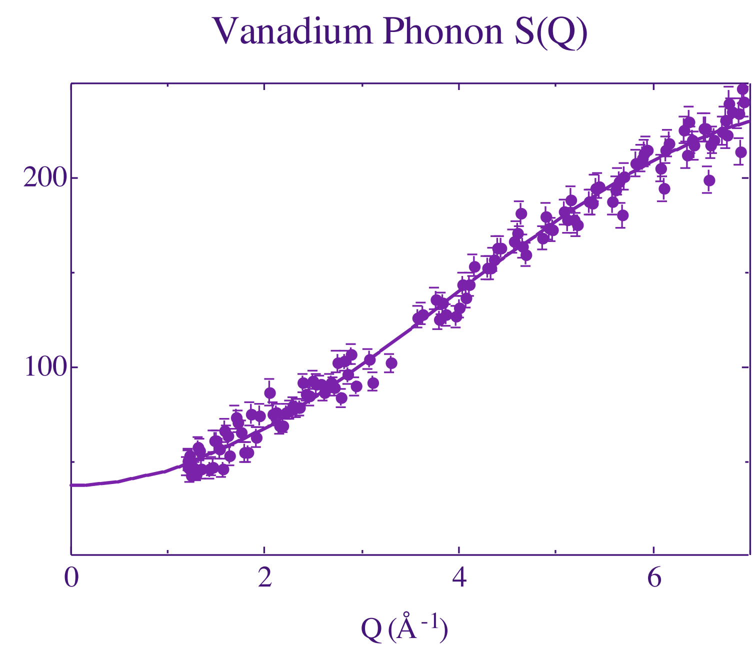

Multi-phonon Scattering

Vanadium Cross Section

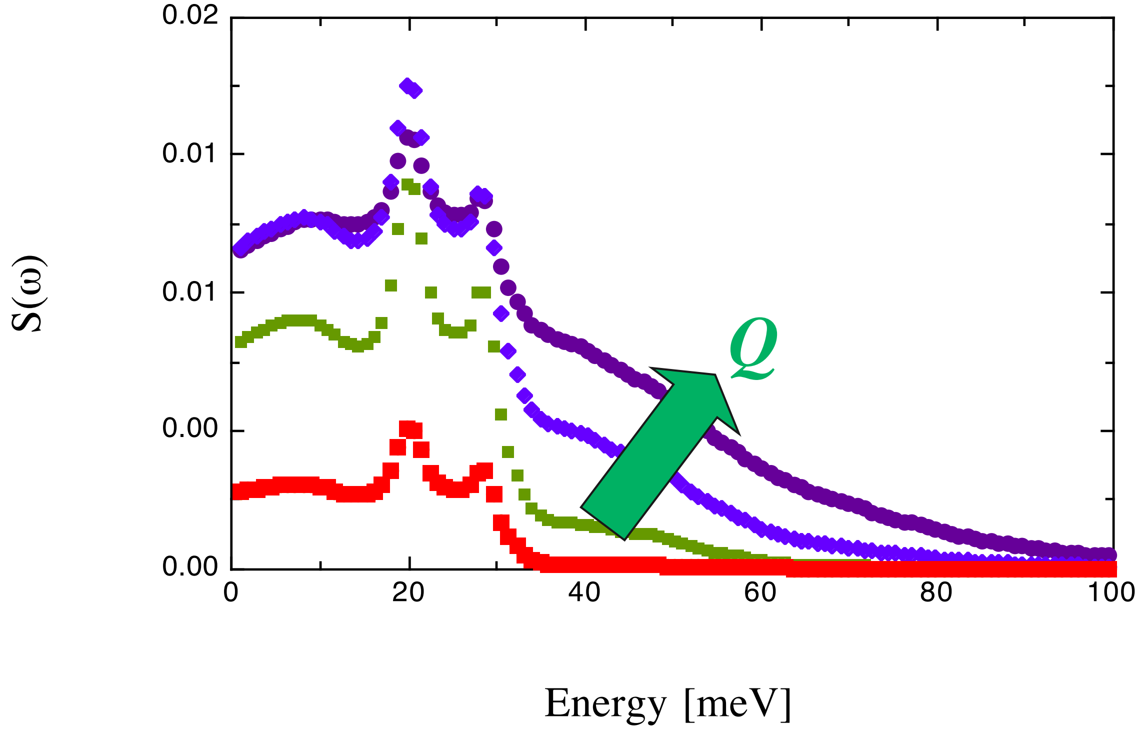

Multi-phonon (n > 1) scattering becomes larger with increasing Q.
Eventually, the different terms merge into a single recoil peak.

$$\langle \hbar\omega \rangle = \hbar Q^2/2M$$

N.B. $S(Q) = \int S(Q,\omega)d\omega = 1$ for all values of Q (theoretically)

MgB_2: A Strongly Coherent Scatterer

- With a coherent scatterer, it is necessary to sum over a wide range of Q to generate an accurate phonon density-of-states

$$S(Q,\omega) = \exp\left[-2W(Q)\right]\left[\delta(\hbar\omega) + \frac{\hbar Q^2}{2M}\frac{Z(\omega)}{\omega}\left\{n(\omega)+1\right\} + \ldots\right]$$

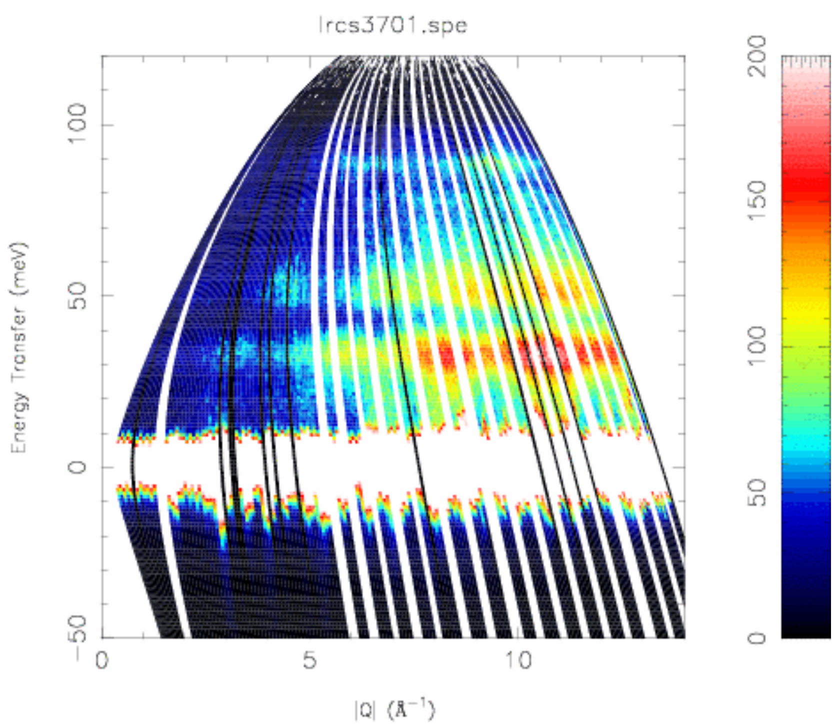

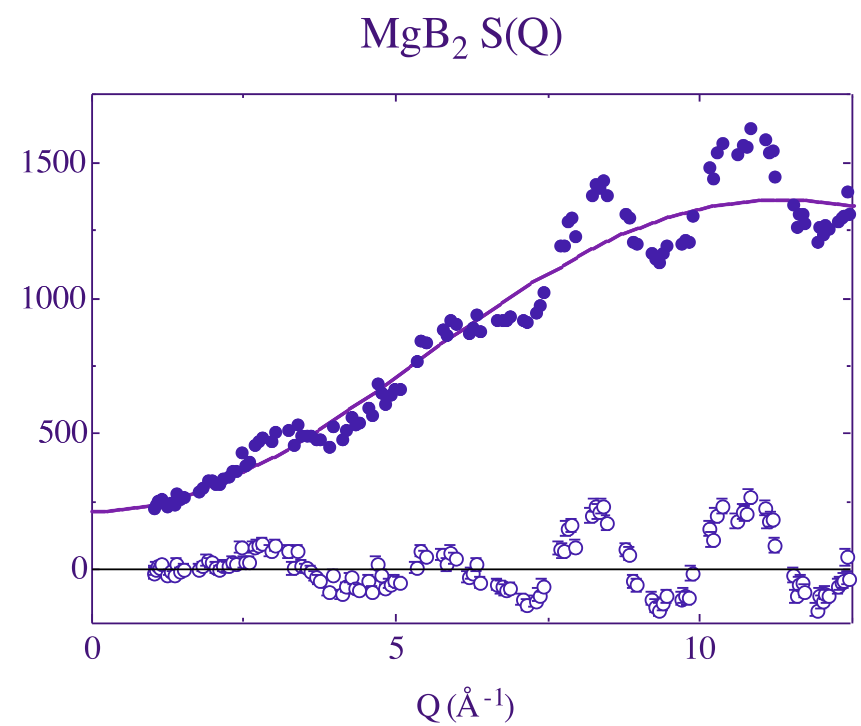

Magnetic Neutron Scattering

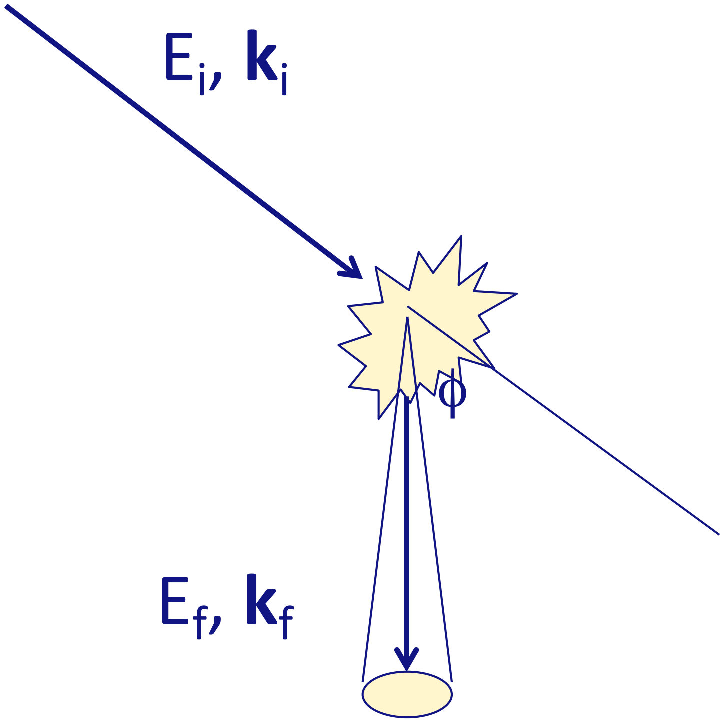

$$\frac{d^2\sigma}{d\Omega\, dE_f} = \frac{k_f}{k_i} S(Q,\varepsilon)$$

Phonon Cross Section

$$S(Q,\omega) \propto \frac{\hbar Q^2}{2M}\frac{Z(\omega)}{\omega}$$

Magnetic Cross Section

$$S(Q,\omega) \propto F^2(Q)\mathrm{Im}\chi(Q,\omega)$$

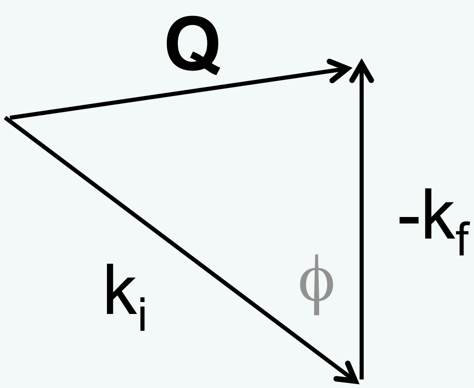

Energy Conservation

$$\varepsilon = E_i - E_f = \frac{\hbar^2}{2m}(k_i^2 - k_f^2)$$

Momentum Conservation

$$\vec{Q} = \vec{k}_i - \vec{k}_f$$

Dynamic Magnetic Susceptibility

$$\chi^{\alpha\beta}(\mathbf{Q},\omega) = \frac{M^\alpha(\mathbf{Q},\omega)}{H^\beta(\mathbf{Q},\omega)}$$

Kramers-Kronig Relations

- This dynamic susceptibility is related to the static susceptibility measured in a conventional susceptometer by the Kramers-Kronig relations:

$$\chi'\left(\vec{Q},0\right) = \frac{1}{\pi}\int_{-\infty}^{\infty} d\omega \frac{\chi''\left(\vec{Q},\omega\right)}{\omega}$$

- So the cross section can be rewritten:

$$\frac{d^2\sigma}{d\Omega dE'} \propto \frac{k'}{k} S(Q,\omega) \propto \frac{k'}{k}\left\{n(\omega)+1\right\}\chi'\left(\vec{Q},0\right)\omega P\left(\vec{Q},\omega\right)$$

- $P(Q,\omega)$ is just a normalized spectral or “shape” function
  - e.g. a delta function or a Lorenzian
- $\chi'(Q \rightarrow 0,0)$ is the bulk static susceptibility

N.B. $S(Q,\omega)$ is the neutron scattering law here, not the F.T. of the spin.

S(Q,ω) of $BaFe_2As_{2-x}P_x$ (x = 0.3)

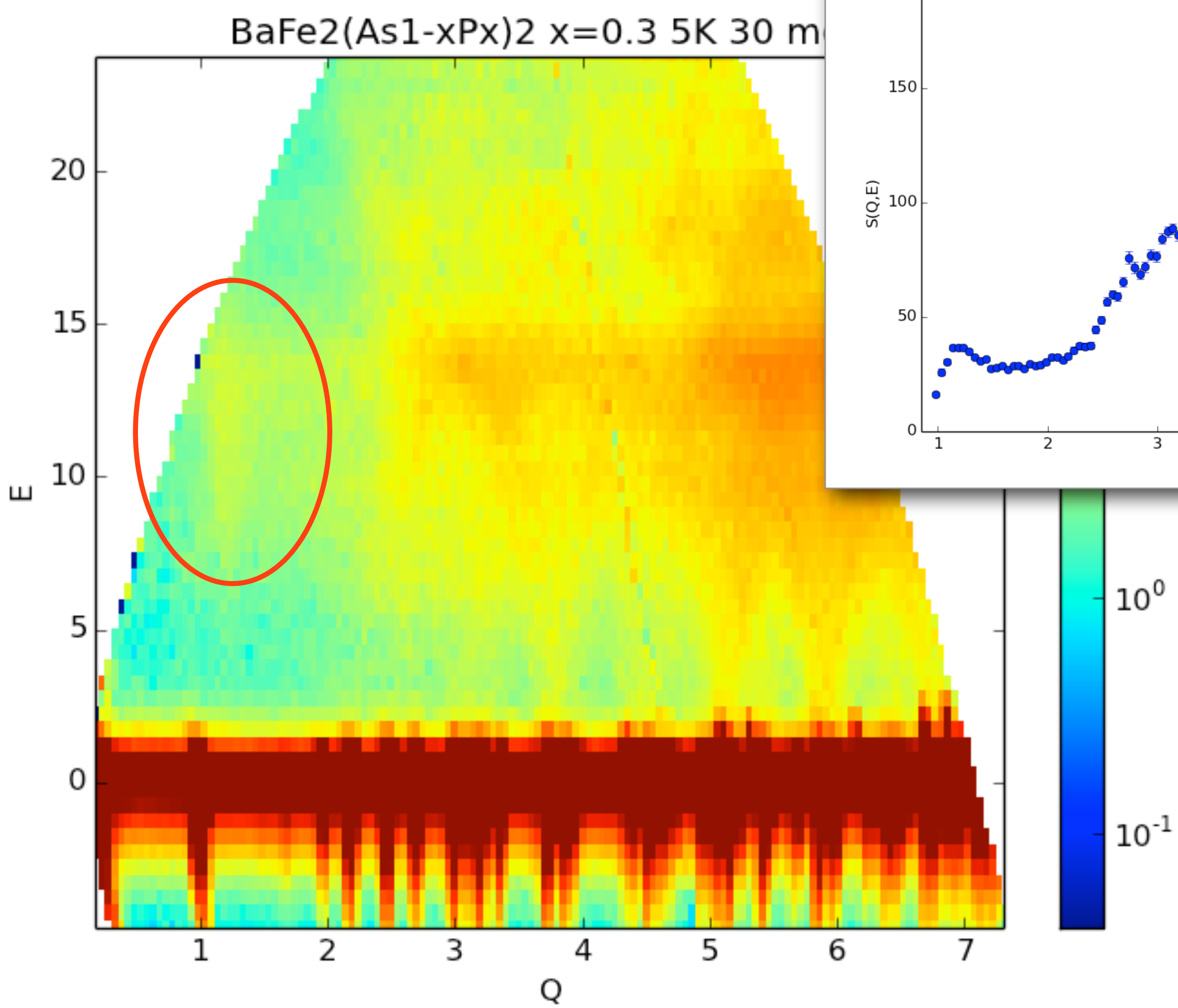

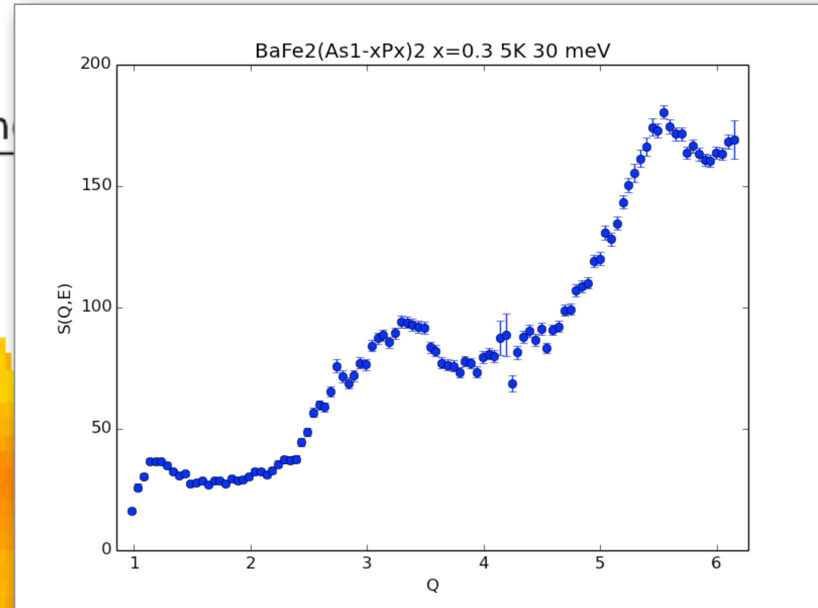

Itinerant Theories of the Resonance

$$\mathrm{Im}\chi_0(\mathbf{Q},\omega) \propto \int d^3\mathbf{k} \left(1 - \frac{\xi_{\mathbf{k+Q}}\xi_{\mathbf{k}} + \Delta_{\mathbf{k}}\Delta_{\mathbf{k+Q}}}{E_{\mathbf{k+Q}}E_{\mathbf{k}}}\right)\delta(\omega - E_{\mathbf{k+Q}} - E_{\mathbf{k}})$$

Resonance Condition

$$\Delta_{\mathbf{k+Q}} = -\Delta_{\mathbf{k}}$$

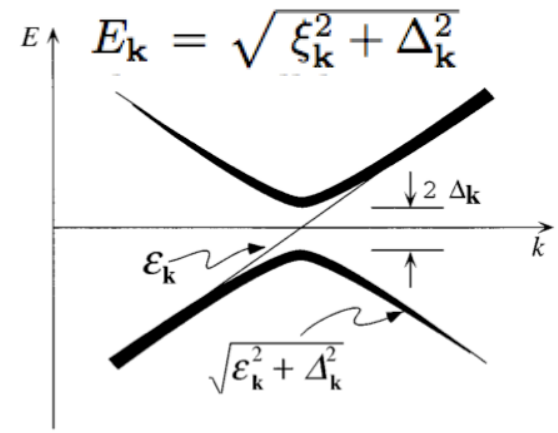

$$\chi(\mathbf{Q},\omega) = \frac{\chi_0(\mathbf{Q},\omega)}{1 - J(\mathbf{Q})\chi_0(\mathbf{Q},\omega)}$$

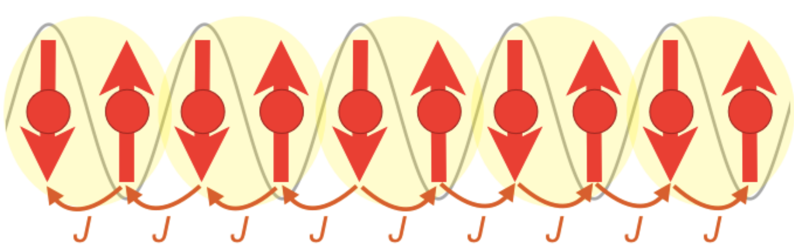

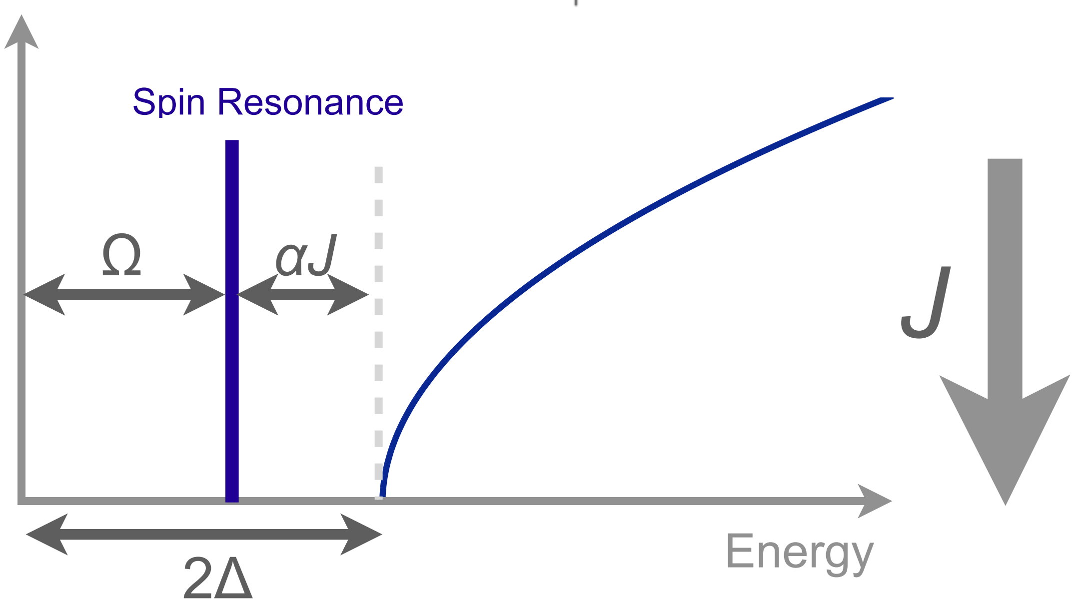

M. M. Korshunov and I. Eremin, Phys. Rev. B. **78**, 140509 (2008)
T. Maier *et al*, Phys. Rev. B **79**, 134520 (2009)

Doping Dependence of the Resonance

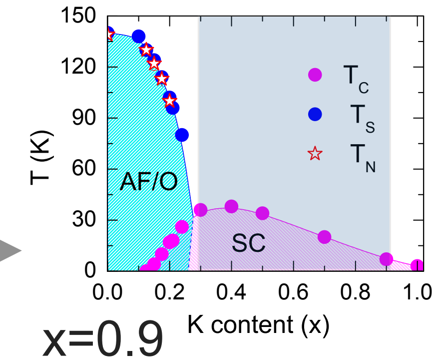

Hole-Doping

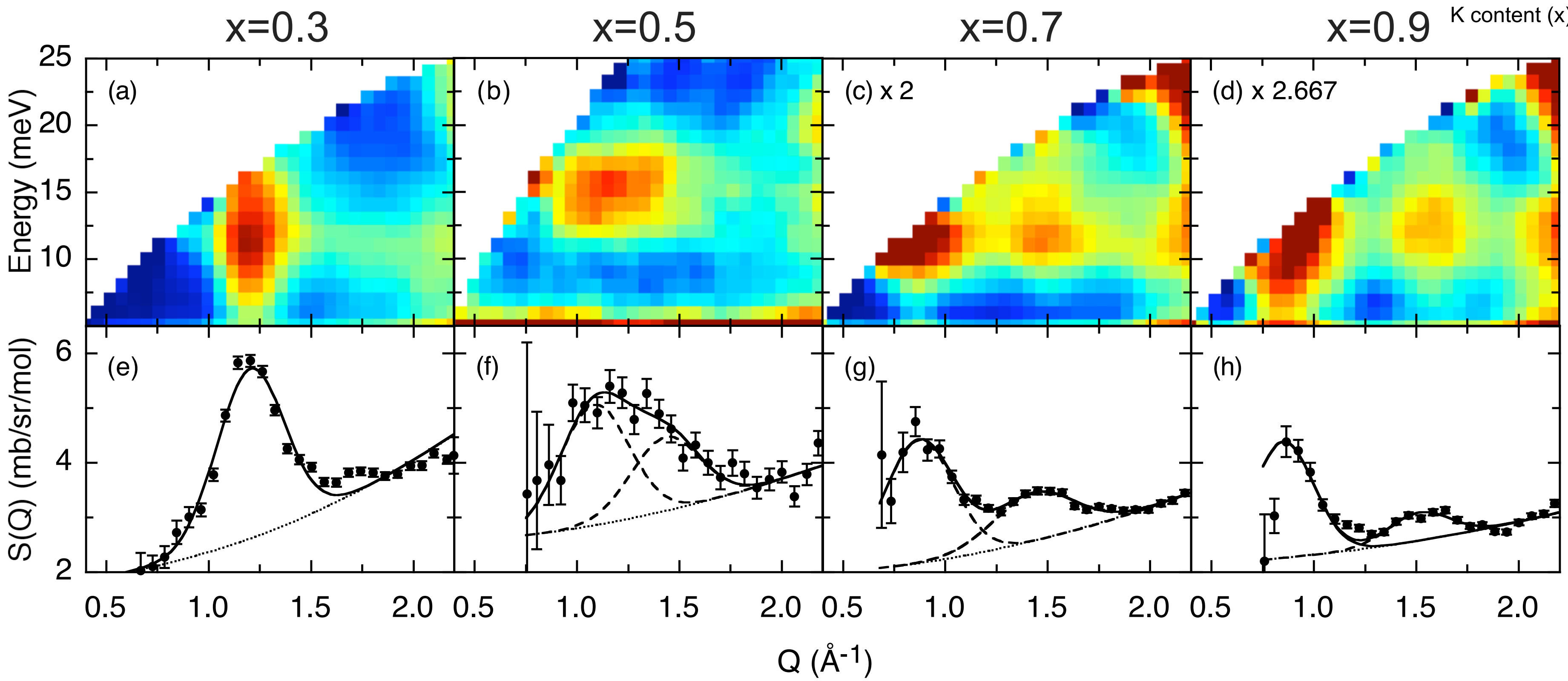

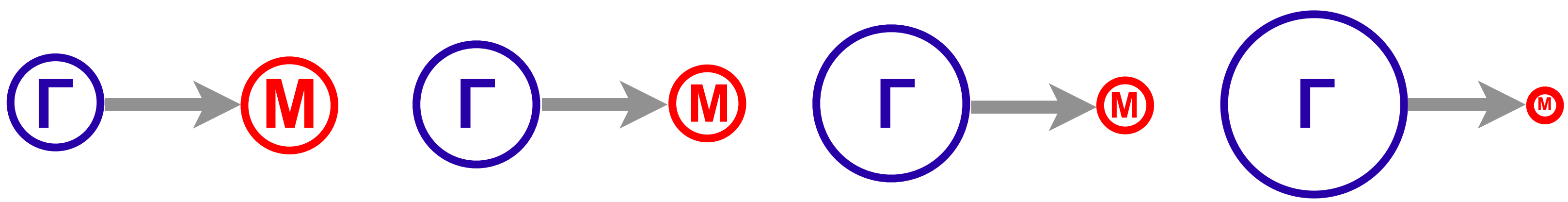

J.-P. Castellan *et al*, Physical Review Letters **107,** 177003 (2011)

Resonant Spectral Weight

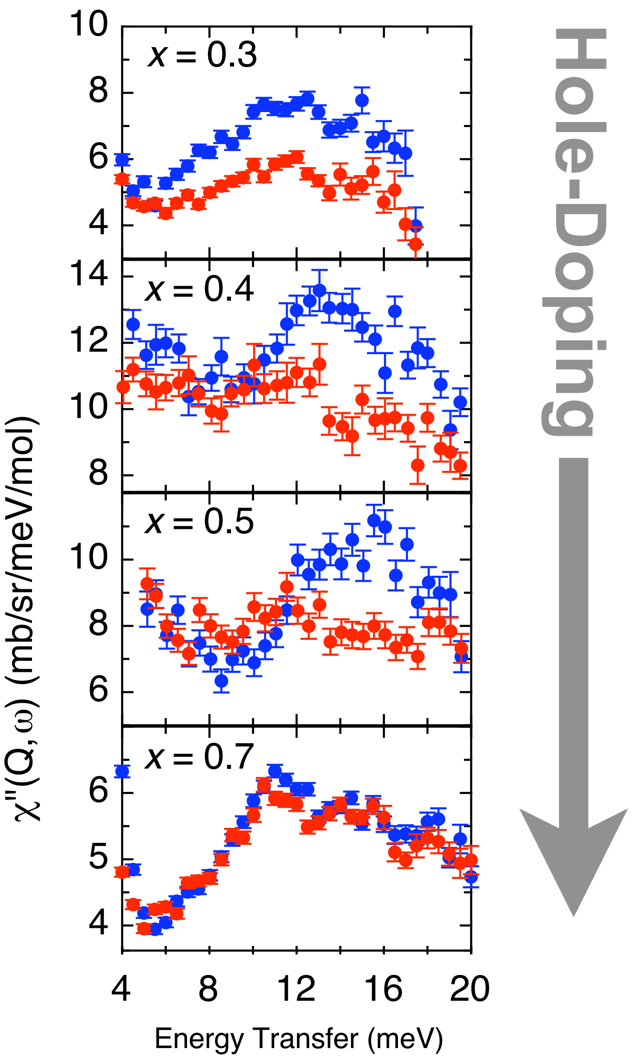

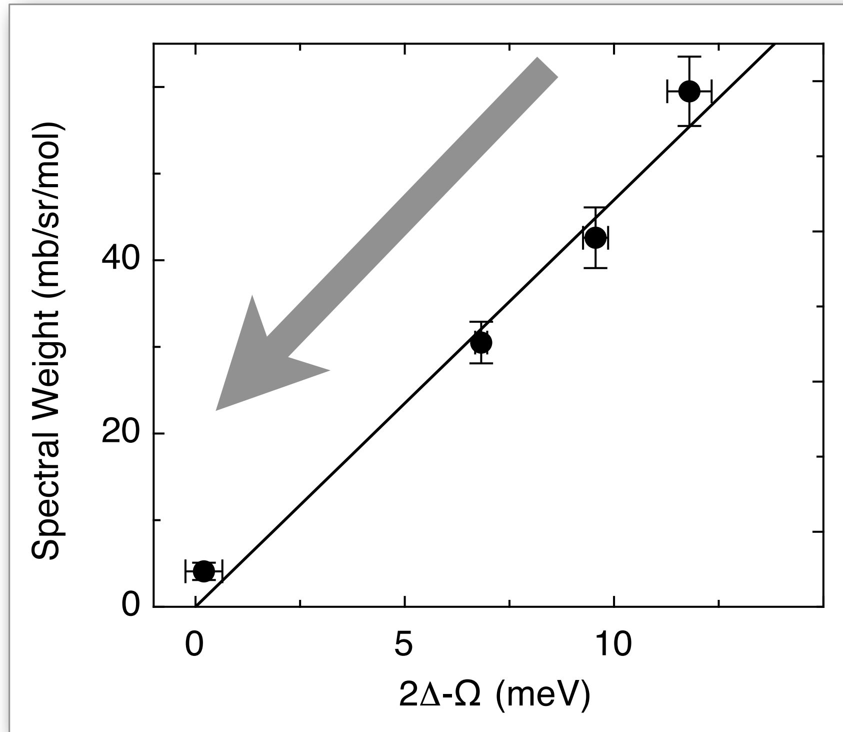

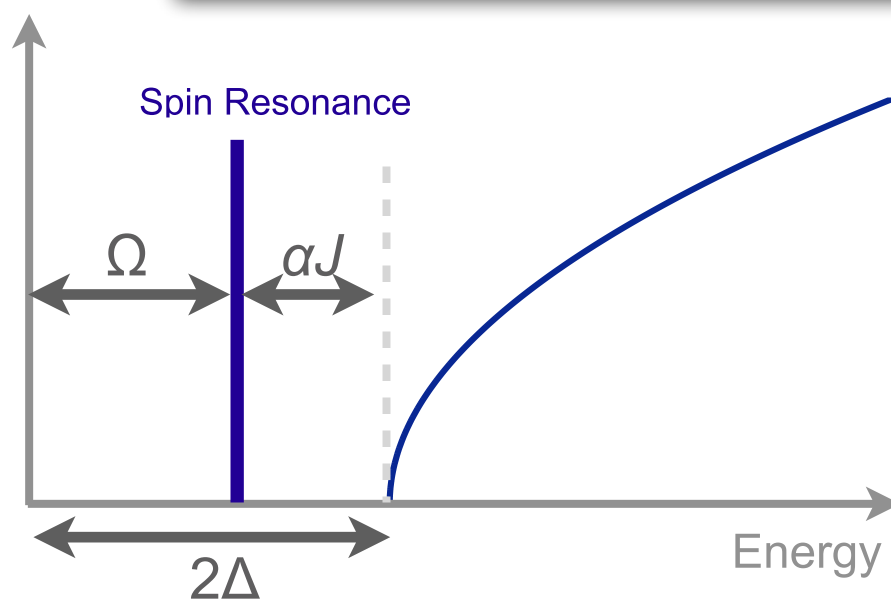

M. Eschrig, Adv. Phys. **55**, 47 (2006)

Crystal Field Spectroscopy

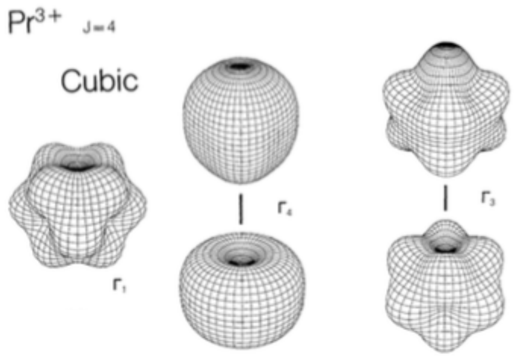

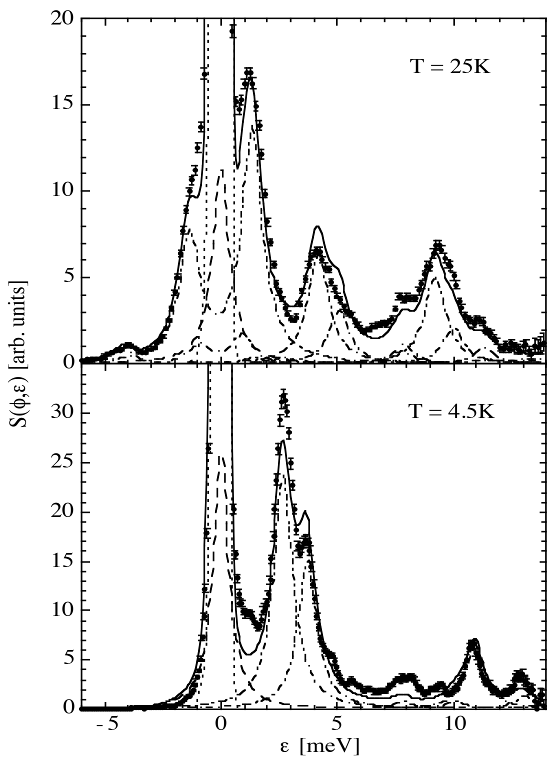

- Localized electronic $4f^n$ wavefunctions may be split by Coulomb repulsion from neighboring anions
- Neutrons can induce transitions between the energy levels if there is a dipole matrix element

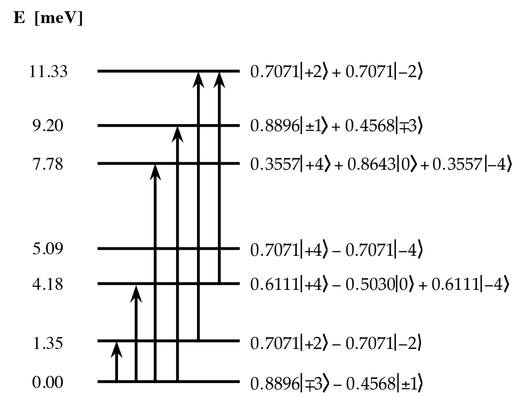

- The crystal field wavefunctions can be determined from the inelastic peak energies and intensities.

$$S(Q,\omega) \propto f^2(Q)\, p_i\, |M_{ij}|^2 \delta(\omega - \Delta_i)$$

where $p_i = \exp(-\Delta_i/k_B T) / Z$

and $Z = \sum_i n_i \exp(-\Delta_i/k_B T)$

Intermultiplet Transitions

- The rare earths have a rich array of excitations between different LSJ multiplets.
- Most of these transitions are non-dipolar.

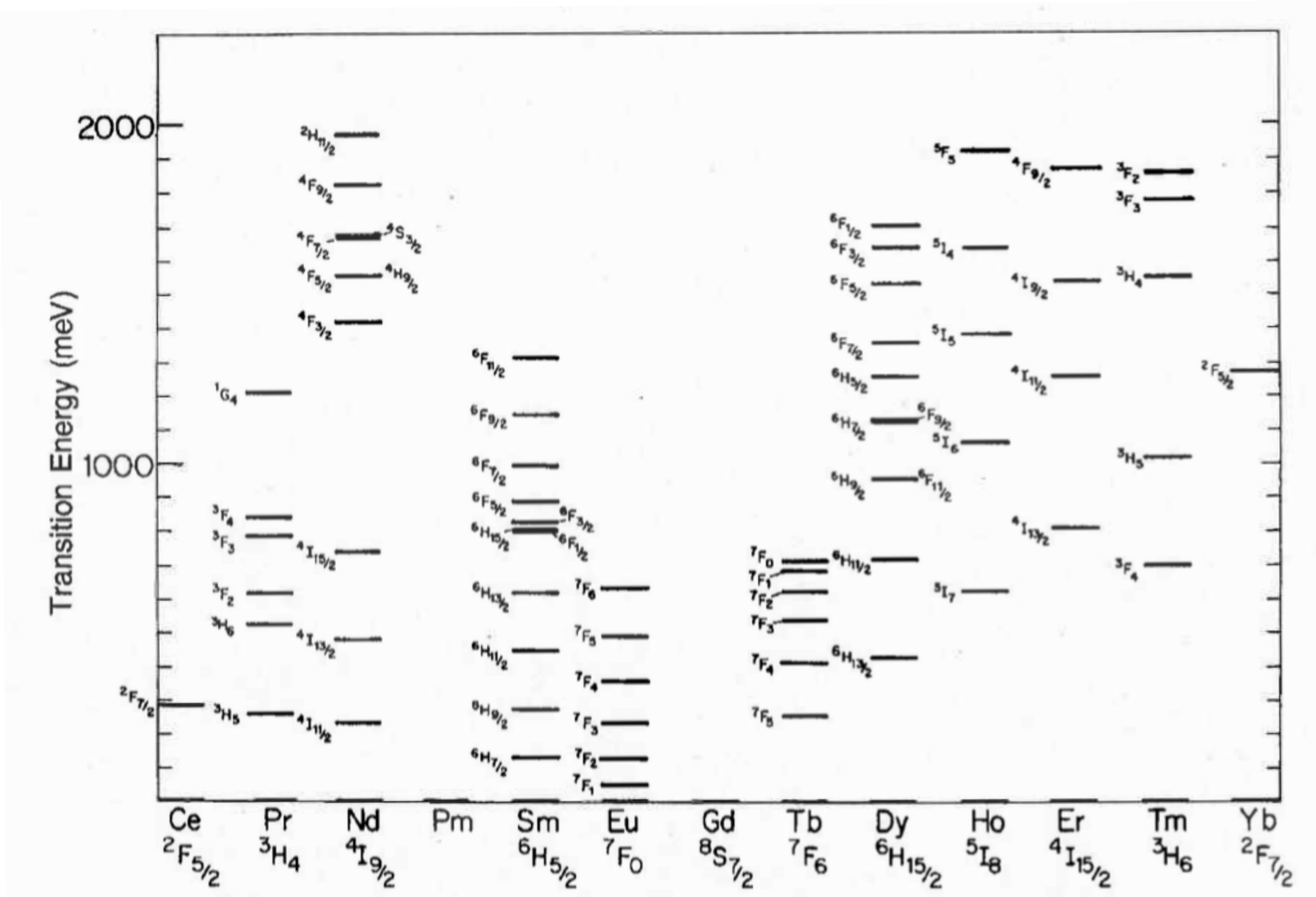

Intermultiplet Excitations in Thulium

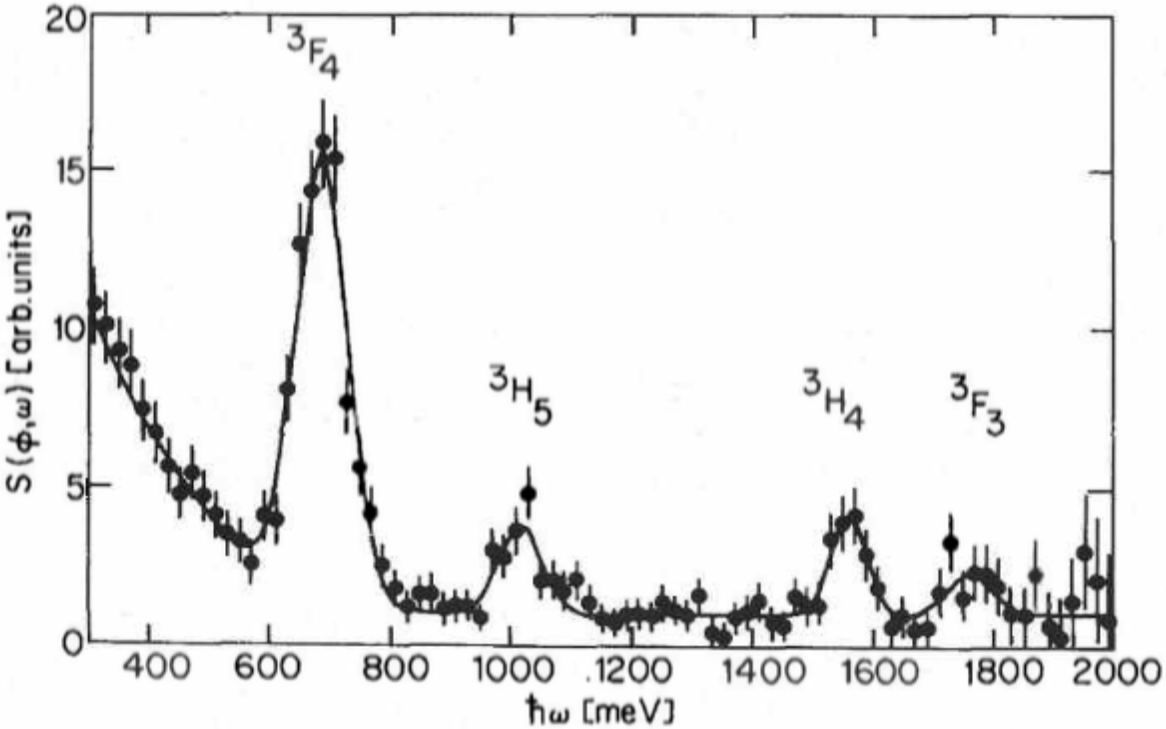

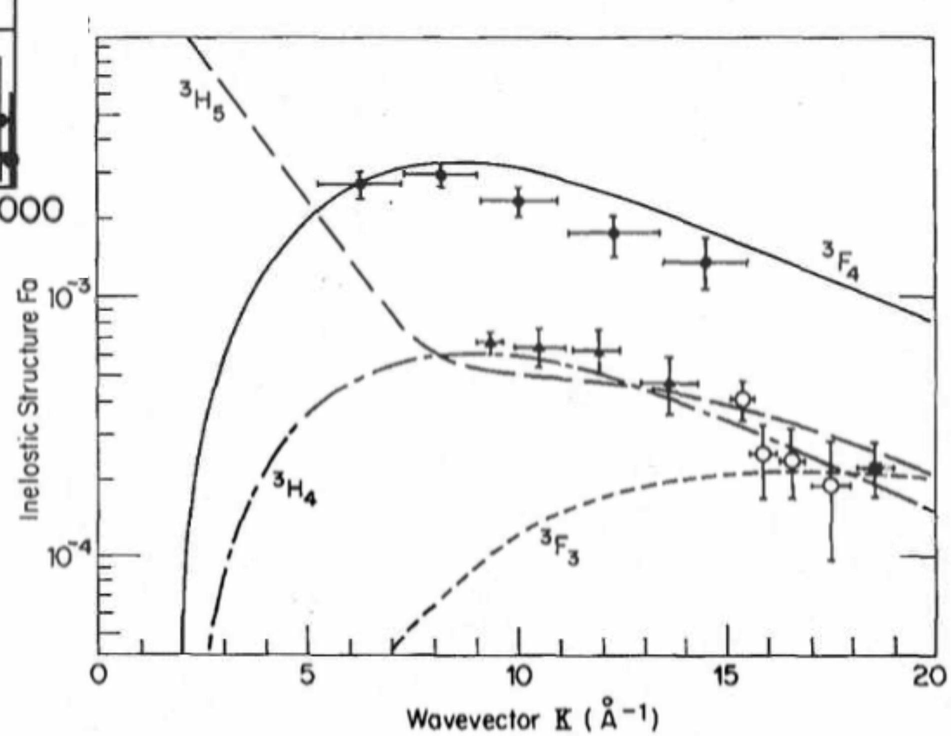

R. Osborn, S. W. Lovesey, A. D. Taylor, & E. Balcar, E. in *Handbook of the Physics and Chemistry of Rare Earths* (ed. Gschneidner, K. A.) **14,** 1–61 (North-Holland, 1991).

Fluctuating Moment Systems

Neutron measurements of spin dynamics have been important for measuring relaxation rates of local moments coupled to conduction electrons .

The temperature dependence Γ(T) has distinctive behaviour in heavy fermions, Kondo lattice and intermediate valence materials.

In particular Γ(T→0) gives a measure of the "Kondo temperature", a key parameter in strongly correlated electron systems.

$Ce_{0.8}La_{0.2}Al_3$

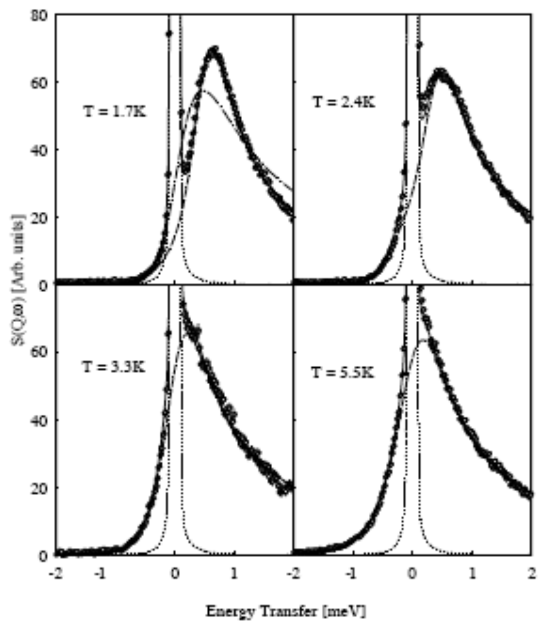

$UCu_{5-x}Pd_x$

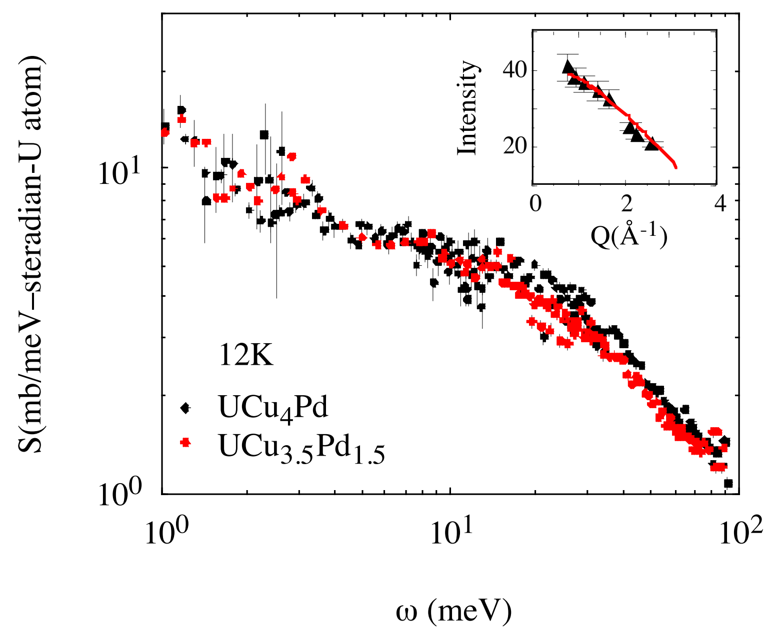

Single Crystal Experiments

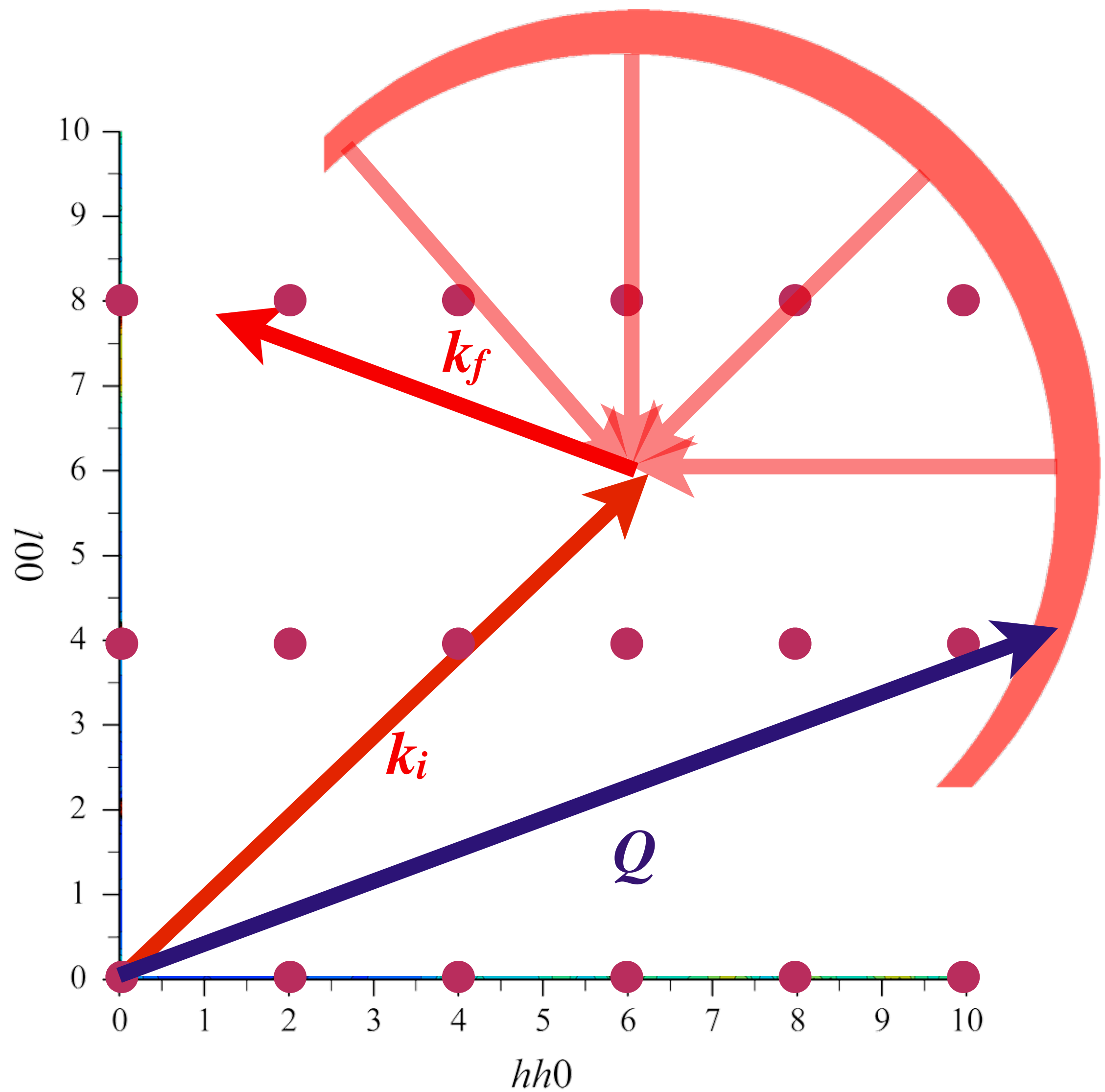

$$k_i = 2\pi / \lambda_i$$

$$k_f = 2\pi / \lambda_f$$

$$\boldsymbol{Q} = \boldsymbol{k_i} - \boldsymbol{k_f}$$

Kinematics Again (in a single crystal)

Can also be expressed in terms of the components of **Q** parallel and perpendicular to the incident wavevector $\mathbf{k}_i$:

$$Q_\perp = k_f \sin(\psi) \qquad Q_{||} = k_i - k_f$$

Hence it follows that

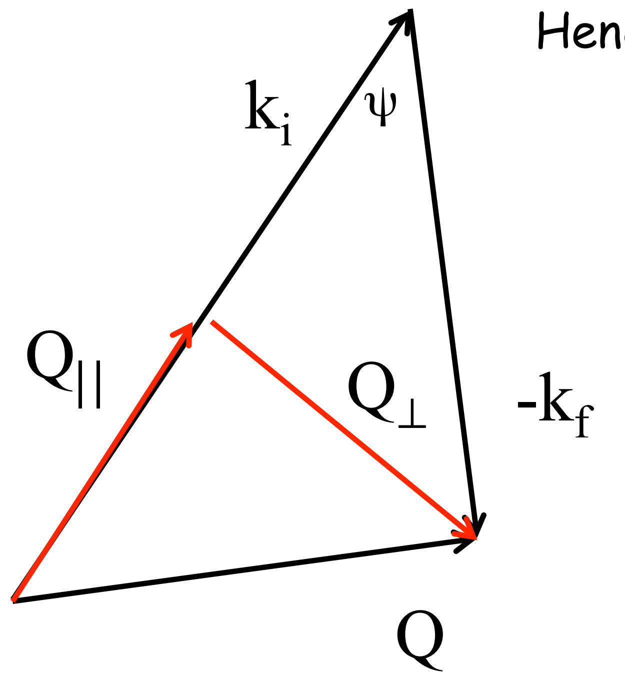

$$Q_\perp = \sqrt{\frac{2m(E_i - \varepsilon)}{\hbar^2}} \sin(\psi)$$

and

$$Q_{//} = \sqrt{\frac{2m}{\hbar^2}} [\sqrt{E_i} - \sqrt{(E_i - \varepsilon)} \cos(\psi)]$$

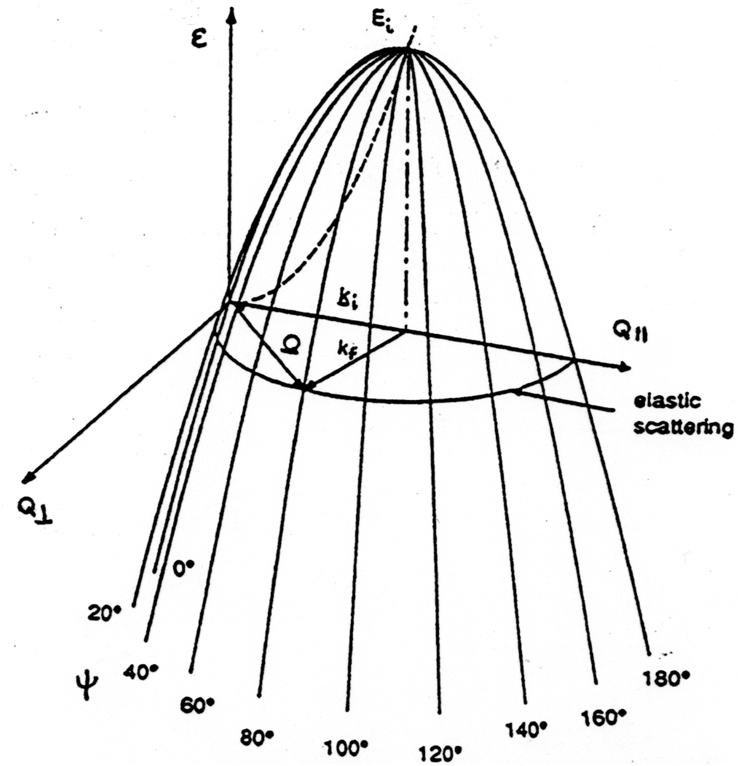

This results in the surface of a paraboloid, with the apex in $(Q_{//}, Q_\perp, \varepsilon)$-space at the point $(k_i, 0, E_i)$.

Kinematics in a Single Crystal (contd)

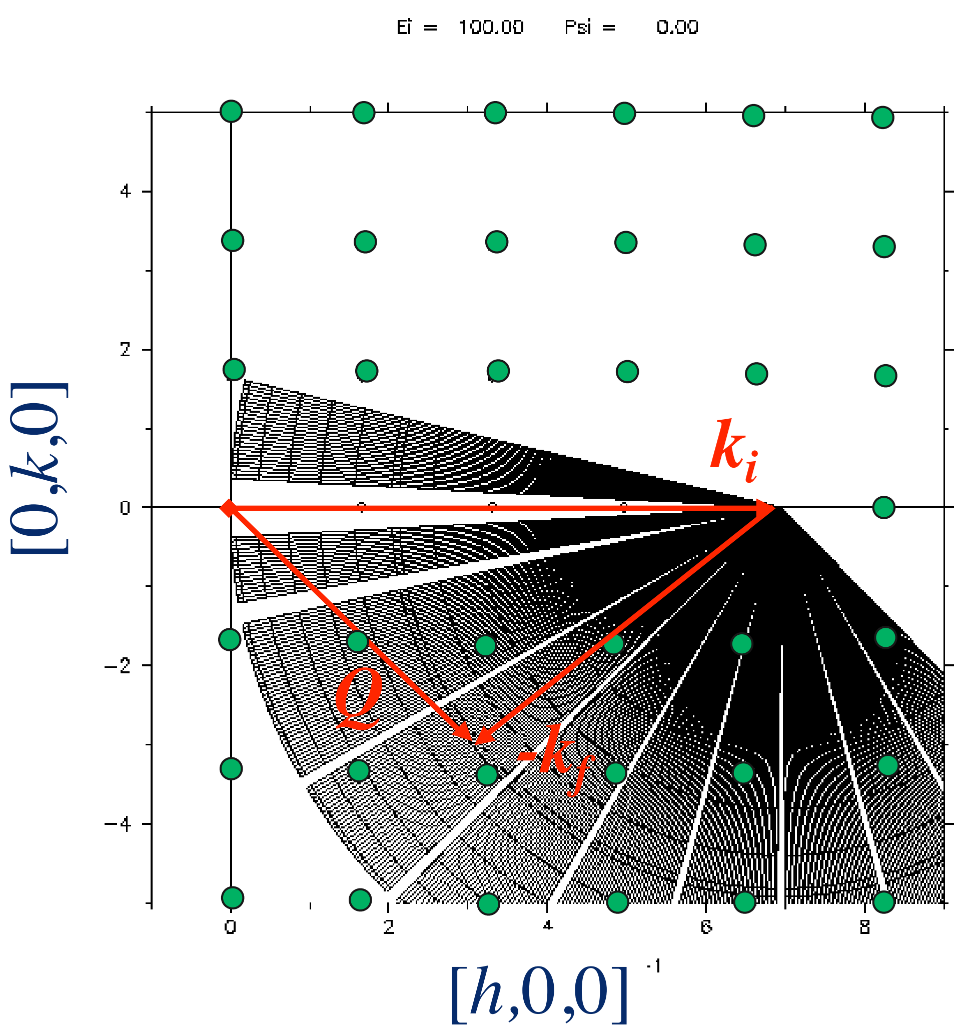

In a single crystal experiment, we need to superimpose the scattering triangle on the reciprocal lattice.

Locus of constant ω is a Q-circle of radius k_f centered on **Q** = $\mathbf{k}_i$

Coherent Spin Waves

- In most magnetic systems, there is a coupling between neighboring spins
  - e,g, Heisenberg exchange

$$H_{ex} = -\sum_{i,j} J_{ij} \vec{S}_i . \vec{S}_j$$

- When one spin changes direction, it induces a wave-like disturbance of all the neighboring spins.

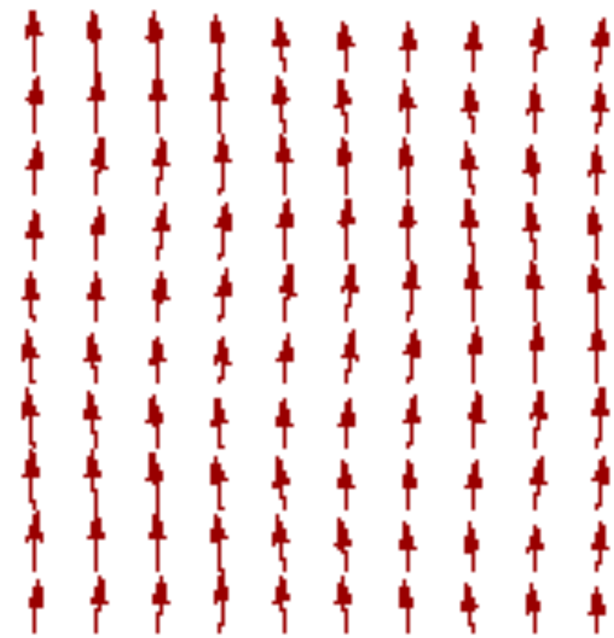

$La_{0.7}Pb_{0.3}MnO_3$ - CMR Ferromagnet

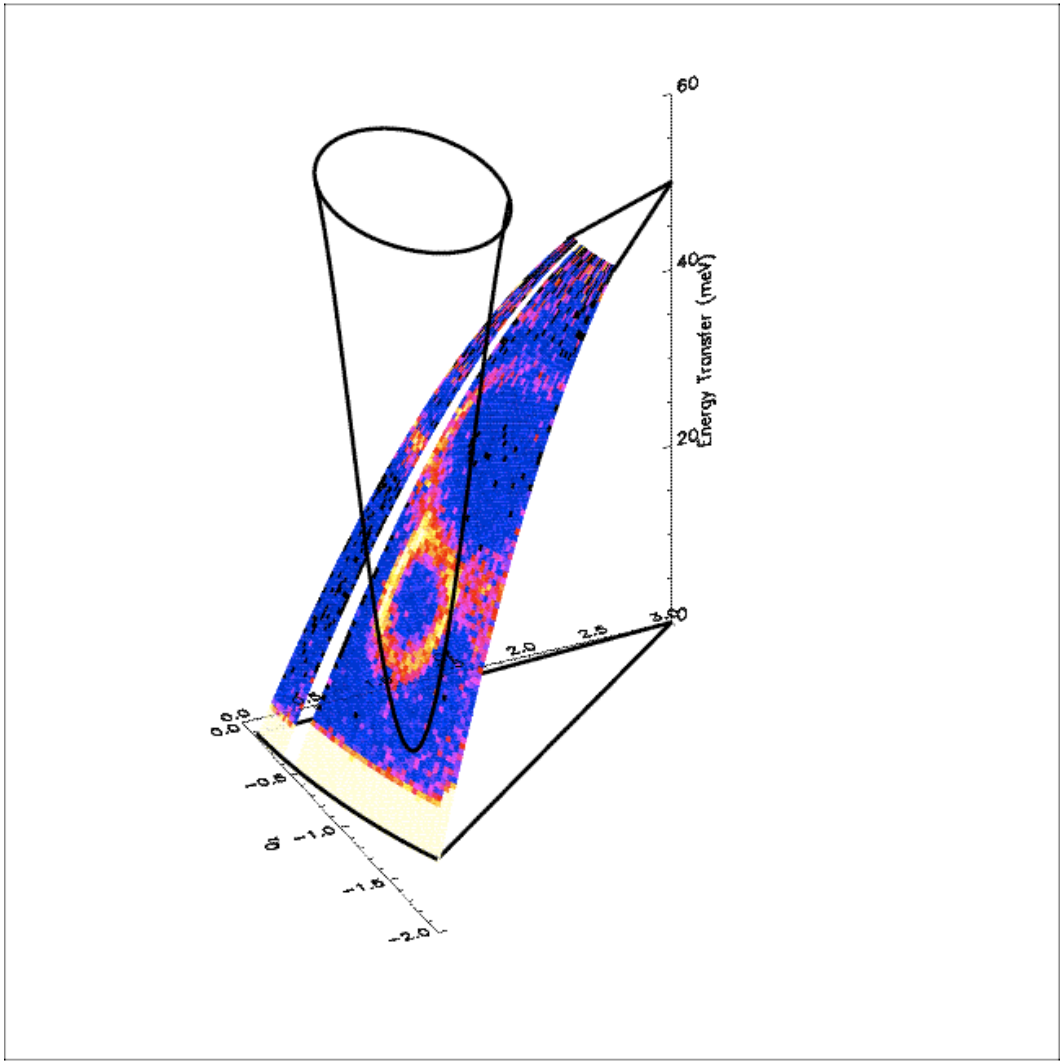

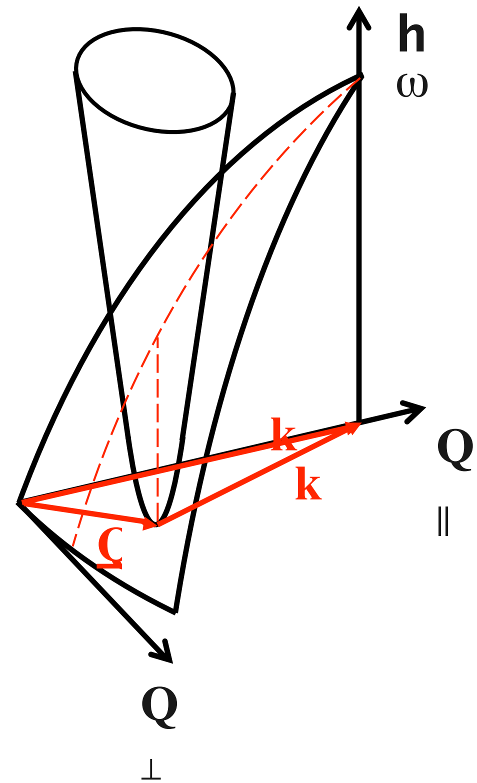

Spin Waves in a CMR Ferromagnet

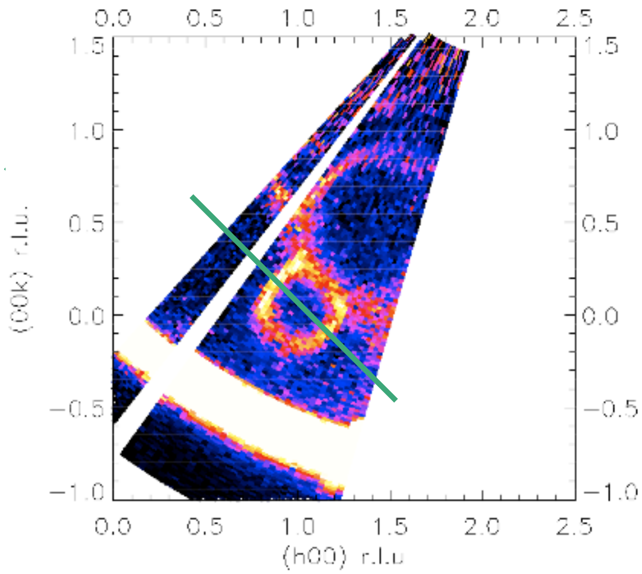

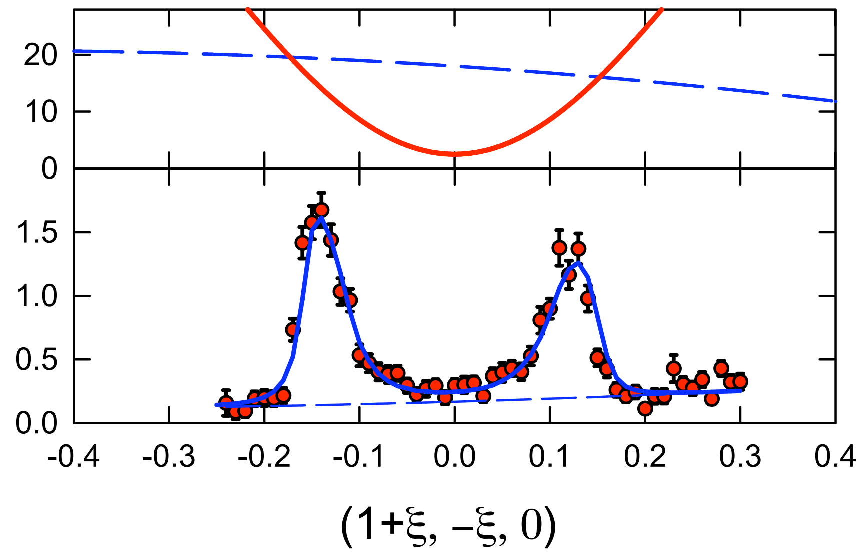

Heisenberg ferromagnet (nearest neighbor)

2JS = 8.8 ± 0.2 meV

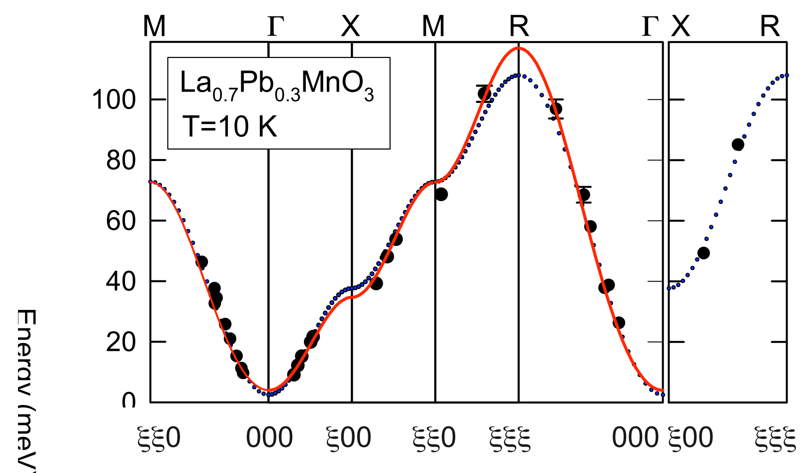

Double exchange model:

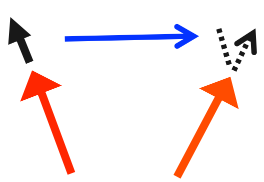

W = 1.6 eV (half band-width)

J_H = 3.2 eV (intra-site exchange)

Perring et al., Phys Rev. Lett. **77,** 711 (1996)

MAPS Spectrometer

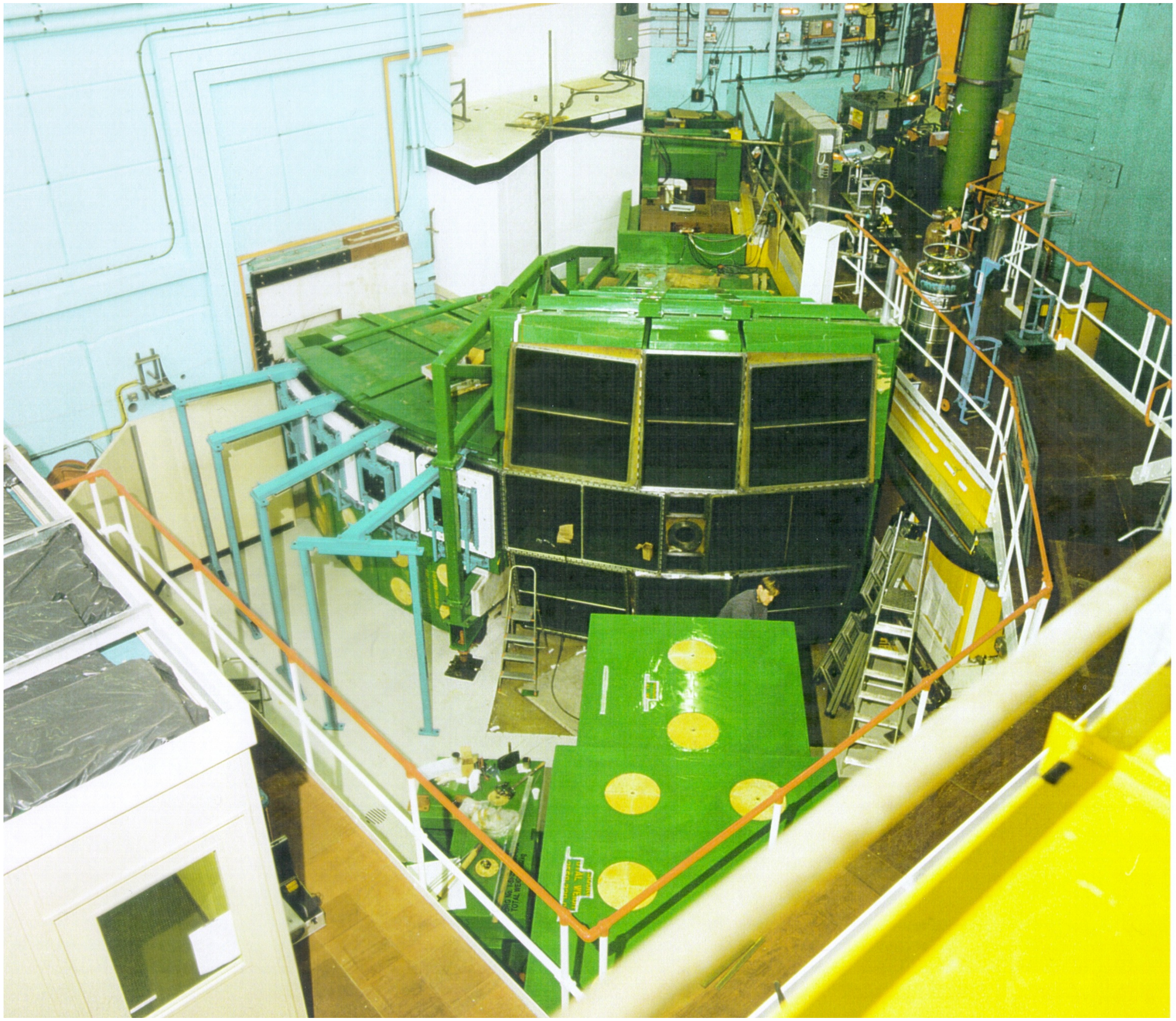

Spin Waves in Cobalt

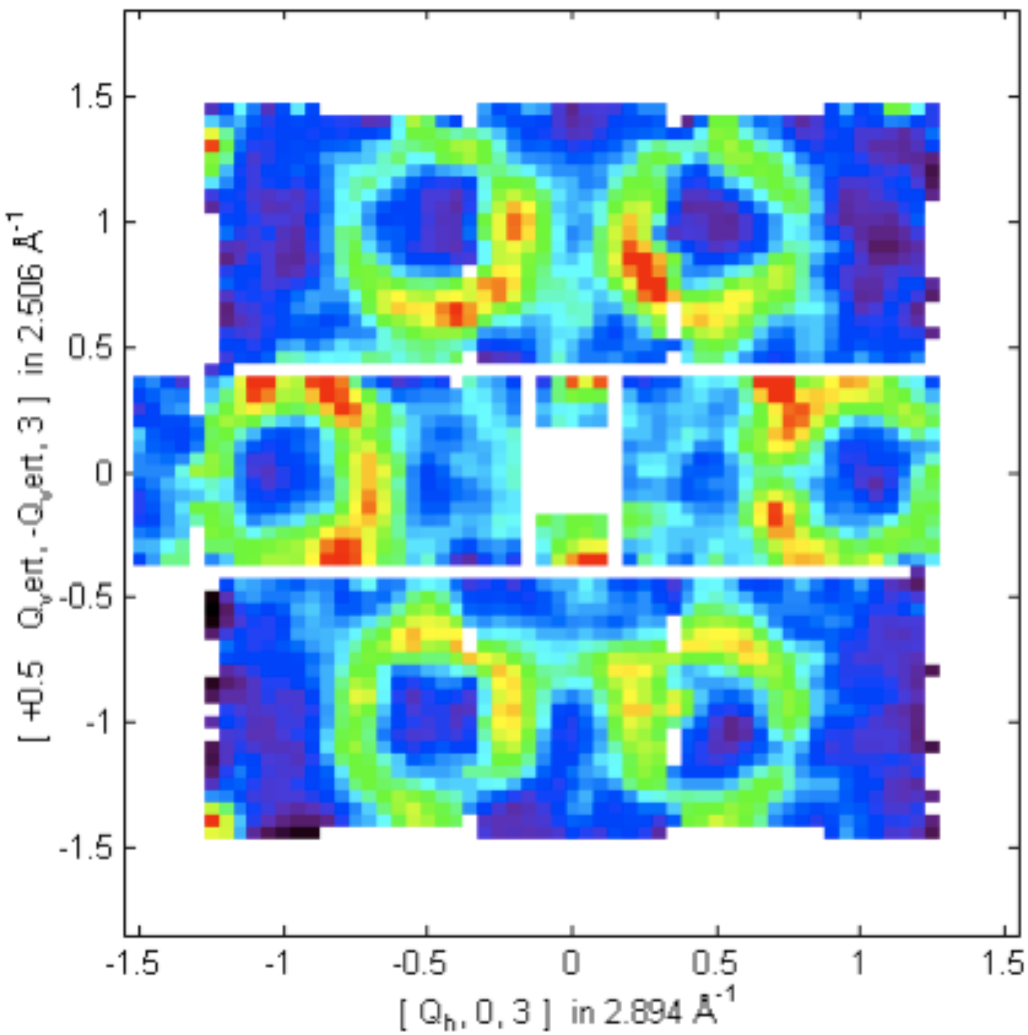

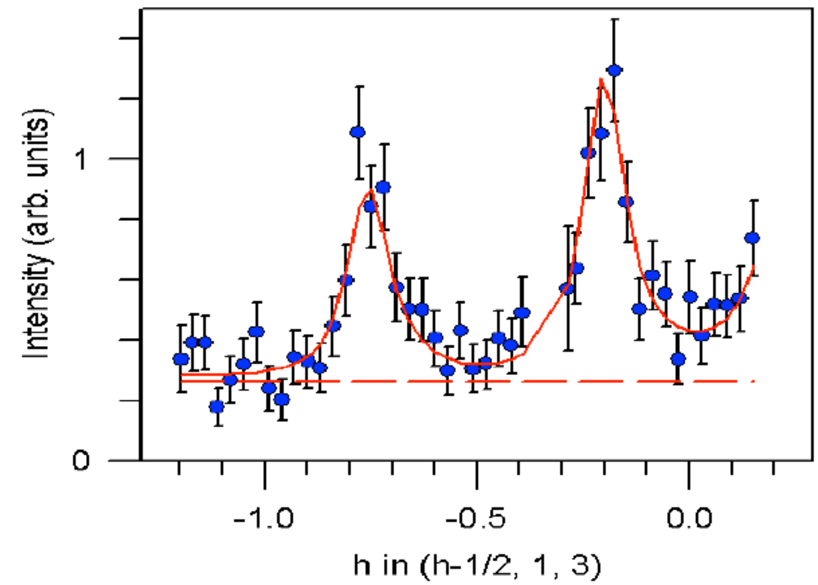

$$H = -J \sum \mathbf{S}_i . \mathbf{S}_j$$

$12SJ = 199 \pm 7$ meV

$\gamma = 69 \pm 12$ meV

Spin Waves in $Fe_{1+y}Te_{1-x}Se_x$

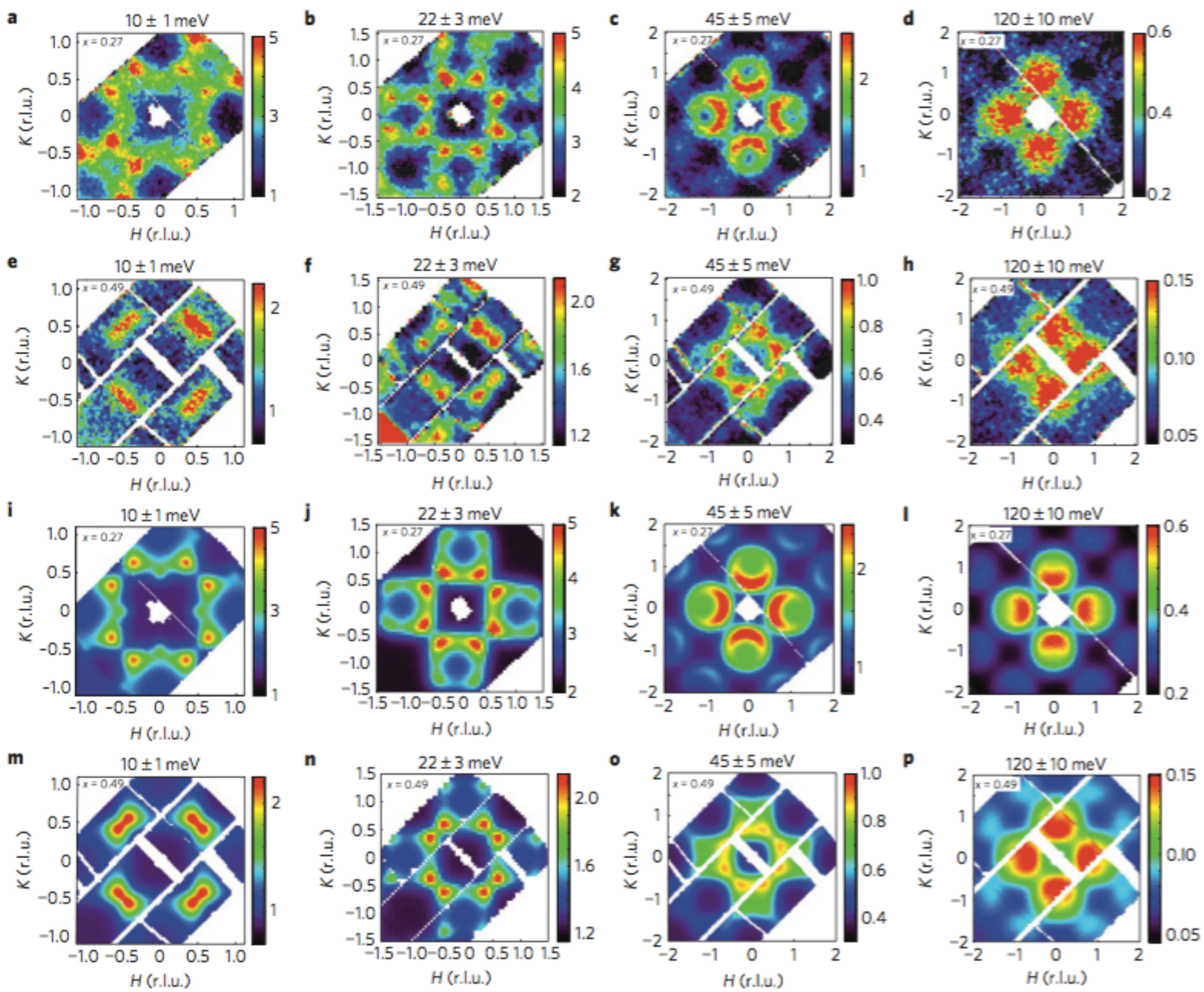

M. D. Lumsden, *et al. Nat Phys* **6,** 182–186 (2010).

$KCuF_3$ - 1D Spin-1/2 Antiferromagnet

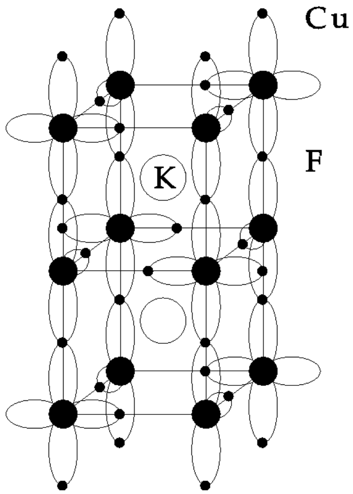

Faddeev and Takhtajan

(Phys. Lett 85A 375 1981)

suggested excitation spectrum:

not spin waves : S=1

but pairs of "spinons" : S=1/2

$$\omega = \omega_1(q_1) + \omega_2(q_2)$$

$$q = q_1 + q_2$$

→ continuum of excitations

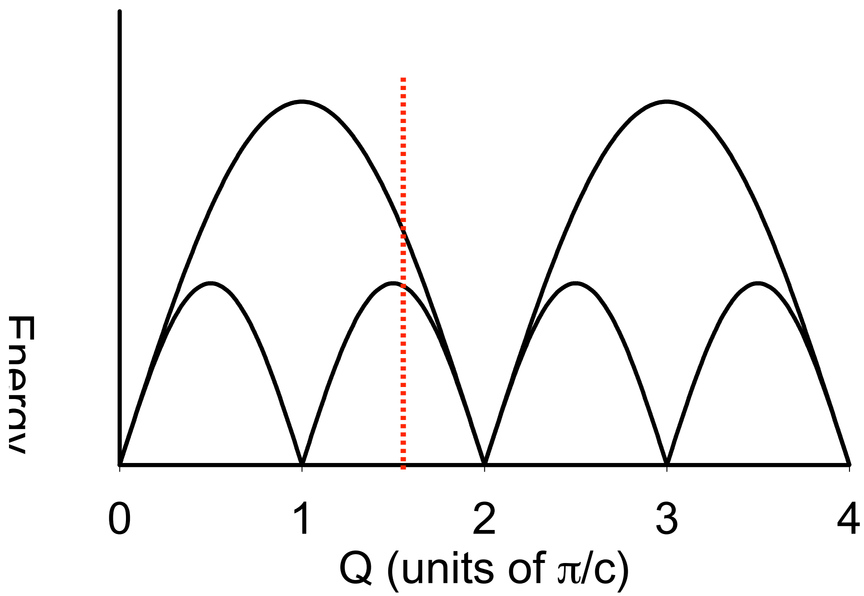

$$\omega_L = (\pi/2)\, J\ |\sin(\pi q)|$$

$$\omega_U = \pi\ J\ |\sin(\pi q/2)|$$

Numerical and analytic work:

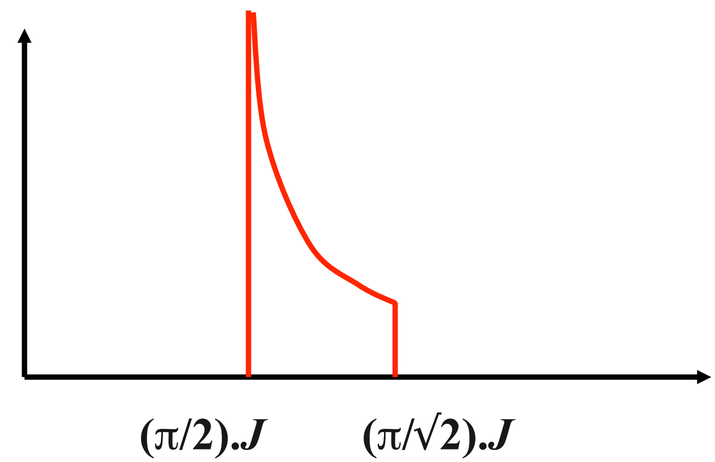

Low-Dimensional Excitations

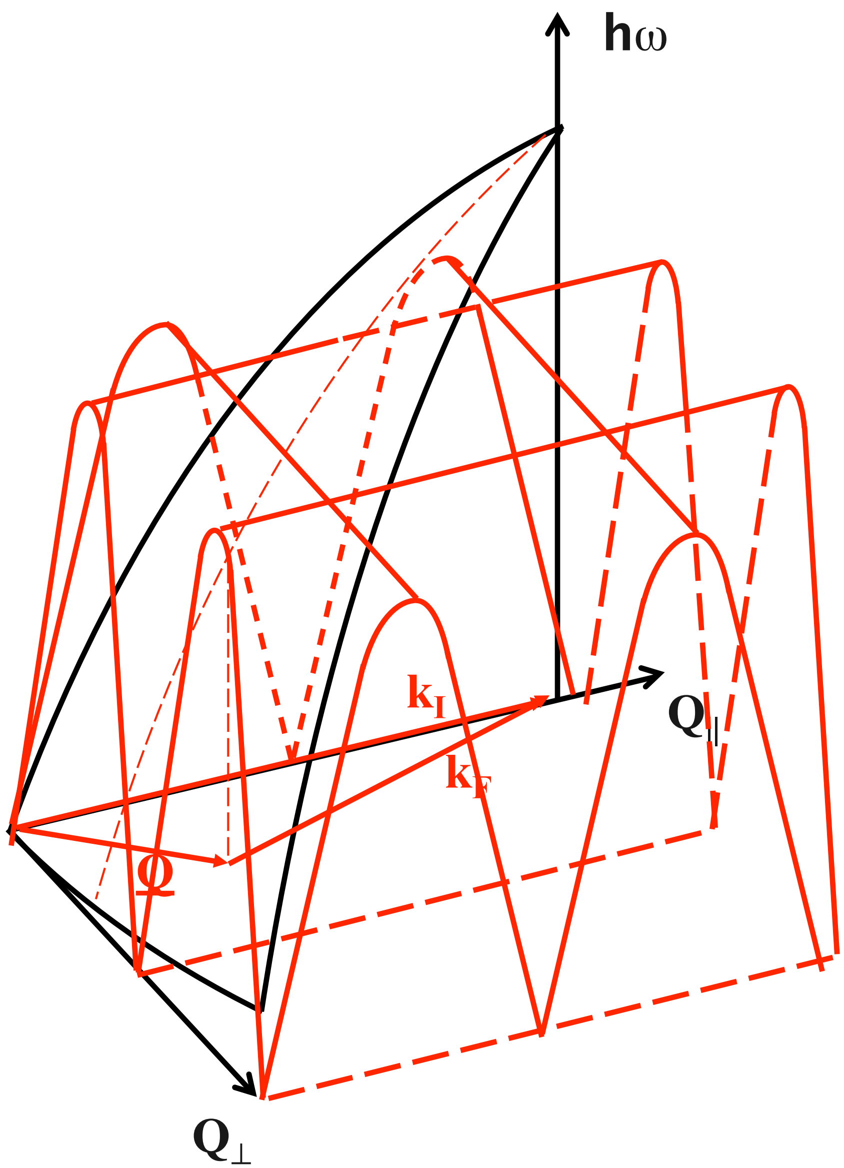

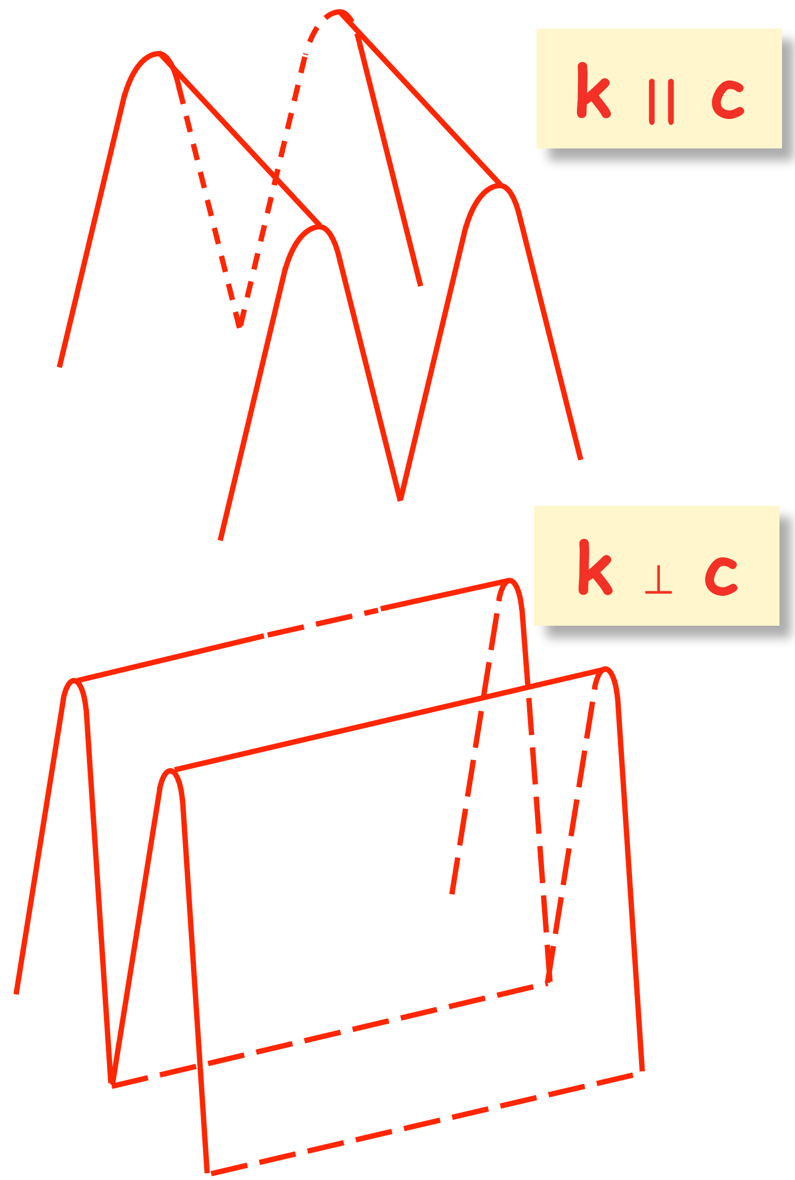

k II c

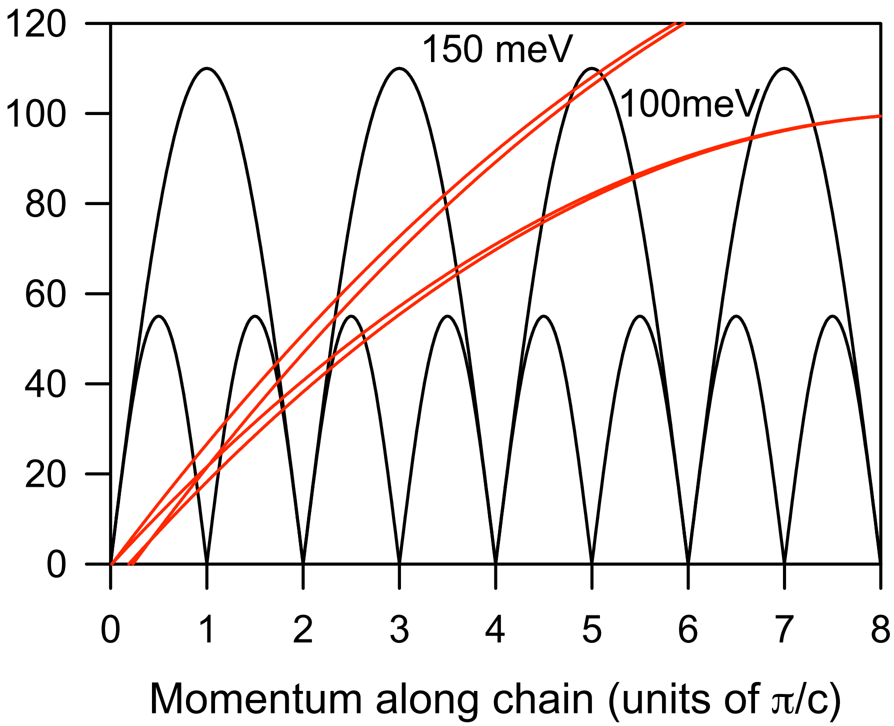
120
100
80
60
40
20
0
0
1
2
3
4
5
6
7
8
150 meV
100meV
Momentum along chain (units of π/c)

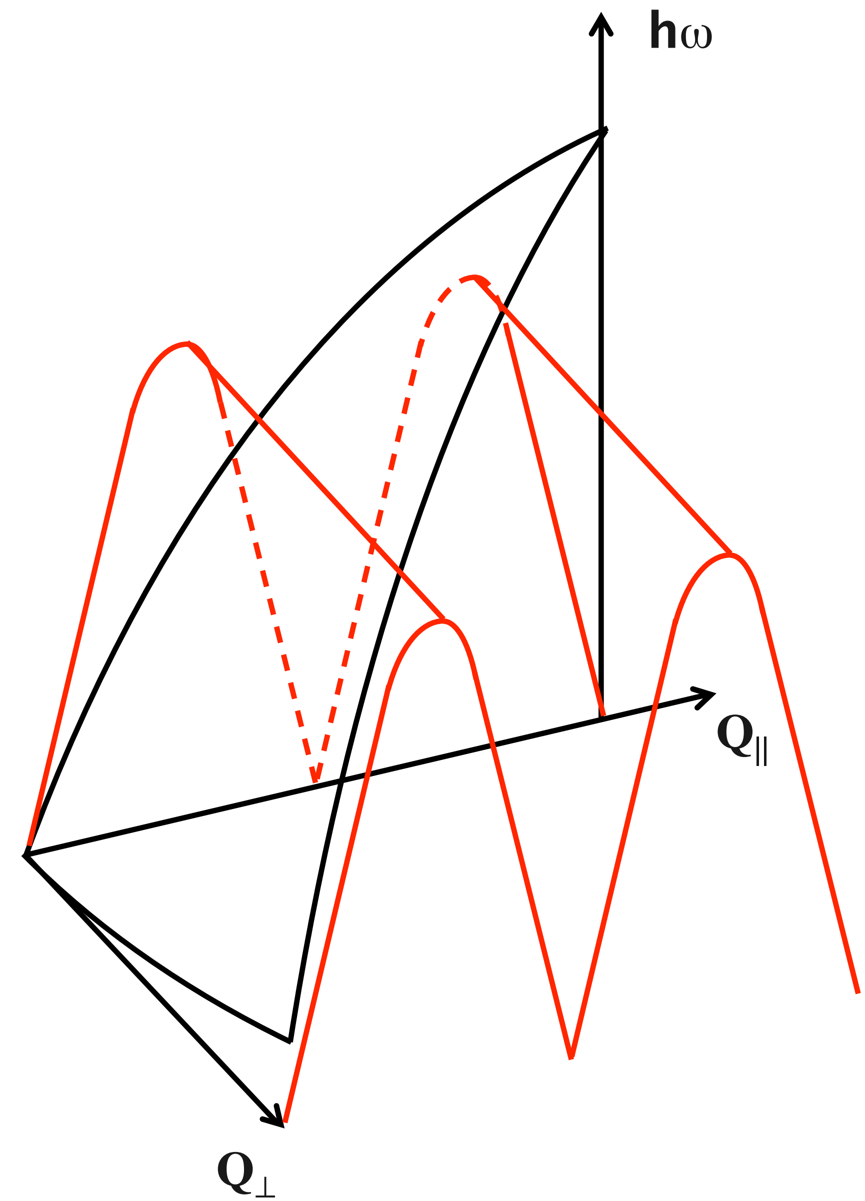
hω
Q||
Q⊥

$KCuF_3$ Excitations

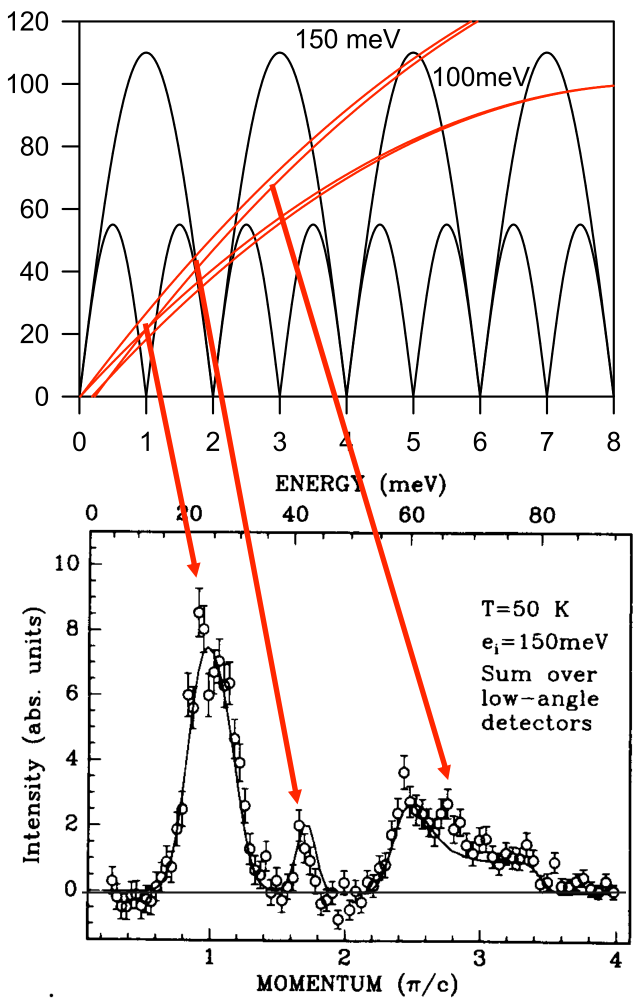

- **Broad peak can only be explained by continuum**

First clear evidence of continuum scattering in S=1/2 chain

- **Intensity scale:**

  A = 1.78 ± 0.01 ± 0.5

c.f. numerical work:

  A = 1.43

- **Coupling constant:**

  J = 34.1 ± 0.6 meV

D.A.Tennant et al, Phys. Rev. Lett. **70** 4003 (1993)

k ⊥ c

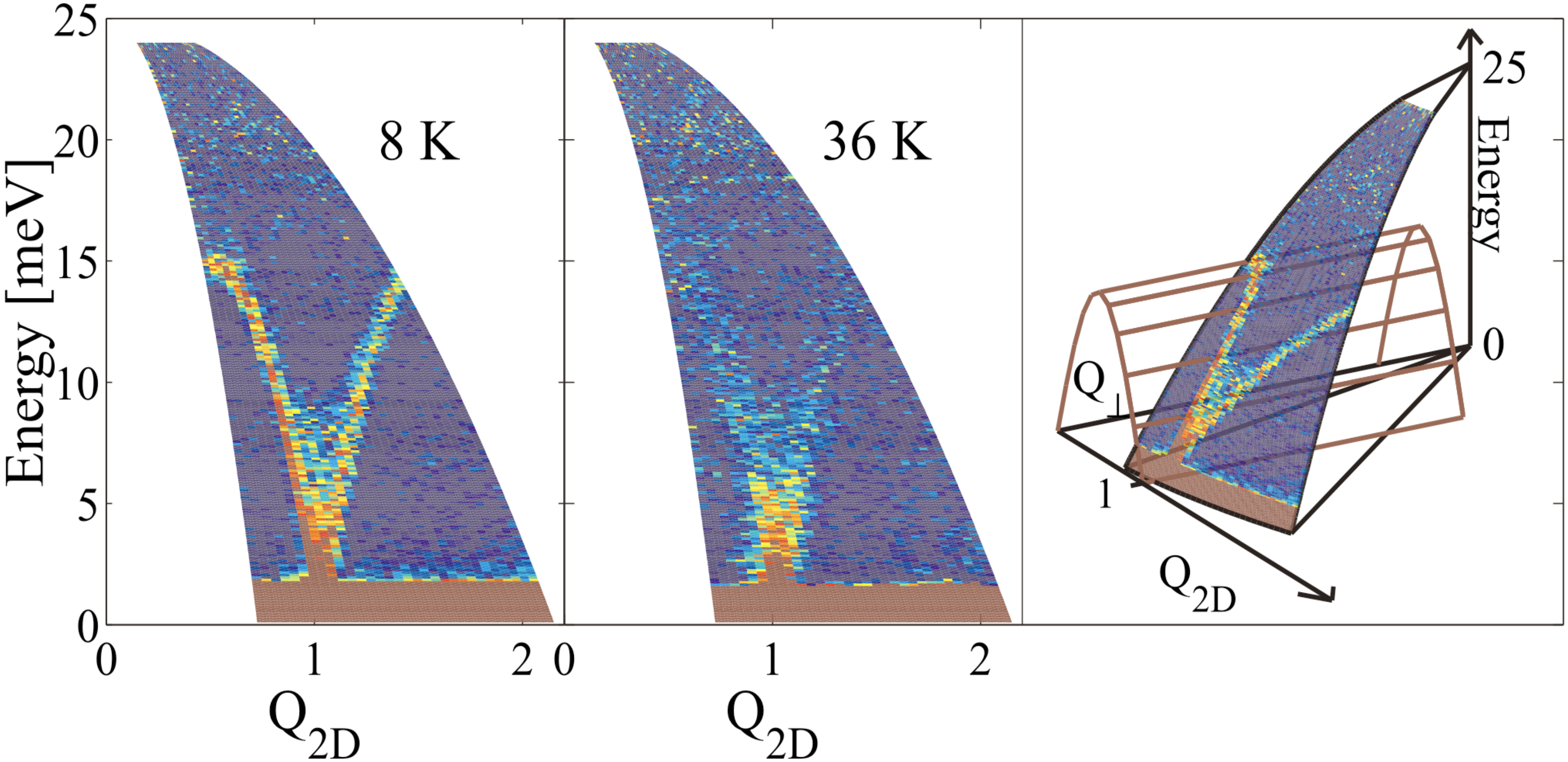

25
20
15
10
5
0
Energy [meV]
0
1
2
Q2D
8 K
0
1
2
Q2D
36 K
25
Energy
0
Q⊥
1
Q2D

$KCuF_3$ Excitations (again)

Direct observation of the continuum

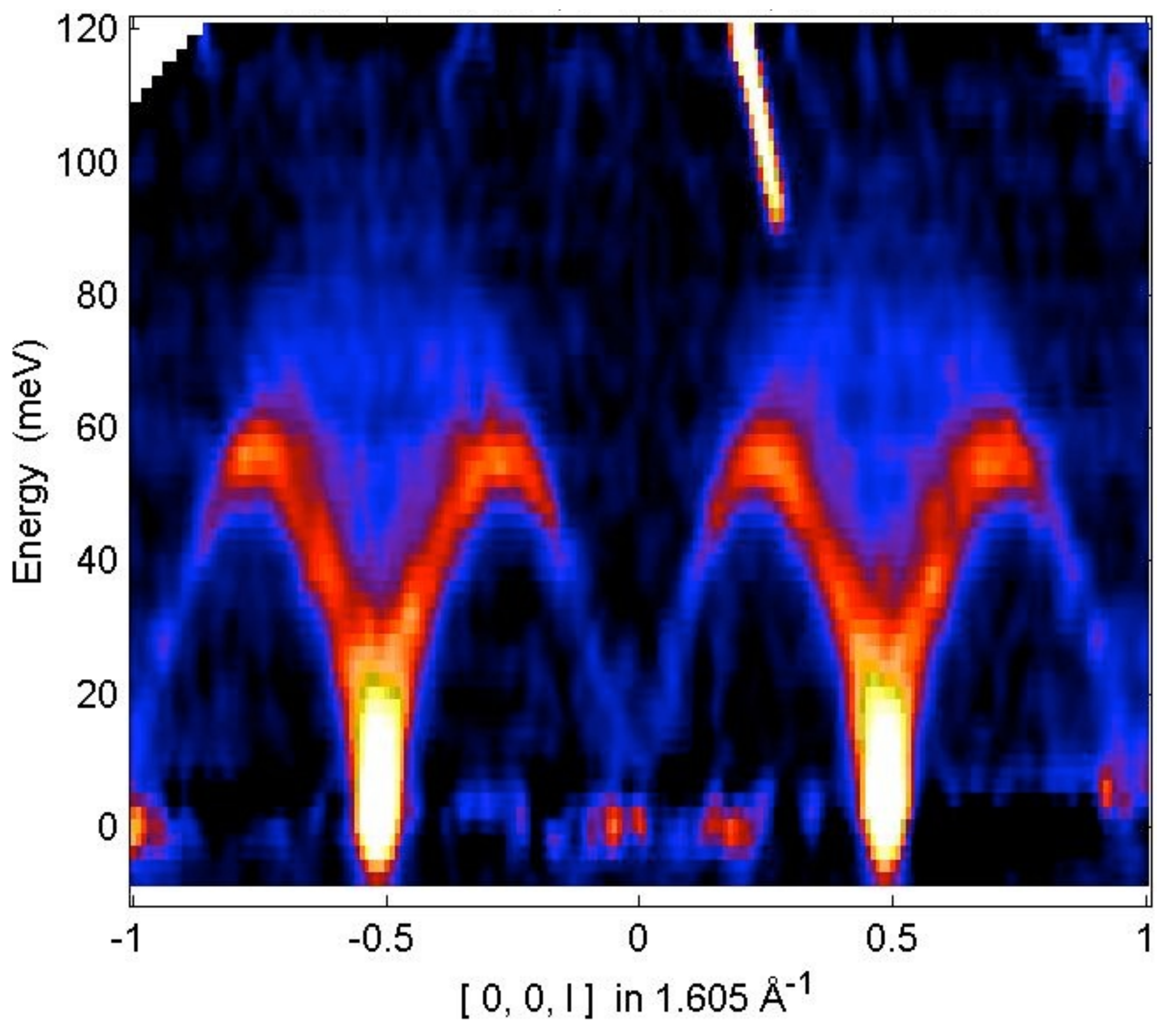

Stephen Nagler (ORNL)
Bella Lake(Oxford)
Alan Tennant (St. Andrews)
Radu Coldea(ISIS/ORNL)

$CuGeO_3$ 1D Spin-Peierls Compound

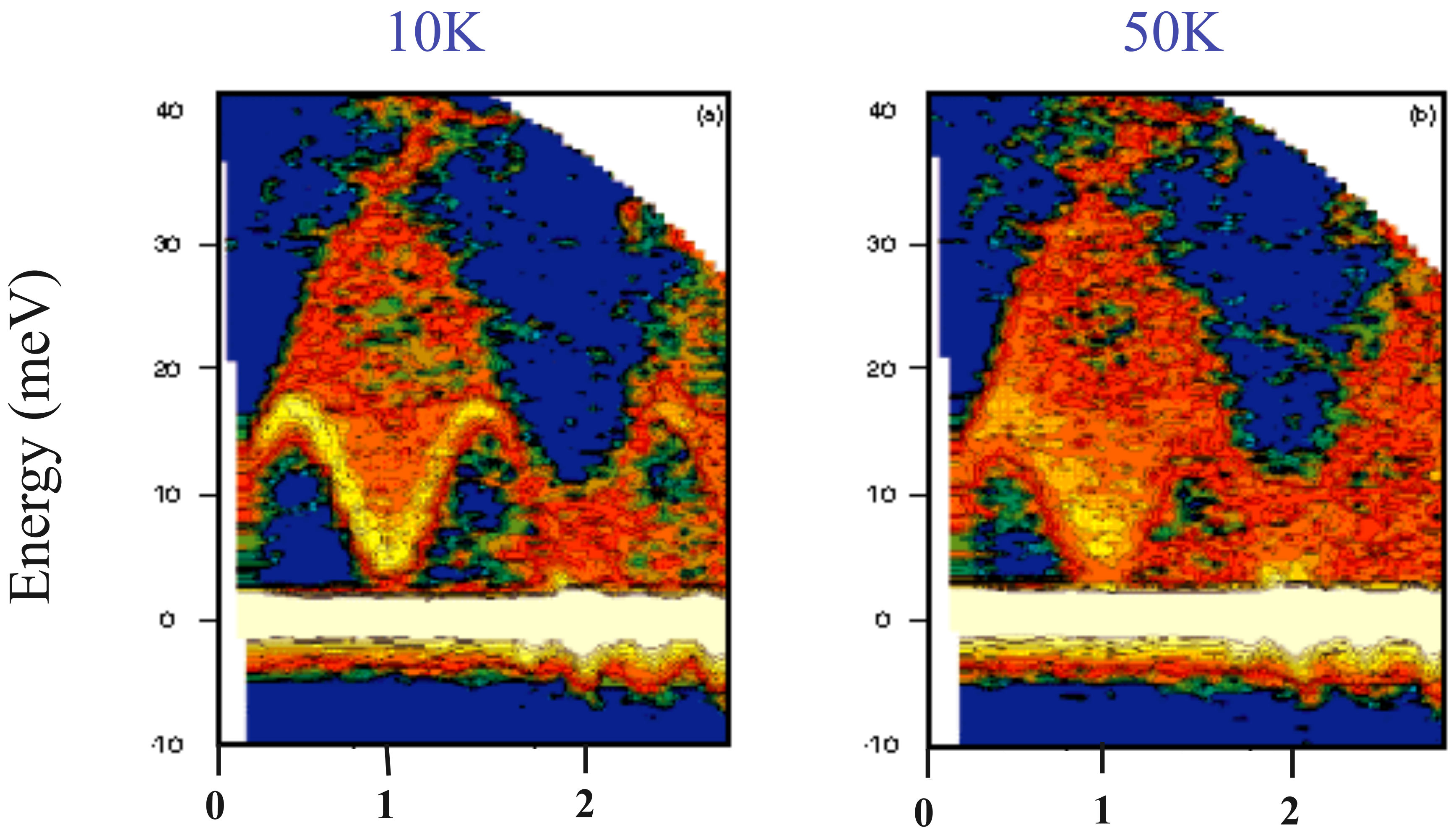

M.Arai et al., Phys. Rev. Lett **77** 3649 (1996)

Measurements of 4D S(Q,ω)

- "Recent developments at pulsed neutron sources promise the most significant advance in neutron spectroscopy since Brockhouse devised the triple-axis spectrometer."

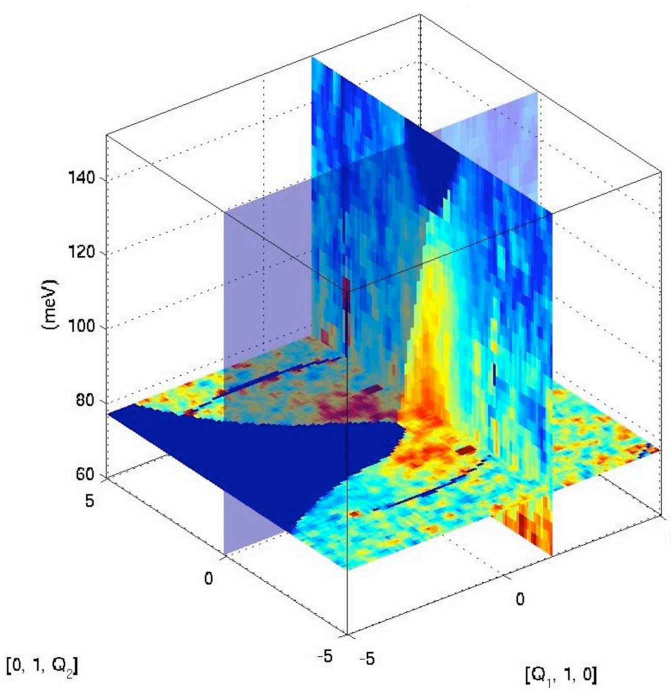

Magnetic Fluctuations in MnSi

R.A.Ewings, T.G.Perring (ISIS)

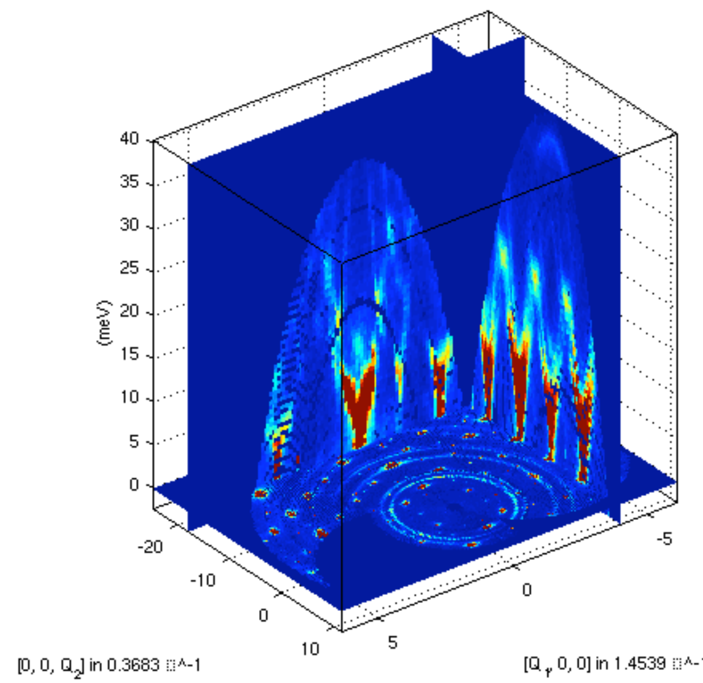

Lattice vibrations in calcite ($CaCO_3$)

Beth Cope, Martin Dove (Cambridge)

Measurement of Electronic Excitations

$$\chi_0(\mathbf{q}) = \sum_{\alpha,\beta,\mathbf{k}} \frac{f(\epsilon_{\alpha,\mathbf{k}}) - f(\epsilon_{\beta,\mathbf{k+q}})}{\epsilon_{\beta,\mathbf{k+q}} - \epsilon_{\alpha,\mathbf{k}} + i\gamma}.$$

$$\chi(q,\omega) = \frac{\chi_0(q,\omega)}{1 - J(q)\chi_0(q,\omega)}$$

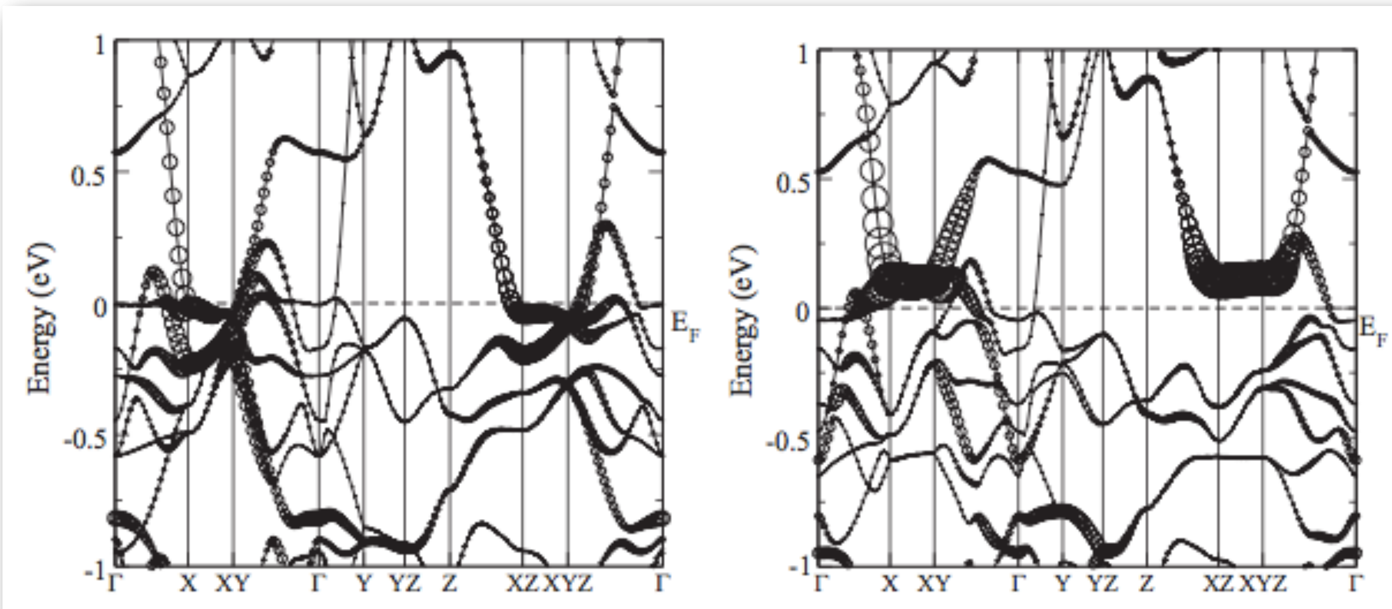

Intersecting the Ewald Spheres

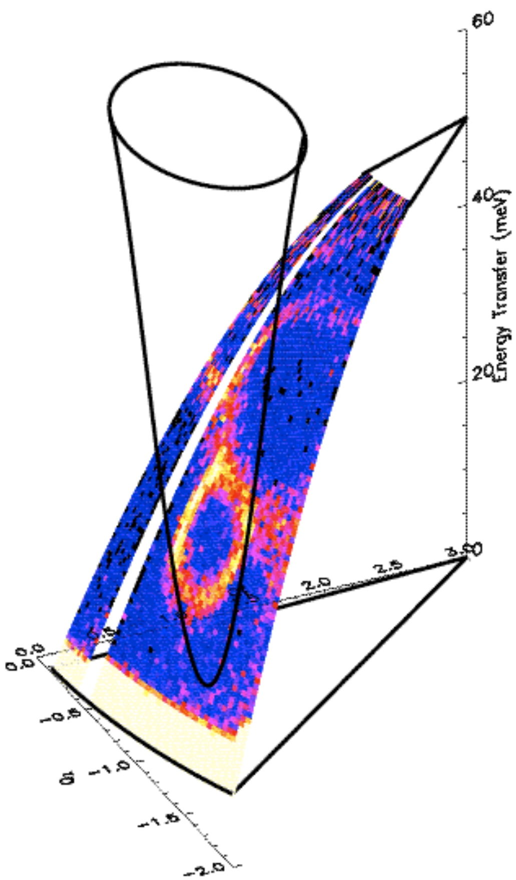

Perring et al., Phys Rev. Lett. **77**, 711 (1996)

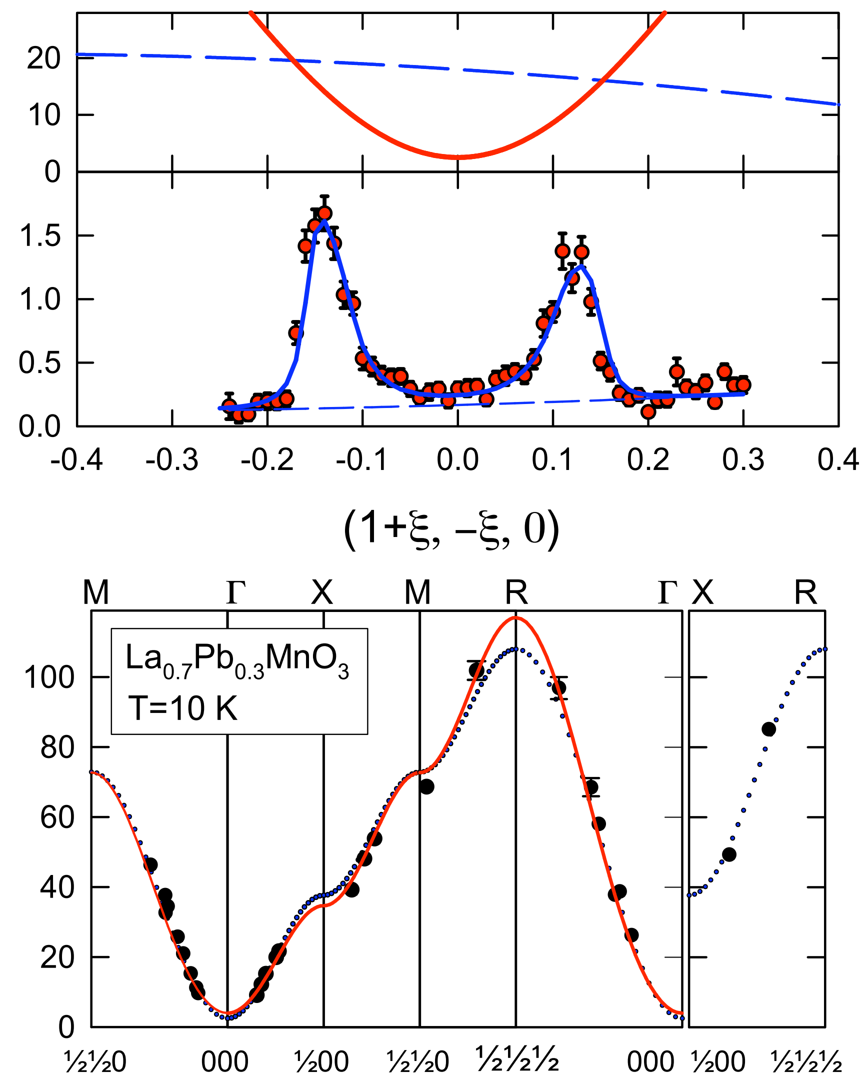

4D S(Q,ω) by the Rotation Method: Horace scans

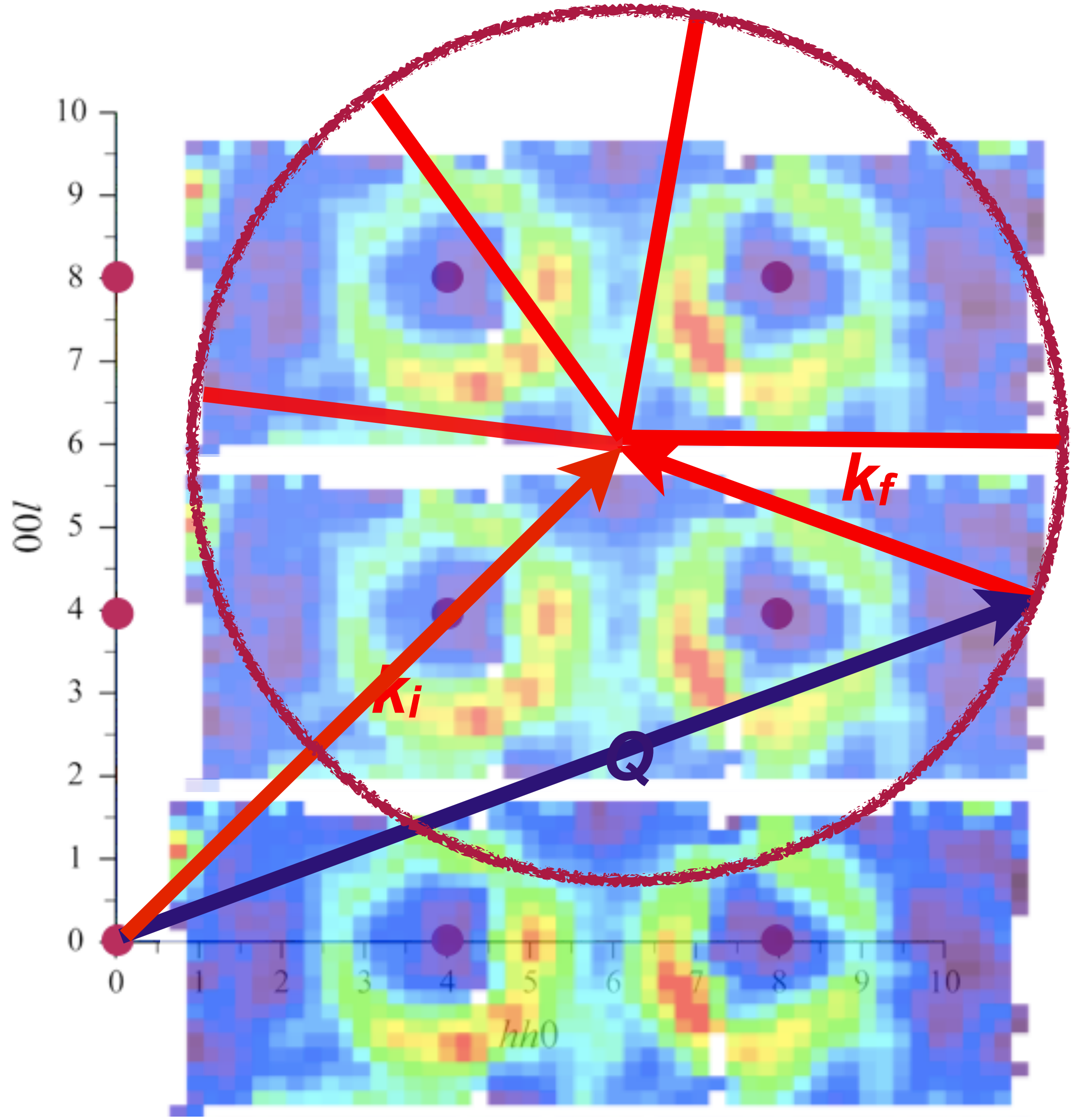

Measurements of S(Q,ω) at ISIS (Horace-mode)

- Experiments at ISIS have already demonstrated the value of measuring four-dimensional volumes of S(Q,ω).
  - Scans typically take 1-2 days: 90 x 1° x 0.5h
  - Similar technique used on NIST's DCS (for a single scattering plane)

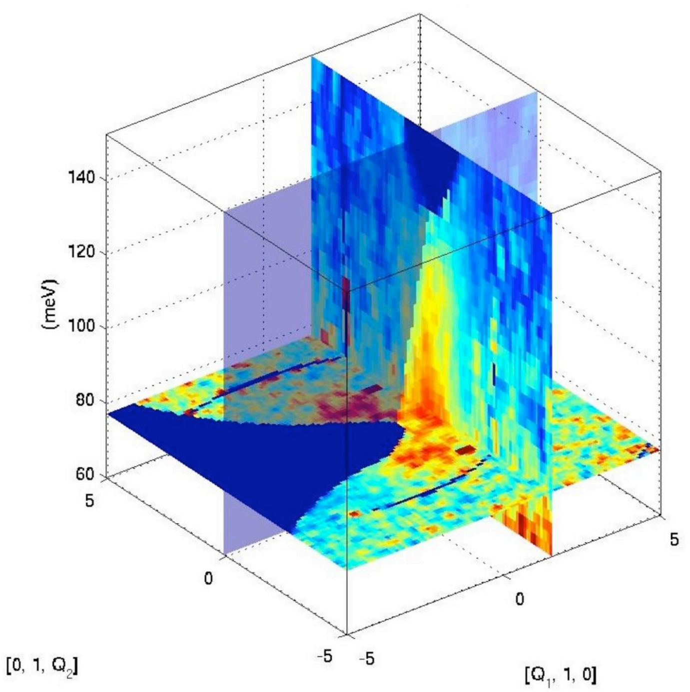

Magnetic Fluctuations in MnSi
R.A.Ewings, T.G.Perring (ISIS)

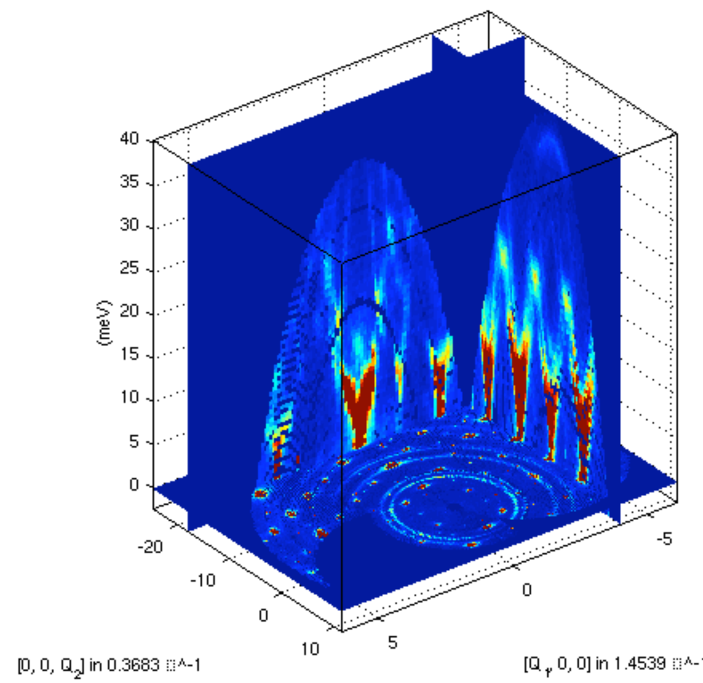

Lattice vibrations in calcite ($CaCO_3$)
Beth Cope, Martin Dove (Cambridge)

Asynchronous rotation measurements on ARCS

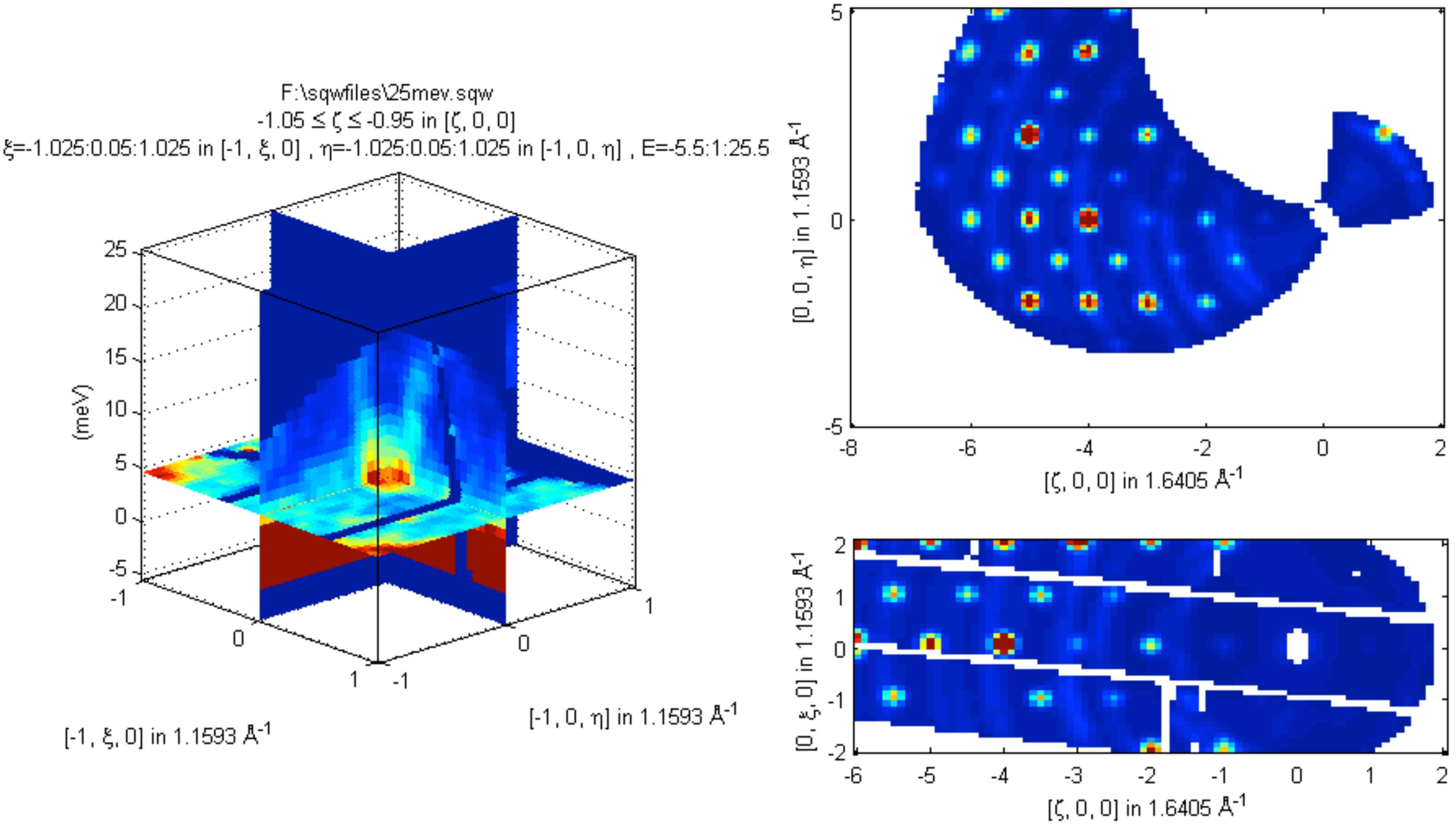

ARCS Network

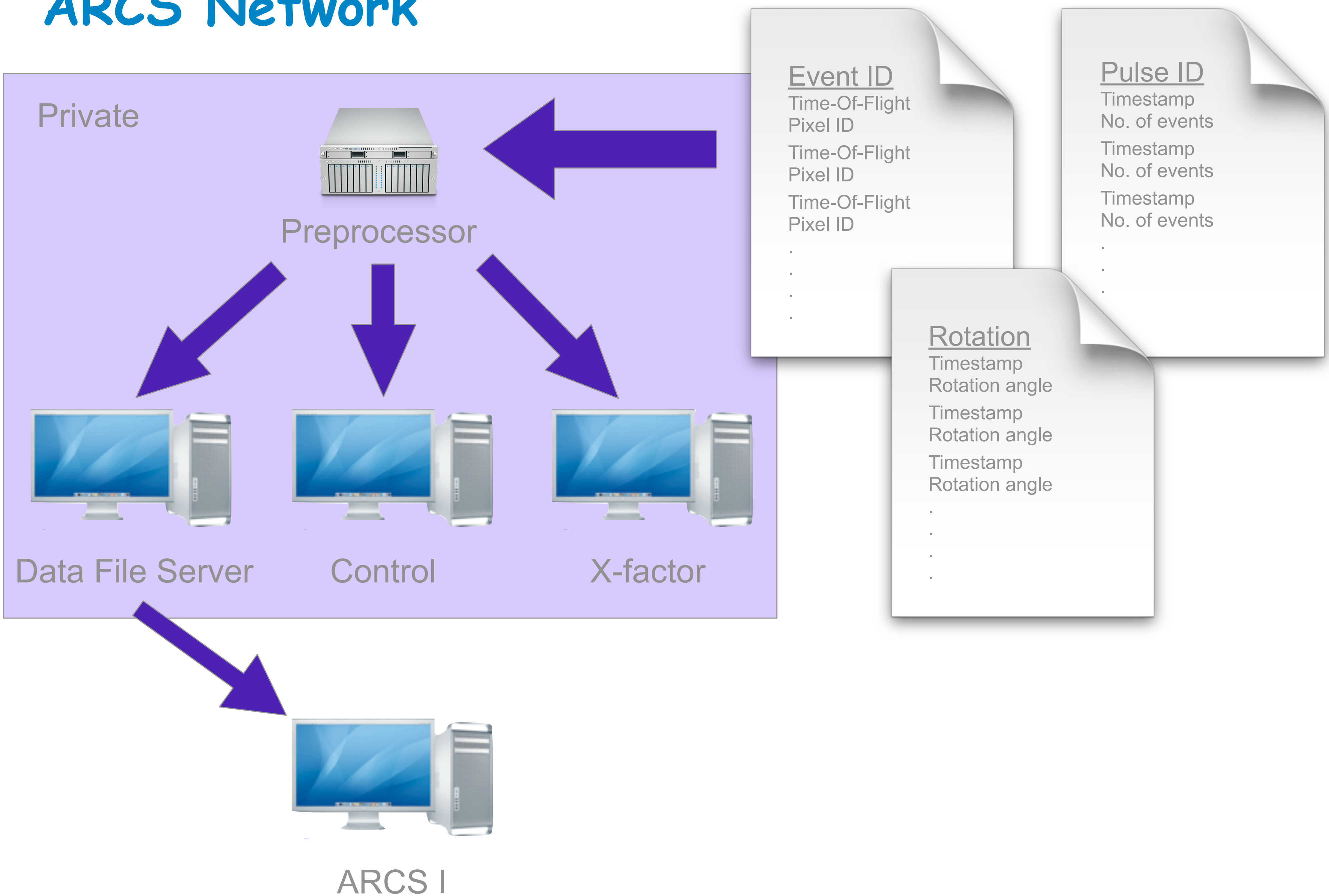

Case study: $LaSr_2Mn_2O_7$

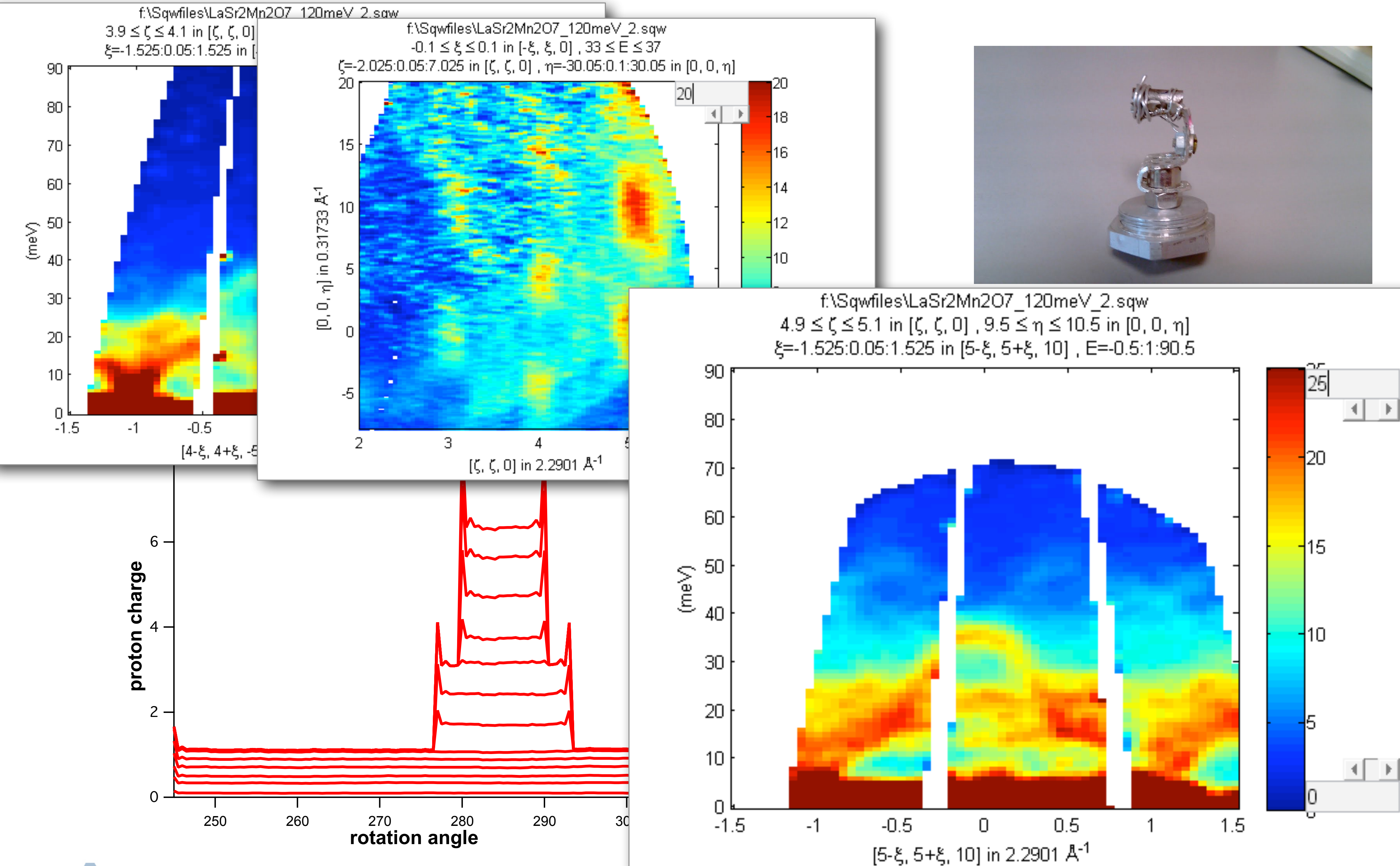

Case study: YNi_2B_2C

$\hbar\omega$ = 102meV

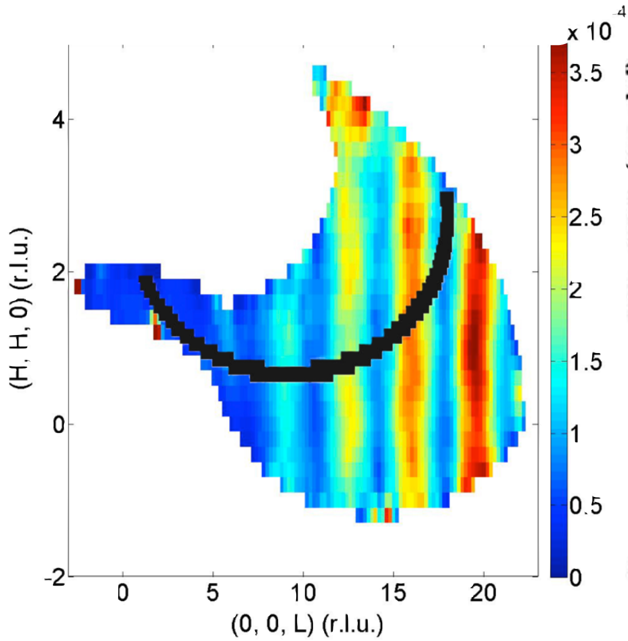

E_i = 160meV

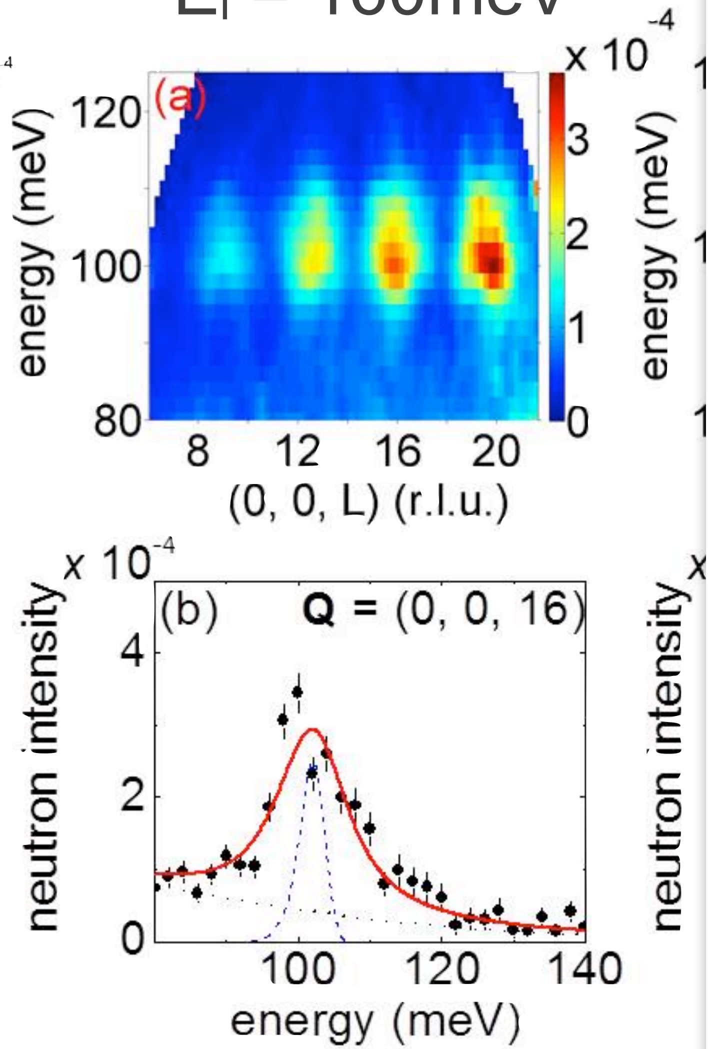

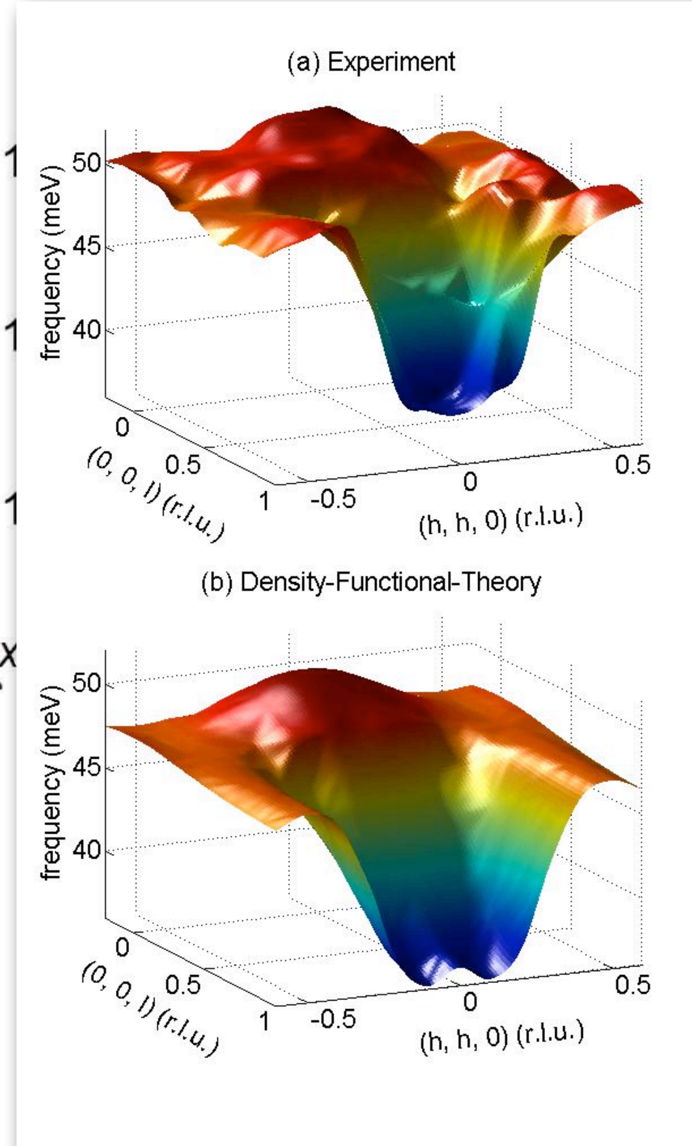

F. Weber, S. Rosenkranz, L. Pintschovius, J.-P. Castellan, E.A. Goremychkin, R. Osborn, W. Reichardt, R. Heid, K.-P. Bohnen, D. Abernathy, PRL **109,** 057001 (2012).

$La_4Ru_2O_{10}$: An Orbital-Peierls System

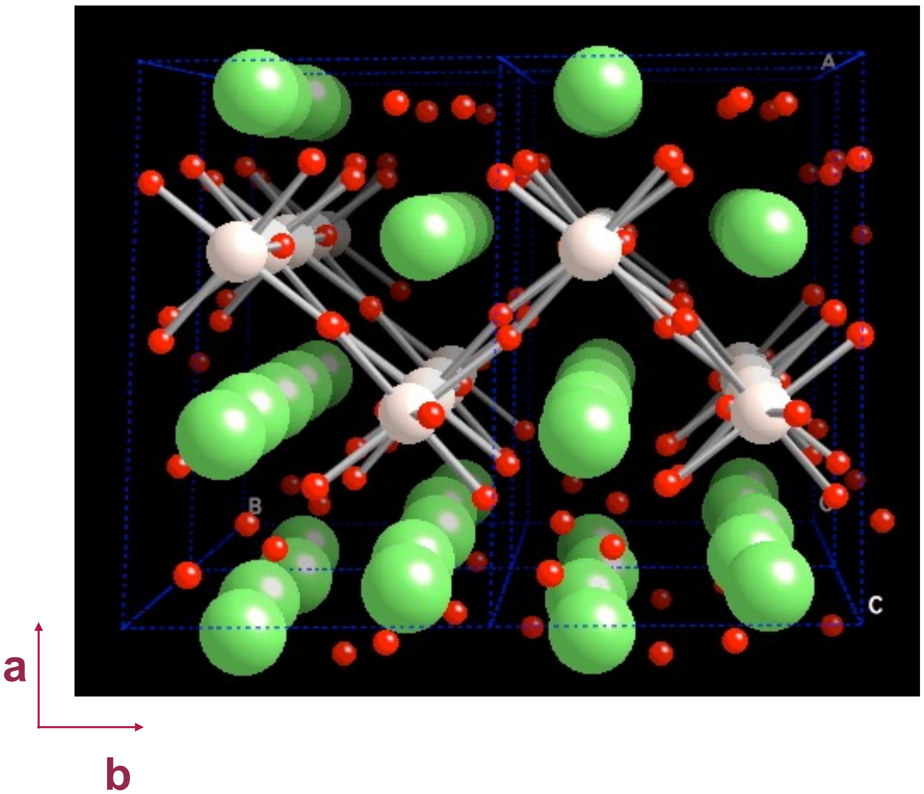

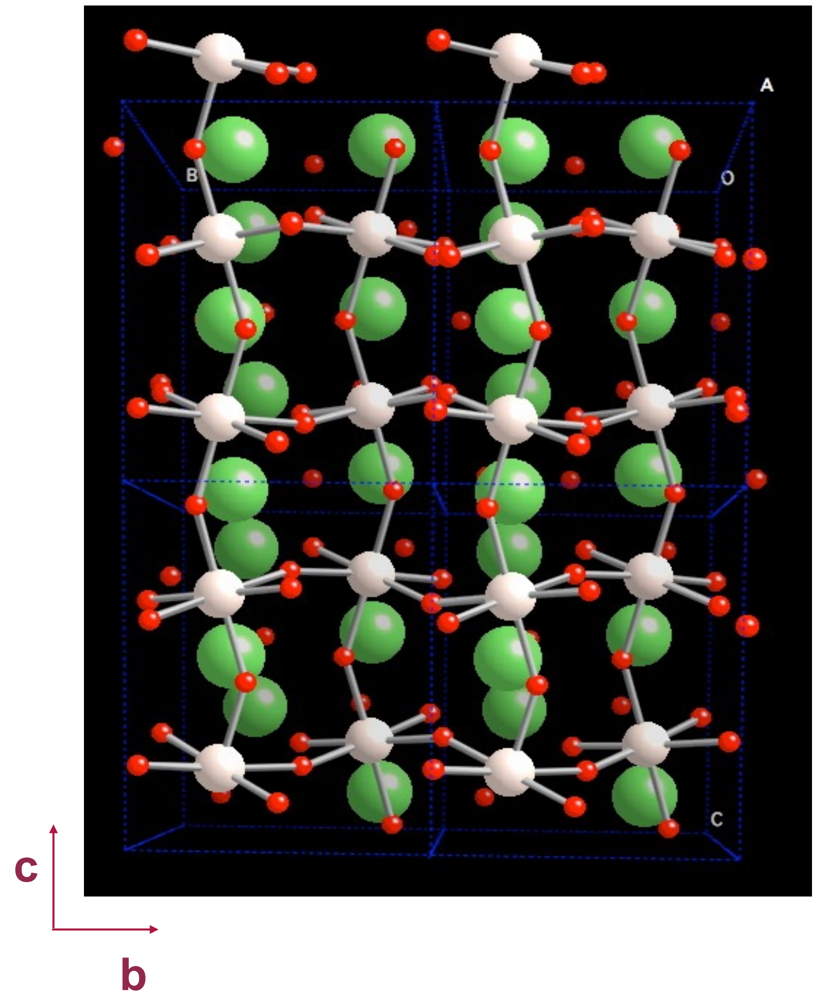

Antiferromagnetic Dimers

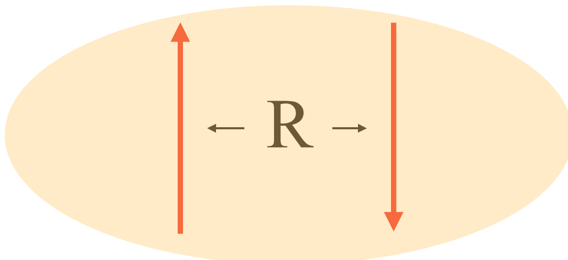

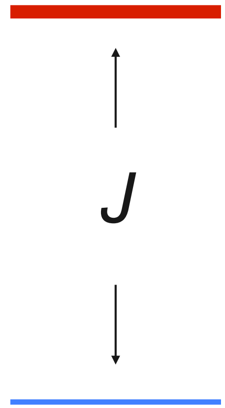

$$|\uparrow\uparrow\rangle, |\downarrow\downarrow\rangle, \frac{1}{\sqrt{2}}\left(|\uparrow\downarrow\rangle + |\downarrow\uparrow\rangle\right)$$

$$\frac{1}{\sqrt{2}}\left(|\uparrow\downarrow\rangle - |\downarrow\uparrow\rangle\right)$$

Hamiltonian: $J\mathbf{S}_1 \cdot \mathbf{S}_2$

$$S^{\alpha\alpha}\left(\vec{Q},\omega\right) = \sin^2\left(\frac{\vec{Q}\cdot\vec{R}}{2}\right)\delta(\omega - J)$$

Magnetic Excitations in Coupled Tetramers

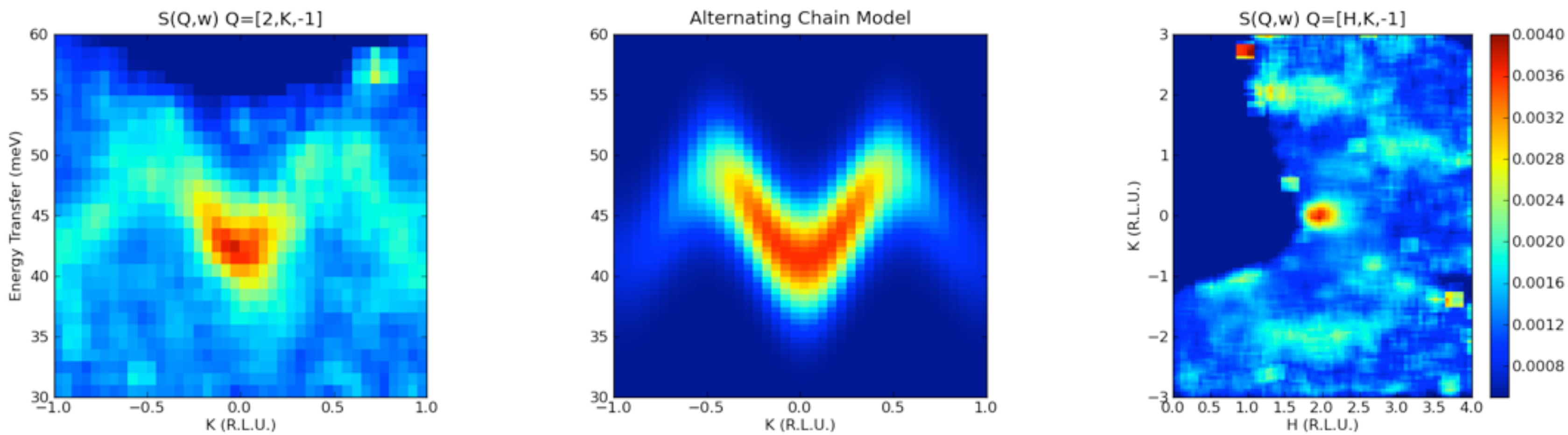

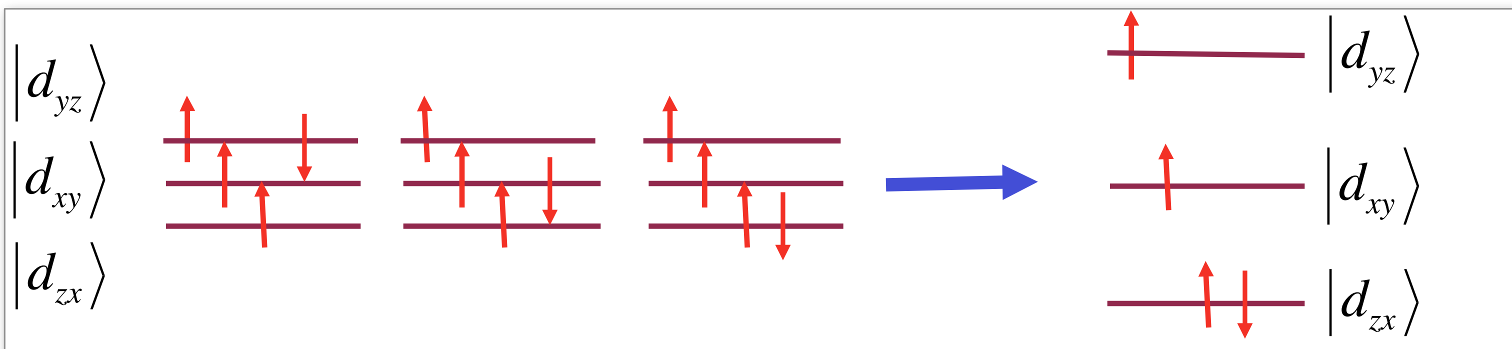

$$J_y = 2J_0(1+\delta)$$
$$J_x = J_0(1-\delta)$$
$$J_z = J_0$$

Khomskii Model: H. Wu *et al.*, PRL **96**, 256402 (2006)

J.P. Castellan, M.B. Stone, P Khalifah, R. Osborn, S. Rosenkranz, S. Nagler, unpublished

Magnetic Fluctuations in $CePd_3$

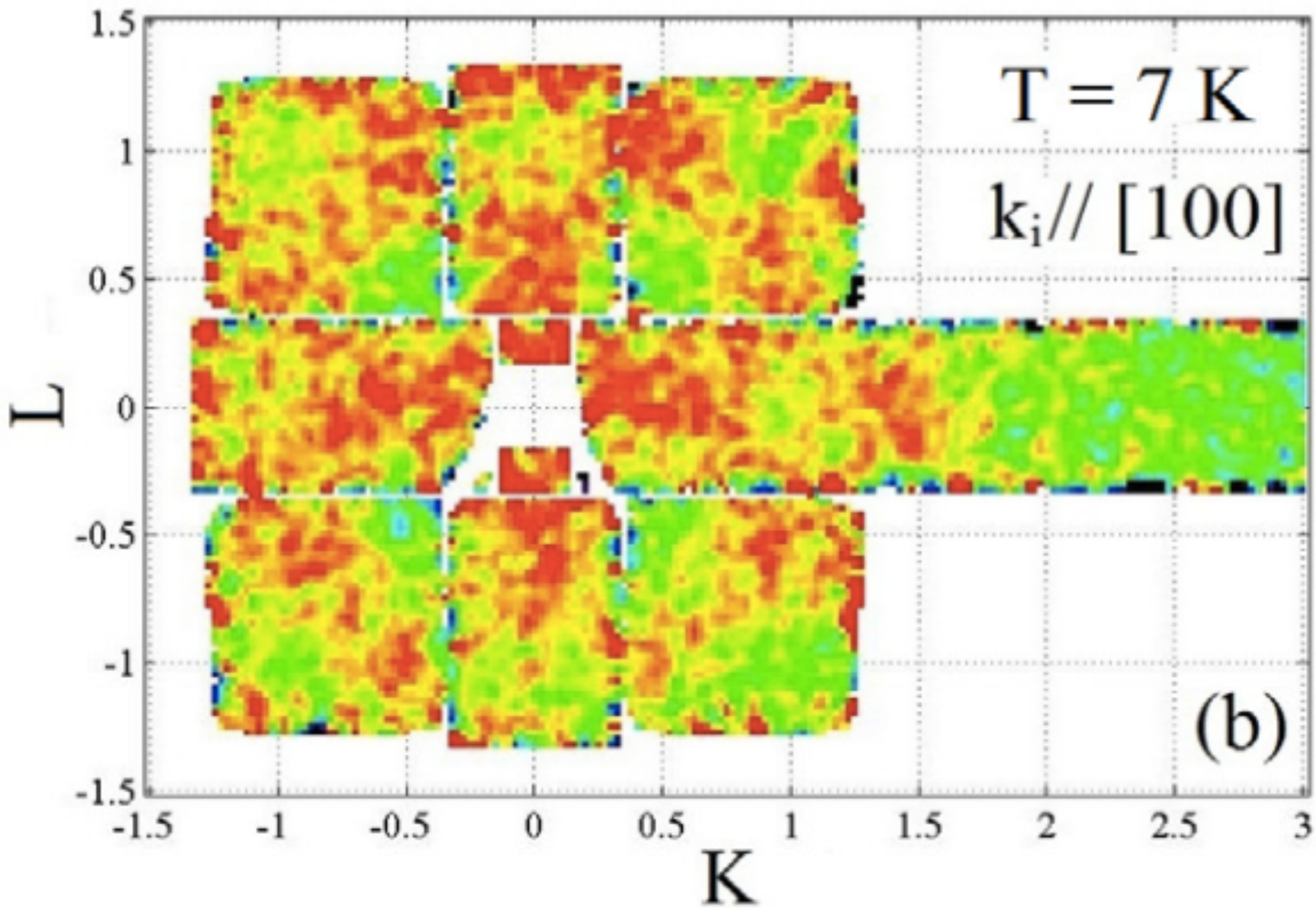

Magnetic Fluctuations in $CePd_3$

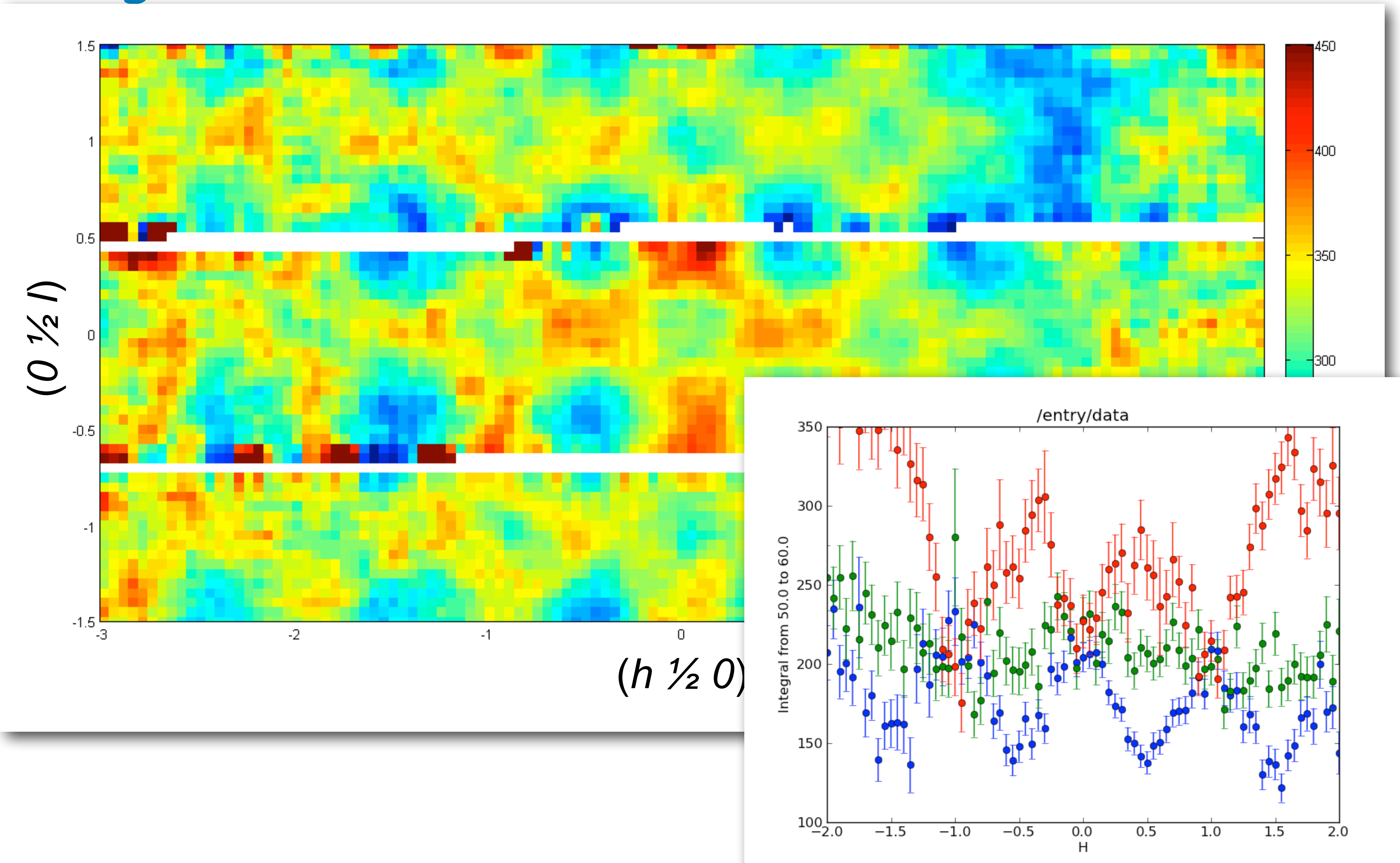

DMFT Calculations of the $CePd_3$ Band Structure

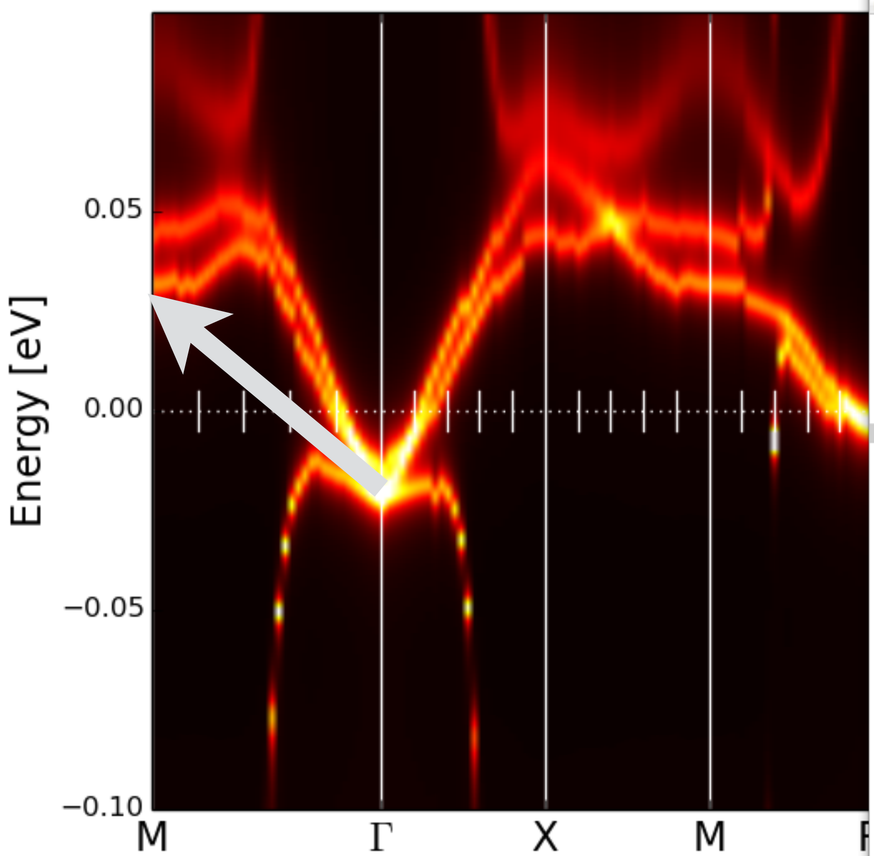

Hyowon Park - Private Communicatio

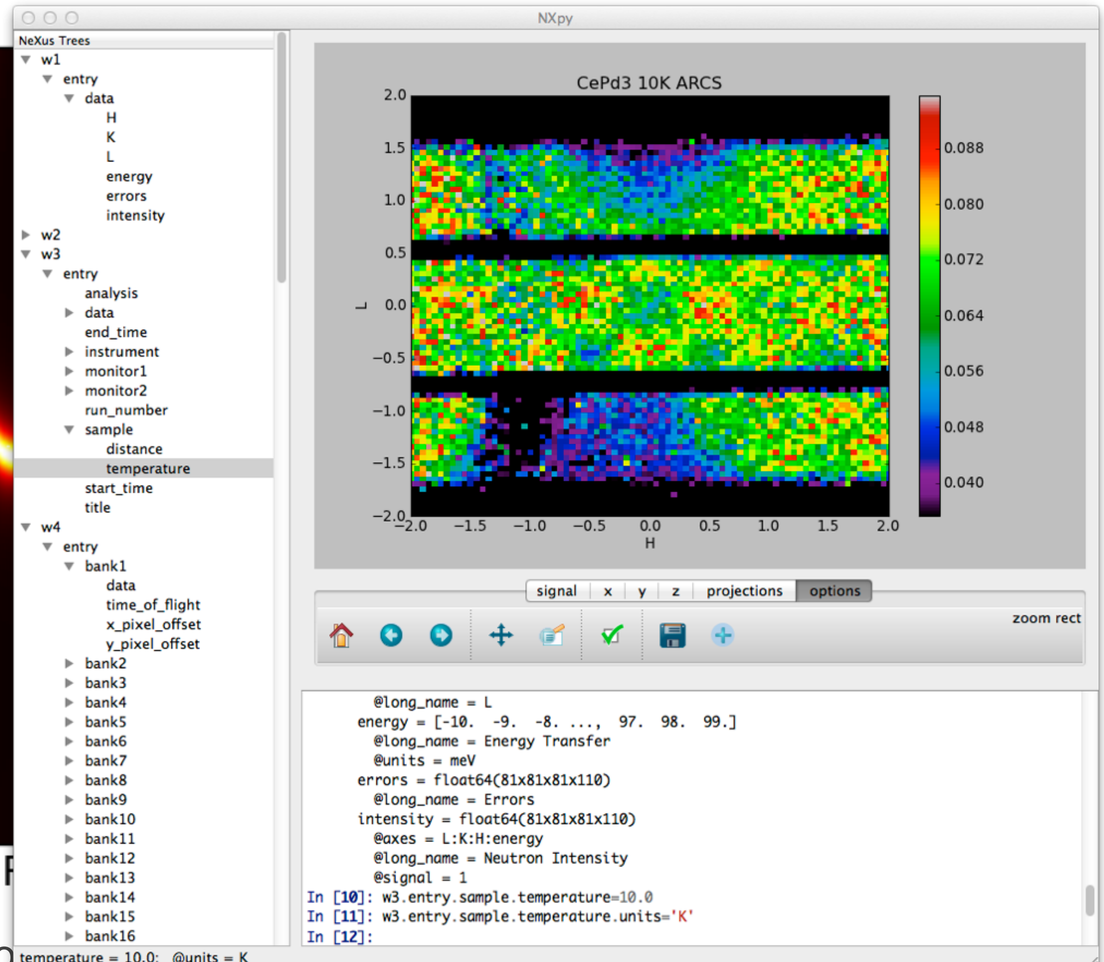

New approaches to data analysis

- The ability to measure 4D S(**Q**,ω) enables new modes of data analysis
- For example, the measurement of the overlapping phonon modes in multiple zones, where they have different structure factors, allows them to be untangled.

$SrFe_2As_2$

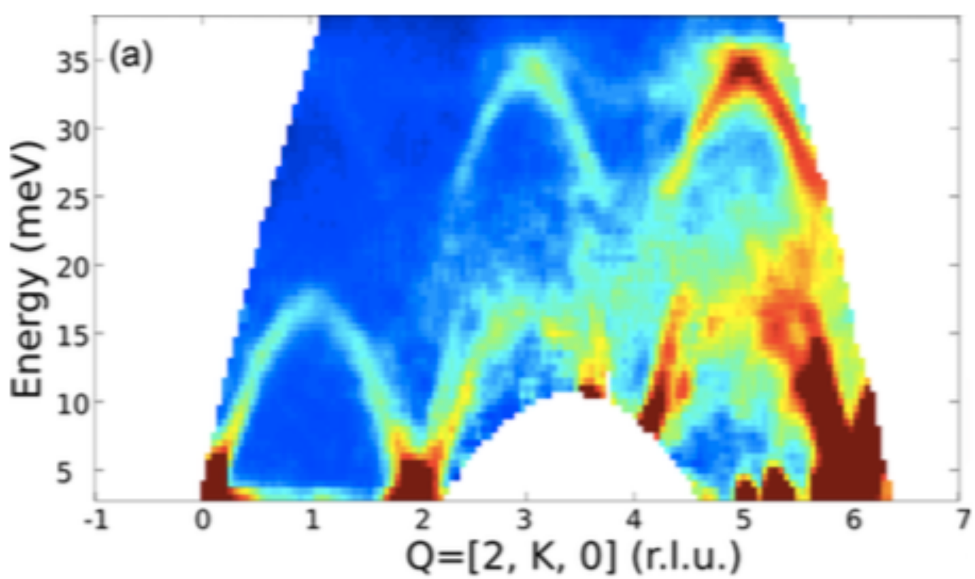

Parshall, D. et al. Phys Rev B **89**, 064310 (2014).

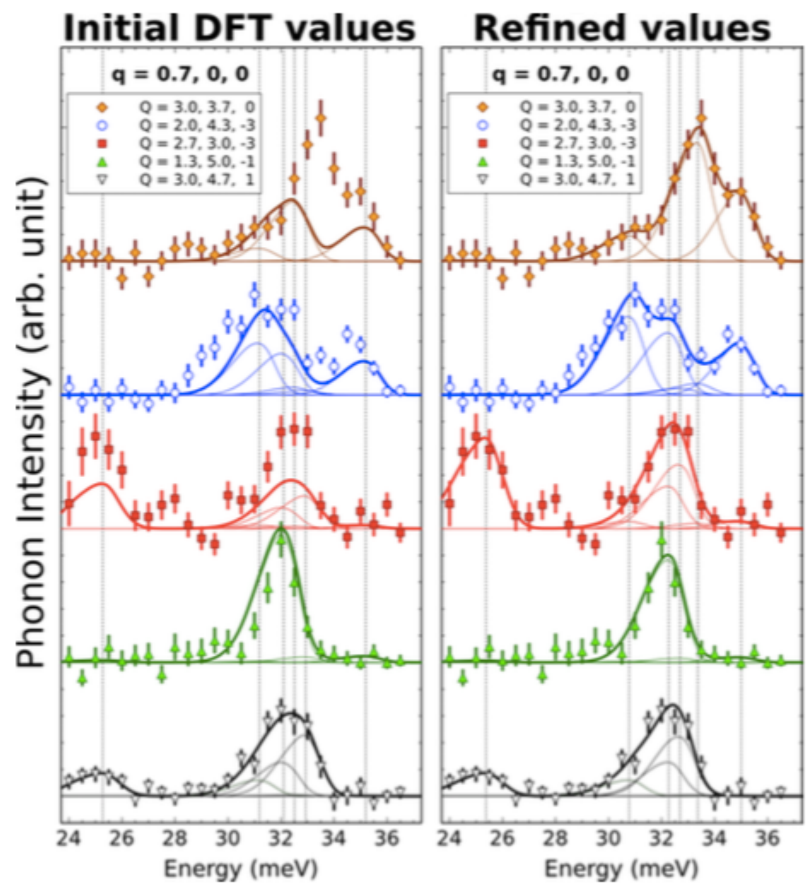

Conclusions

- Measurement of 4-dimensional S(**Q**,ω) are becoming routine.
  - This has the potential for revolutionizing how we do inelastic scattering - not just in 3D systems.
  - The technique would be ideally suited to rep-rate multiplication.
- This allows a much closer coupling of experiment to ab initio theories of electronic structure.
- This should also encourage the development of advanced algorithms for analyzing the data.
  - Advanced data mining, merging rep-rate volumes, four-dimensional optimization